Technology and Health Care 12 (2004) 81–154
IOS Press

I. Bioengineering

1. Methods

Reduction of entrance doses to patients during X-ray examinations

Diana Adliene[a], Gediminas Adlys[a], Reda Cerapaite[a], Egle Jonaitiene[b] and Inga Cibulskaite[b]
[a]*Kaunas University of Technology, Studentu street 50, LT-3031 Kaunas, Lithuania*
Tel.: +370-37300342; E-mail: diana.adliene@ktu.lt
[b]*Kaunas Medical University Clinics, Eiveniu 2, LT-3000 Kaunas, Lithuania*

Introduction: Registration of surface entrance doses (SED) to patients during X-ray examinations is very important solving the problems of radiation protection of patients. However individual dosimetry of patients is very new in Lithuania. It was achieved in last years that every diagnostic X-ray equipment used in health care institutions of Lithuania was tested and quality control programmes were introduced, but reference levels of entrance doses based on *in situ* dosimetrical measurements were not set until now.

The aim of this investigation was to perform measurements of SED to patients during different procedures of X-ray examinations using TLD technique and to discuss the possibilities to reduce this dose.

Methods: The investigation was carried out at the Radiology Clinic of Kaunas Medical University. SED of 20 randomly selected patients in each case were measured *in situ* during urography procedure using Siemens Multix Pro/Vertix Pro X-ray machine and during mammography procedure using Alpha RT mammograph.

Measurements were performed using TLD dosimeters consisting of 2 LiF:Ti,Mg $(3.1 \times 3.1 \times 0.9)\text{mm}^3$ pieces, which were put into small plastic bags. Dosimeters were calibrated at Radiophysics Department of Malmo University Hospital (Sweden). Dosimeters were placed on the patient's skin surface in the centre of exposure field (urography) and in the middle of exposure field at the distance of 5–6 cm from the breastbone (mammography).

Results: The results of our investigation showed that the measured values of ESD of patients during urography procedure do not exceeded recommended dose level limit (10 mGy / image) in all cases, but varied in a very broad area from total dose value of 1,641 mGy to 40,045 mGy for different patients depending on their individual characteristics (mass, length, thickness). Total exposure of patients was similar to those measured in Scandinavian countries, but the number of images made in Lithuania was 2–5 times smaller. Based on these results it could be assumed that there is some space for the reducing of entrance dose levels.

Surface entrance doses measured during mammography procedure were used for the evaluation of average glandual dose (AGD) of the breast. It was determined that the recommended (AGD) dose limit of 4 mGy/image was exceeded in two cases. This fact could be explained taking into account the individual parameters of the patients and assuming that TLD technique is not very suitable for the entrance dose measurements in mammography because of scattering effects.

Despite of small discrepancy the results of our investigation will be included into initial database for radiation protection of patients during X-ray examinations in Lithuania and will be used for the determination of reference entrance dose levels.

References

[1] Radiation Protection 109. Guidance of diagnostic reference levels (DRL,s) for medical exposures // EC Directorate-General environment, Nuclear safety and Civil protection, 1999.
[2] SSI FS 2002:2 The Swedish Radiation Protection Authority's regulations and general advice on diagnostic standard doses and reference levels within medical X-ray diagnostics, 2002.
[3] J. Zoetelief and F. Schultz, Patient dosimetry in diagnostic radiology using TLD. Proc. of the int. conf. "Biomedical Engineering and Microtechnologies", Riga, 2002, pp. 57–61.

Science, Knowledge and Technology in Organ Replacement

Vittorio Bonomini
Professor Emeritus, University of Bologna, Italy

This report deals with the present relation between Science-Technology and Science-Humanism, a problem probably still insufficiently appreciated its present being and future prospects.

While in the Ancient World, Medicine was seen in a multicultural cosmological context, and from the Renaissance on in a prevailing anthropological vision (aimed at understanding Man not only Sapiens, but also Human), present-day Medicine sees the dominion of Technology and Economy, which rule the roost of Medicine, and so it grows more and more impersonal. "Treat the patient as a human being" is steadily becoming a cliché, rather than a strongly felt ethical principle.

In Medicine, the present-day dominion of Technology over Science and Knowledge involves teaching and clinical practice.

The teaching problem emerges when the hiatus between Humanistic and Technological Disciplines is adequately pondered. Here the dominance of Technology over Science at all costs means the loss of the latter's deepest roots, while not ruling but being ruled by technological doctrines is a real danger.

Science and Knowledge, therefore, should be properly balanced, and the Humanistic Disciplines should be revalued in a context of all-inclusive universal Knowledge.

The unfortunate effects of the technological bias are most tangibly felt in Clinical Medicine, where Science, Knowledge and Technology do not run parallel, and the gap between basic knowledge and applicative knowledge is quite evident, particularly in the "new forms of life" that the most up-to-date Medical Biotechnology allows. They include: computer science; biological manipulation (cloning, assisted fecundation, genetic manipulation, transgenization, etc.); artificial organ replacement; organ transplantation; bioengineered new organs; gene therapy, etc. Although such "miracles" would have been unthinkable 30–40 years ago, they are by no means free from criticism, raising, as they do, a series of problems (cultural, ethical, economic, social, etc.). By and large these new forms of life result: unpredicted by natural physical laws; still inadequate biological codification; while solving one problem, they generate others; they represent today's transitional state of knowledge (and at the same time the permanent state of confusion in Medicine).

Among these new forms of life, Organ Replacement has made the greatest public impact. Death of a vital organ no longer necessarily means death of the individual. Of the various organs, the kidney affords the greatest experience, and is commonly taken as a yardstick for the status of current organ substitution.

What we know, what we don't know, what the merits are, what the drawbacks are, only become clear over the course of many years of R.R.T.

The spectacular survival is a proven fact, especially with living donors, but, at the same time, an associated specific co-morbidity emerges, together with several biological repercussions and the appearance of a new biology risk.

The factors behind these unpredicted expectations can be various: logistic: adequacy of facilities; centre experience and policy; technical: unphysiology of treatment; unbiology of immunomodulation; cultural: applicative knowledge outweighing theoretical knowledge. The latter is likely the most important and makes it hard for organ replacement to be defined as a "True Science".

Such a definition presupposes that theoretical and applicative knowledge run parallel. Few disciplines in Medicine attain that status (one example is infectious disease). In 90% the cause of disease remains unknown. We know the effects, not the cause. In Organ Replacement Therapy the dissonance in knowledge comes from "continuing application despite what we know" (as in Dialysis) and "continuing application despite what we don't know" (as in Transplantation).

We should do well to ponder this problem since, despite the fact that such shortcomings have been known for many years now, they have never been corrected: nevertheless, the demand for therapy is steadily growing, due to at least three factors: a) the higher incidence of Renal failure; b) relaxation of Entry requirements; c) financial incentives for the ESRD Medical Industry Complex.

The main consequences of Application outweighing Theory in Organ Replacement Therapy are: a growing detachment from the patient; a new patient is created, not an ex-patient; society and the patient need to be properly informed; the time has come for a new Culture.

This new Culture, which we might term "the new millennium project", should include both rehabilitation of the patient and humanization of Techno-medicine. Complete patient rehabilitation, above all, means improving basic knowledge via: 1. explaining; 2. transforming; 3. innovating. Knowledge is the key to future development, but to be of real benefit to both the patient and society it must evolve into innovation. In this regard, it should be stressed that the indispensable economic support for Scientific Research should not involve the old-economy or the simple new-economy. What is needed is a wise-economy, which occurs when the new-economy meets innovation.

Unfortunately, the climate of present Medicine makes it difficult to apply these assumptions in Organ Replacement. For example, the prospected evolution from Medicare to Managed-care of the Health support and funding research system, involves a scheme where the main targets are: reduction of costs by all means; transforming the doctor's role into a new task (from treating the patient to managing the cost of doing so, etc.). Reducing the costs, but not the benefits, while 70–80% of the doctor's time becomes devoted to clinical and routine bureaucracy, and only 7% to research is at least questionable. Uncertainties apart, what is certain is that if Europe is to invest in knowledge and innovation, it must receive specific research funding. Too often research into basic (theoretical) knowledge is blocked by the short-sighted distribution of national research funds.

We said Knowledge and Innovation. All true progress in fact implies transformation and innovation. And the "science of discovery" is the real central dynamo of learning; and innovation sets the seal on it. Informed, innovative knowledge is the only hope for rehabilitating the patient in Organ Replacement in clinical terms. The core of the problem is: specific – not aspecific – immunotherapy in transplantation; and a bioartificial – not just artificial – organ in dialysis. What is needed for such results is: simultaneous evolution of scientific thought and research; evaluation of results in terms of Science and Art; interdisciplinary research; updating of Academic and other Institutions; all geared to RRT therapy. Likewise, a bridge must be built between Science, Society and Ethics. I can only sketch some of the points for cultural guidelines: professionalism of judgement in planning programmes; need for pluralistic cultural programmes; acceptance of any changing reality without dogma or prejudice; a greater tendency toward humanizing Techno-medicine.

To humanize Organ Replacement, lastly, apart from using a bio-artificial device in dialysis and specific immunotolerance in transplantation, we need to rediscover Man, the prime target of ethical-medical learning.

Conclusions

1. In Organ Replacement (the most updated reference point of the new forms of life that present applied Biotechnology affords) Science, Knowledge and Technology do not run parallel with time. Technology outweighs theoretical knowledge.
2. The cultural dissonance is among the most important factors of the real reality of Organ Replacement solving one problem (survival); but activating many others (clinical, ethical, social, economic).
3. A new culture is needed, aimed at balancing Science and Knowledge in a more appropriate context tending to equate Science-Technology and Science-Humanism.
4. Humanizing Techno-Medicine means recapturing the essence and purpose of Knowledge (which otherwise remains mere erudition), via more appropriate guidelines for bridging Science, Society and Ethics.
5. In Organ Replacement it means rediscovering Man as a person and patient; improving his quality of life; reducing cost/benefit, and, last but not least, guaranteeing long-life to Medicine itself, and finally restoring the doctor to his ethical role (which the dominion of technology tends to undermine).

The application of infrared spectroscopic imaging in medical diagnostics

Patrick Garidel
Martin-Luther-University Halle/Wittenberg, Institute of Physical Chemistry, Muehlpforte 1, D-06108 Halle/Saale, Germany
E-mail: Patrick.Garidel@t-online.de

Introduction: Traditional microscopic methods for the histophathological characterisation of tissues require complicated and time consuming procedures for sample analysis and yield only reduced information concerning the biochemical composition of samples.

The presented study utilises the combination of microscopy and the power of infrared vibrational spectroscopy to analyse medical relevant samples as e.g. skin [3–6].

Since a few years, micro infrared spectroscopy is used to investigate the biochemical composition and characterisation of tissues [7,8,13,14]. Paschalis, Mendelsohn and Boskey ([1,11,12] and references cited therein) have shown the power of this technique for the characterisation of bone samples. A number of quantitative and qualitative information can be derived from these data concerning the relative amount of mineral and carbonate, mineral composition, or crystal perfection in bone samples. Max Diem and coworkers ([8] and references cited therein) have demonstrated that this technique has a large potential in the field of cancer research.

Micro infrared spectroscopy (also known as infrared microscopy) combines a Fourier transform infrared spectrometer with an infrared microscope [2]. The infrared beam probing the sample is focused at the microscope's focal plane. Actually, this method is applied in the transmission as well in the reflection mode. Infrared microscopy utilises the chemical composition of the tissue as an indicator for the state of the cells in the tissue. No stains nor chemical treatments of the sample are required. Micro

infrared spectroscopy uses the inherent optical property of the sample. The first reports utilised the so called mapping procedure. However, this method is extremely time-consuming, due to the fact that only one single detector is utilised. The term mapping describes a method, where the investigated sample is moved stepwise under a single channel detector while taking a spectrum after each sample movement. Due to the fact, that this is a laborious procedure, it is often necessary to focus the investigation on only a limited number of spots [13]. The variable size aperture defines the investigated area from which an infrared spectrum is collected.

The application of infrared array detectors (focal plane array detectors) reduces the time for an imaging experiment considerably [9]. The used imaging method is based on a procedure taking all spectra of the chosen sample area at once under an array detector without moving the sample. Such an array detector typically contains 4096 (64×64) elements, and from each element a single infrared spectra is collected, thus that one imaging experiment generates simultaneously 4096 infrared spectra.

Examples are shown how this method can be used for the biochemical characterisation of stratum corneum and monitoring the lateral distribution of topically applied drugs in a skin sample .

Method: Skin samples were taken from a Göttingen pig. Thin sample sections (4 micrometer) were obtained by cryosectioning, mounted on a calcium fluoride infrared window and dried on air. Micro infrared spectroscopy data were collected (at room temperature) via a Bruker IRScope II coupled to Bruker IFS66 v/s Fourier transform infrared spectrometer equipped with liquid nitrogen cooled Mercury-Cadmium-Telluride detector. Imaging data were obtained using a Bruker Hyperion IR imaging unit. For more detail see references [2–4].

Results: Infrared spectra are recorded by infrared microscopy from the investigated sample utilising small apertures of 20–50 micrometer of typical spots and single cells of the sample [3]. Infrared bands which are characteristic for one component in the tissue are determined. These are the so called marker bands, which are specific for one component in the sample. Stratum corneum consists mainly of lipids and corneocytes (horney cells). Marker bands for the lipids are the symmetric and asymmetric methylene bands found at 2920 cm^{-1} and 2851 cm^{-1} [3]. In addition, the lipid fraction is characterised by the carbonyl band with its maximum at $\sim$ 1738 cm^{-1} (see Fig. 1). The main chemical compounds in corneocytes are proteins, which are characterised by the asymmetric methyl vibration ($\sim$ 2957 cm^{-1}), the amide I (1655 cm^{-1}), amide II (1545 cm^{-1}) and amide B ($\sim$ 3080 cm^{-1}) bands (for more details see [3]). The intensity of these marker bands varies within the sample and the integrated intensity of the corresponding spectral parameter is calculated for the whole data set obtained by infrared imaging and converted in a colour or grey scale code. Thus, infrared images shown in this paper are generated with the following code: black (dark) large amount, white (light) low amount of the imaged component (see Fig. 1).

The spatial resolution achievable by infrared microscopy is determined by the diffraction limit of about one half of the wavelength of the infrared radiation. Thus the spatial resolution of the lipid distribution is limited to $\sim$ 3.5 micrometer (utilising the methylene marker bands), whereas the spatial resolution of the protein fraction is limited to $\sim$ 6 micrometer (utilising the amide I marker band). However, due to the size of the elements on the focal plane array detector, the spatial resolution is technically limited to $\sim$ 7 micrometer.

In Fig. 1(A) a photomicrograph of a pig skin sample taken parallel to the skin surface at a depth of 6 μm is shown. The sample thickness is 4 μm. As can be seen from the photomicrograph the optical information obtained from this sample is quite low. It looks like a homogeneous tissue with no morphological characteristics. However, utilising the infrared imaging technique reveals a completely other view. Figure 1(B) namely represents the lipid distribution as obtained by integrating the asymmetric

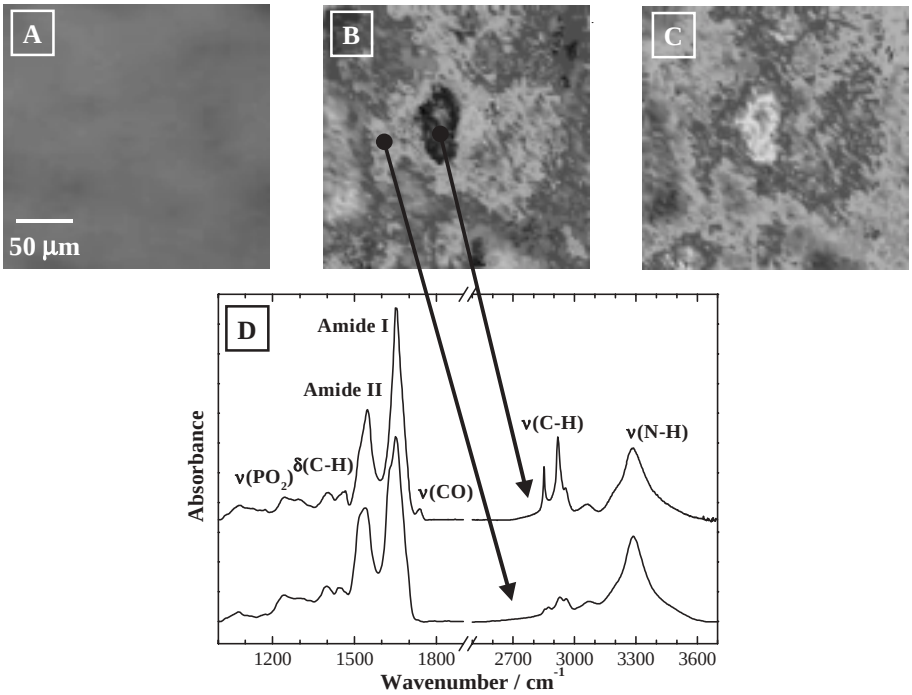

Fig. 1. (A) Photomicrograph of a pig skin sample obtained parallel to the skin surface at a depth of 6 μm. (B) Biochemical imaging of the lipid and (C) protein distribution with: white (light) low amount, black (dark) large amount of the imaged component. (D) Infrared spectra of different spots on the sample.

methylene band within this sample. Dark areas in Fig. 1(B) correspond to a high amount of lipid, whereas white areas are characteristic for a reduced concentration of lipid. This is also obvious by analysing the infrared spectra obtained on different spots of the sample (Fig. 1(D)). The lower spectrum of Fig. 1(D) is marked by a low amount of methylene bands and the absence of the carbonyl band. In the upper spectrum, the intensity of the methylene bands has increased largely.

Representing the lipid fraction by means of the integral intensity of the carbonyl band reveals a similar result (data not shown). The amide I marker band is used for imaging the protein fraction (Fig. 1(C)). Comparing the two infrared images (Figs 1(B) and (C)) it becomes obvious that both images are nearly complementary. Areas with a high amount of lipid show the absence of proteins and vice versa. This documents a heterogeneous distribution of the lipid and protein fraction within the stratum corneum.

The distribution of various topically applied drugs in the skin can easily be monitored by infrared imaging. It necessitates a specific marker band, which is not overlapping with intrinsic vibrations of the sample matrix. This can be achieved by utilising isotopically labelled components (e.g., molecules with deuterium labelled hydrocarbon chains, adsorbing between 2050–2250 cm $^{-1}$) or using other vibrational bands outside the region of the matrix marker bands. Recently, this was demonstrated with a sun screen containing the UV B blocker octocrylene [10], which contains a nitrile group with a vibrational band at $\sim$ 2220 cm^{-1}. Depending on the used formulation, the sun screen distribution within the skin can be quite different (for more details [4,10]).

Conclusions: A method is presented which utilises the intrinsic infrared spectroscopic information of the sample for the biochemical characterisation of a tissue, at a high spatial lateral resolution of $\sim$ 7 micrometer. Examples are described and presented for the utilisation of infrared microscopy and

imaging for the diagnostic of tissue samples. Further potential applications are e.g.: differentiation of normal versus pathological states (e.g. cancer), spatial distribution, adsorption mechanisms and kinetics of external agents in the tissue, development of topically applied drug delivery systems and formulations.

Acknowledgements: The author would like to thank the Studienstiftung des deutschen Volkes (Germany) for supporting this work with a BASF grant and Dr. W. Hübner and Bruker Optics for technical support.

References

[1] E. Atti, S. Gomez, S.M. Wahl, R. Mendelsohn, E. Paschalis and A.L. Boskey, Effect of transforming growth factor-β deficiency on bone development: a Fourier transform infrared imaging analysis, *Bone* **31** (2002), 675–684.
[2] M. Boese, IR Spekroskopie als neues Bildgebungs-Verfahren, *G.I.T. Labor-Fachzeitschrift* **45** (2001), 434–435.
[3] P. Garidel, Mid-FTIR microspectroscopy of stratum corneum single cells and stratum corneum tissue, *Phys. Chem. Chem. Phys.* **4** (2002), 5671–5677.
[4] P. Garidel, Insights in the biochemical composition of skin as investigated by micro infrared spectroscopic imaging, *Phys. Chem. Chem. Phys.* **5** (2003), 2673–2679.
[5] P. Garidel, H.C. Chen, D.J. Moore, E. Paschalis and R. Mendelsohn, Fourier transform infrared microscopic imaging of stratum corneum and its components, *Eur. Biophys. J.* **29** (2000), 363.
[6] P. Garidel, FTIR chemical mapping: a tool for spatially resolved characterization of stratum corneum, in: *The Essential Stratum Corneum*, Chapter. 52, R. Marks, J.L. Levêque and R. Voegli, eds, Martin Dunitz Ltd, 2002, pp. 335–338.
[7] W. Hübner, A. Blume, R. Pushnjakova, Y. Dekhtyar and H.-J. Hein, The influence of X-ray radiation on the mineral/organic matrix interaction of bone tissue: An FTIR microscopic investigation, *Calcif. Tissue* (2003) submitted.
[8] P. Lasch, L. Chiriboga, H. Yee and M. Diem, Infrared spectroscopy of human cells and tissue: detection of disease, *Tech. Cancer Res. Treat.* **1** (2002), 1–7.
[9] E.N. Lewis, P.J. Treado, R.C. Reeder, G.M. Story, A.E. Dowrey, C. Marcott and I.W. Levin, Fourier transform spectroscopic imaging using an infrared focal plane array detector, *Anal. Chem.* **67** (1995), 3377–3381.
[10] R. Mendelsohn, M.E. Rerek and D.J. Moore, Infrared spectroscopy and microscopic imaging of stratum corneum models and skin, *Phys. Chem. Chem. Phys.* **2** (2000), 4651–4657.
[11] L.M. Miller, V. Vairavamurthy, M.R. Chance, R. Mendelsohn, E.P. Paschalis, F. Betts and A.L. Boskey, In situ analysis of mineral and crystallinity in bone using infrared micro-spectroscopy of the ν_4 PO_4^{3-} vibration, *BBA* **1527** (2001), 11–19.
[12] E.P. Paschalis, O. Jacenko, B. Olsen, R. Mendelsohn and A.L. Boskey, Fourier transform infrared microspectroscopic analysis identifies alterations in mineral properties in bones from mice transgenic for type X collagen, *Bone* **19** (1996), 151–156.
[13] R. Salzer, G. Steiner, H.H. Mantsch, J. Mansfield and E.N. Lewis, Infrared and raman imaging of biological and biomimetic samples, *Fresenius J. Anal. Chem.* **366** (2000), 712–726.
[14] J. Schmitt, M. Beekes, A. Brauer, T. Udelhoven, P. Lasch and D. Naumann, Identification of scrapie infection from blood serum by Fourier transform infrared spectroscopy, *Anal. Chem.* **74** (2002), 3865–3868.

Assessment of thermal tests used in laser Doppler measurement of blood perfusion

A. Skora[a], M. Kacprzak[a], J. Obidzinska[b], A. Zbiec[a], W. Staszkiewicz[b] and R. Maniewski[a]
[a]*Institute of Biocybernetics and Biomedical Engineering PAS, Trojdena 4, 02-109 Warsaw, Poland*
Tel.: +48 22 659 91 43; Fax: +48 659 70 30; E-mail: angela@ibib.waw.pl
[b]*Department of Vascular Surgery CPMS, Ceglowska 80, 01-809 Warsaw, Poland*

Introduction: The laser Doppler technique enables non-invasive and continuous monitoring of tissue perfusion in microcirculation. Generally, the perfusion index is given only in relative values. Thus, accurate and reproducible results can be only obtained when using a well controlled provocation test [1,

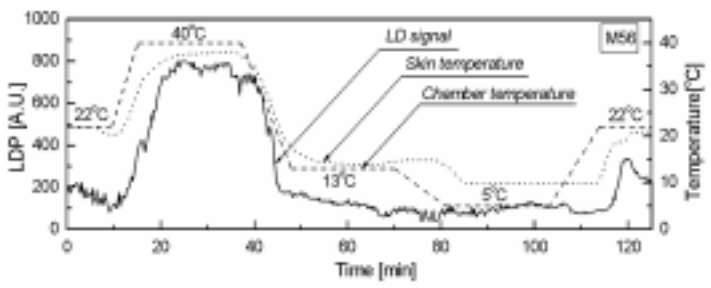

Fig. 1. Blood perfusion and skin temperature changes during the thermal test with air, measured with laser Doppler multichannel system on the second finger of Raynaud's syndrome patient.

Fig. 2. The blood perfusion images of the hand obtained during thermal test with cold water for Raynaud's patient: reference before stimulation (a), reaction caused by stimulation (b).

2]. The aim of this study was evaluation of two types of thermal tests, in which air or water were used. The tests were performed in the temperature range of 5°C to 40°C.

Methods: Two types of thermal tests were prepared. In the first stimulation test, the thermal chamber (Heraeus Instruments, Germany) was used to warm and cool the patient's hand with air. This test consisted of five phases: two resting phases in basal conditions (22 °C), warm phase (40°C) and two cool phases (13°C and 5°C). Each phase lasted about 20 min, and it took about 10 min to change the phase and obtain stable temperature. For the skin microcirculation measurement in this test, the multichannel laser Doppler system (Oxford Array, UK) was used. The second thermal test was performed using cold water. The patient's hand was immersed in 10°C water for 4 min. The skin microcirculation changes were evaluated at temperature of environment (22°C) with the laser Doppler scanner (LDI Moor Instruments, UK), in this case.

In the study, fifteen Raynaud's syndrome patients and ten normal volunteers were examined.

Results: The first thermal test using air was applied to observe of dynamic changes in skin microcirculation on the hands. Clear and quick changes of LD and temperature signal were observed during heating to 40°C. A similar result was obtained during cooling to 13°C. During the 5°C phase an interesting cold-induced vasodilation, called the hunting response or Lewis wave can be often seen in normal volunteers, but is not usually observed in Raynaud's patient [3]. In the resting phase (22 °C) the perfusion and temperature increased quickly in normal volunteers, and the reaction was often delayed in Raynaud's patients. An example of results of the thermal test was presented as laser Doppler and temperature signals in Fig. 1.

Results of microcirculation changes during the thermal test with application of cold water are presented in Fig. 2. A typical vasoconstrictive response was observed after cooling (Fig. 2(b)) compared to the

control image before provocation (Fig. 2(a)). The mean value of LD signal decreased from 41.7 to 9.5 units. As a result of the thermal test, the hyperemic reaction was observed in normal volunteers.

Conclusion: Both during the thermal tests with application of cold water and during the thermal test with air, pronounced changes in skin microperfusion were noted. Application of the multichannel instrument provides visualisation of dynamic changes in the skin microcirculation in selected spots on the body. Laser Doppler Imager provides complete information about the distribution of the microvascular perfusion in the whole of the scanned area, but the measurement time is too long to observe fast changes during the thermal test. Application of both technique and thermal test proposed might give complete information about the microvascular system disfunction in Raynauld's patients.

References

[1] R. Maniewski and A. Liebert, Laser Doppler method for measuring of blood microcirculation (in Polish), EXIT, Warszawa 2003.
[2] R. Maniewski, P. Leger, P. Lewandowski, A. Liebert, P. Bendayan, H. Boccalon, L. Bajorski and K.O. Möller, Spectral analysis of laser Doppler perfusion signal measured during thermal test, *Technology and Health Care* **7** (1999), 163–169.
[3] T. Lewis, Observations upon the reactions of the vessels of the human skin to cold, *Heart* **15** (1930), 177–208.

Individual adaptation of functional electrical stimulation of paraplegics in different cycling tasks

Johann Szecsi[a], Martin Fiegel[a], Philipp Krause[a] and Jochen Quintern[b]
[a]*Department of Neurology, LMU-Munich, Germany*
[b]*Department of Neurology, Bad-Aibling, Germany*
Tel.: +49 89 7095 4829; E-mail: jszecsi@nefo.med.uni-muenchen.de

Introduction

To fully benefit from leg-propelled FES cycling, paraplegic patients must exercise not only with a tricycle at the hospital, but also at home with home-trainers. Thus, there is a need for diverse devices to be adapted to patients with unique features and capabilities. Our goal was to find a convenient method for identifying the best fit between the individual patient and the technically very diverse devices.

Starting from the empirical successful method of "positives torques only" strategy [4], we took the uniform angular speed (smooth pedal stroke) of the crank as an optimality criterion for this fitting.

Methods

A. Experimental Approach

Cycling: Three commercially available tricycles were chosen to cover a broad range of possible geometries. Each tricycle was provided with an 8-bit shaft encoder, driven synchronously by the cranks. To control pedalling speed, a throttle potentiometer adjusted simulation between threshold and maximum. Orthoses held the ankle joint of the patients at 90° and constrained the motion to the sagittal plane. We stimulated the muscle groups quadriceps, gluteus and hamstrings presuming a constant electromechanical delay of 140 ms.

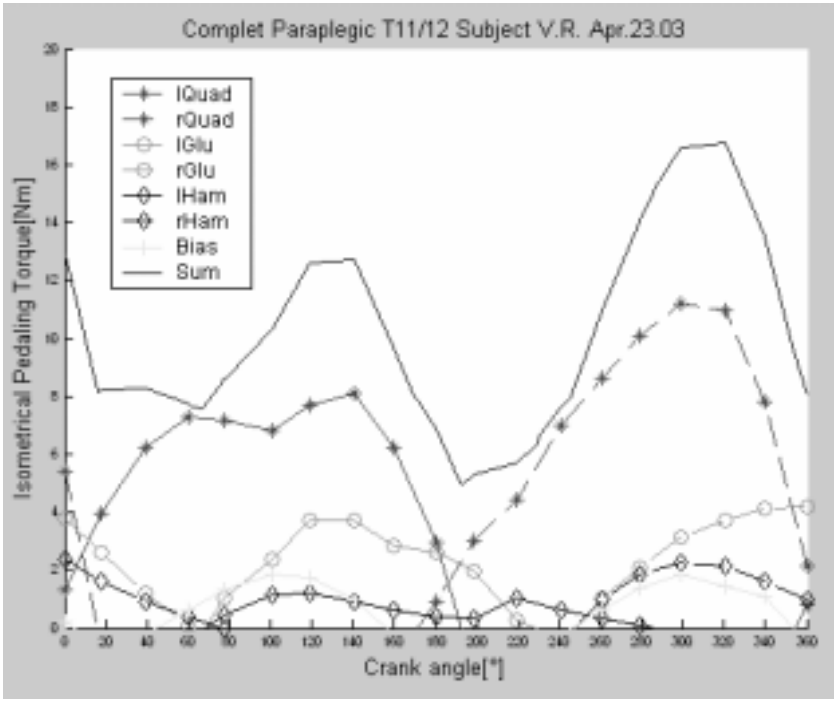

Fig. 1.

Isometric torque measurement: To convert the tricycle into a torque-measuring test bed, the front wheel was removed and the fork of the tricycle was fixed on a stationary frame, bearing a torque-measuring sensor. The torque on the crank was transferred to the sensor via a drive chain.

One full rotation of the crank was divided into 18 equiangular positions. The crank was moved manually by means of a lever into a certain angular position and was locked; then we stimulated all six muscle groups individually and sequentially, the torque responses were recorded, the crank nut was relaxed, and so on. In this way isometric moment/angle characteristics were obtained for each muscle group.

By subtracting the bias in each angle position, the active isometric moment/angle characteristics of every muscle group due to pure stimulation were obtained. The bias itself represents the isometric torque caused by gravitational and joint–elastic effects.

Those muscle groups that "were switched" on according to the Positives Only Strategy together with the sum of these positive isometric torques are depicted in Fig. 1.

A commercially available 8-channel surface stimulator giving pulses up to 500 μs and 99 mA was used in both customer mode (cycling) and remote mode (measuring). The stimulation frequency was 20 Hz.

Setup: Six completely paraplegic subjects with spastic lesions (Th5-Th10), all FES-cycling beginners, volunteered for the measurement and cycling session.

B. Modeling Approach

The model of the rider/tricycle system was devised in the simulation environment of SimMechanics.

Even though the rider/tricycle system was essentially modeled as a planar rigid body consisting of five segments (thigh, shank, crank, arm, and diagonal) and possessing a single degree of freedom (e.g. crank

Table 1
In the case of the one degree of freedom closed loop mechanism model of the rider/cycle system and presuming uniform crank rotation, there exists a linear summation rule of the muscle torques not only in the static case (left side), but as well in the dynamic case (right side)

Static isometric summation	Dynamic isokinetic summation
$M_{\mathrm{Quad}}^{\mathrm{crank}} + M_{\mathrm{Glu}}^{\mathrm{crank}} + M_{\mathrm{Ham}}^{\mathrm{crank}} = M_{\mathrm{total}}^{\mathrm{crank}}$	$c_{\mathrm{Quad}} \cdot M_{\mathrm{Quad}}^{\mathrm{crank}} + c_{\mathrm{Glu}} \cdot M_{\mathrm{Glu}}^{\mathrm{crank}} + c_{\mathrm{Ham}} \cdot M_{\mathrm{Ham}}^{\mathrm{crank}} = 1$

Table 2
Transformation of joint coefficients into muscle coefficients (at crank angular velocity of 40 rpm), considering for sake of simplicity only one side. J_i is the obvious static jacobian transforming the torque in the joint into an endpoint (manipulator) torque, and **r** are moment arms

Quadriceps coefficient	$c_{\mathrm{Quad}} = \frac{c_{\mathrm{Hip}}}{J_{\mathrm{Hip}} + J_{\mathrm{Knee}} \cdot \frac{r_{\mathrm{KneeQ}}}{r_{\mathrm{HipQ}}}} + \frac{c_{\mathrm{Knee}}}{J_{\mathrm{Knee}} + J_{\mathrm{Hip}} \cdot \frac{r_{\mathrm{HipQ}}}{r_{\mathrm{KneeQ}}}}$
Hamstrings coefficient	$c_{\mathrm{Ham}} = \frac{c_{\mathrm{Hip}}}{J_{\mathrm{Hip}} + J_{\mathrm{Knee}} \cdot \frac{r_{\mathrm{KneeH}}}{r_{\mathrm{HipH}}}} + \frac{c_{\mathrm{Knee}}}{J_{\mathrm{Knee}} + J_{\mathrm{Hip}} \cdot \frac{r_{\mathrm{HipH}}}{r_{\mathrm{KneeH}}}}$
Gluteus coefficient	$c_{\mathrm{Glu}} = \frac{c_{\mathrm{Hip}}}{J_{\mathrm{Hip}}}$.

angle) it was necessary to model two sides because of the obvious side difference of isometric torques and anthropomorphic dimensions.

However, in the case of one degree of freedom closed loop linkage with fixed trajectory (particularly with uniform speed), we have a relationship analogous to the obviously isometric summation rule (see Table 1).

M_i^{crank} represents the isometric active torques generated in the crank axis by the quadriceps, gluteal, and hamstring muscles, respectively, and $M_{\mathrm{total}}^{\mathrm{crank}}$ the combined active isometric torque in case of simultaneous action of all muscles together (Fig. 1). The coefficients c_i (muscle coefficients) are functions of the constant angular speed of the crank which arise for the intrinsic muscle properties and of course for all inertial, coriolis-centripetal, elastic, viscous, and frictional effects of rotating parts.

The dynamic isokinetic summation relation can obviously be interpreted as the load profile of the cycle/rider system at a given rotation speed of the crank, because they show the torque requirements the rider must fulfill in order to move the crank uniformly.

Simulations lead directly to the joint cofficients c_{hip} and c_{Knee}, whereas the formulas given in Table 2 transfer this coefficients into the muscle coefficients (taking into view the jacobians [1] and the ratio of moment arms [3]).

The difference between the calculated gravitational torque (under isometric conditions) and the experimentally determined bias torque gives the elastic joint torque $M_{\mathrm{Hip(elast)}}$ [2]. Because our simulations showed that up to 75% of the elastic torque on the crank originates from the hip joint, a scaling factor $1 - c_{\mathrm{Hip}} \cdot M_{\mathrm{Hip(elast)}}$ was introduced for the muscle coefficients.

Because the ratio of 'dynamic' jacobian c_i and 'static' jacobian J_i is constant, the above table shows that all muscles are equally weighted, and the right side equation in Table 1 looks like

$$c \cdot (M_{\mathrm{Quad}}^{\mathrm{crank}} + M_{\mathrm{Glu}}^{\mathrm{crank}} + M_{\mathrm{Ham}}^{\mathrm{crank}}) = 1$$

The interpretation of is the warranted sum of active muscle torques $1/c$ in the case of uniform rotation of the crank.

Results

A. Simulation Results

Experimental and simulation methods were applied to the three tricycles.

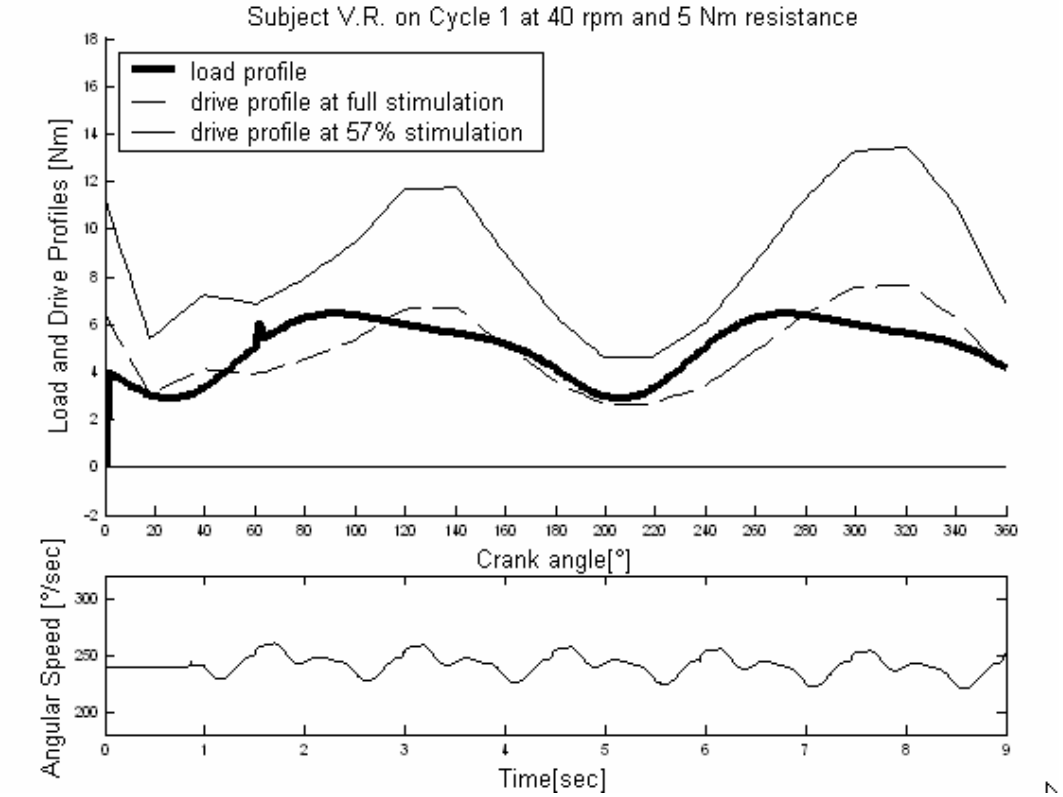

Fig. 2.

The load profiles $1/c$ were compared in the plots (Figs 2 and 3) with the isometric sum of active muscle torques(drive profile). Figure 2, shows for example, that patient VR would drive cycle 1 with the stimulation intensity 57% at a crank rotation speed of 40 rpm (240°/sec) against a rolling drag of 5 Nm (plain floor, no wind). This drive curve balances the load curve. Amplitude deviation and phase shift from the load profile lead to non-uniform pedaling (beating).

Figures 2 and 3 also show the different angular speed courses obtained by simulation, of the same patient riding on two different cycles. With cycle 1 there was a good coincidence between the balancing drive curve (57%) and the required load curve, which results in very smooth pedaling with angular speed deviations of 15ª/sec from the nominal 240°/sec.

A worse "roundness of pedaling" ("smooth pedaling") was observed with cycle 2.

B. Experimental Results

During the 3 months of this first German study, four of our six untrained complete paraplegics repeatedly cycled 500 m at one time, and 1.5–2 km pro cycling session with cycle 2 (on near level ground outdoors).

Our cycling experiments showed that deviations of maximally ($\pm 40°$/sec from the nominal angular speed can be considered smooth pedaling.

All six patients drove cycle 2, three also cycle 1, and one drove all three cycles. In all cycling experiments a smooth movement (video-documented) was observed, and the best results were achieved with cycle 1, as expected.

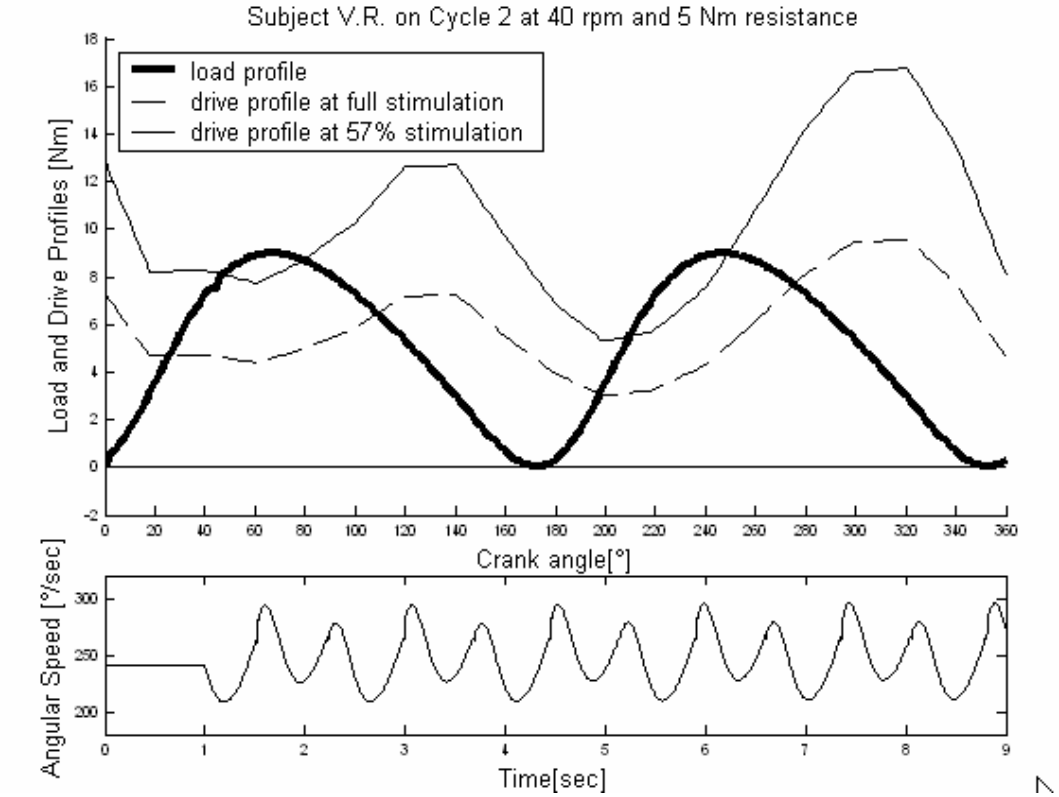

Fig. 3.

Discussion

During dynamic movements with higher angular velocities, the muscle force depends on the shortening velocity and will split the load profile into six muscle-specific profiles. Nevertheless, simulations predict that during 40 rpm angular velocity this splitting will remain less than 10°.

Although this method builds on a physiological (not a black-box) model that informs the physician about the patient's actual condition, it is not over-sophisticated.

References

[1] K. Asada, Robot analysis and control, N.Y. Wiley, 1986 T. Edrich, R. Riener, J. Quintern, Analysis of passive elastic joint moments in paraplegics, *IEEE Transactions on BME* **47**(8) (Aug. 2000).

[2] T. Edrich, R. Riener and J. Quintern, Analysis of passive elastic joint moments in paraplegics, *IEEE Transactions on BME* **47**(8) (Aug. 2000), 1058–1065.

[3] M.G. Hoy, F.E. Zajac and M.E. Gordon, A muscluskeletal model of the human lower extremity: the effect of muscle,tendon, and moment arm on the moment-angle relationship of musculotendon actuators at the hip, knee, and ankle, *J-Biomechanics* (23), (1990), 157–169.

[4] T.A. Perkins, N. Donaldson, N.A.C. Hatcher, I.D. Swain and D.F. Wood, Control of leg-powered paraplegic cycling using stimulation of the lumbo-sacral anterior spinal nerve roots, *IEEE Transactions on Neural Systems and Rehabilitation Engineering* **10**(3) (Sept. 2002), 156–164.

2. Tissue and Cell Engineering

Influence of the proteinase inhibitors Aprotinin® and Marimastat® in tissue engineering of cartilage with fibrin glue

T. Balzer, R. Wittenzellner, S. Milz, B. Ziegelaar, M. Wenzel, A. Naumann and R. Staudenmaier
Klinik und Poliklinik für HNO-Kranke der LMU München, Universitätsklinikum Großhadern, Marchioninistr. 15, 81377 München, Germany
Tel.: +49 89 7095 3898; E-mail: Theda.Happ@gmx.de

Introduction: The aim of cartilage tissue engineering is to produce biological implants from autologous cells in order to avoid foreign body reactions and donor site morbidity during the reconstruction of defects. Due to its moldability, mechanical stability and complete resorption fibrin glue seems to be a promising biomaterial to produce 3-dimensional constructs of cartilage. Our first results with porcine chondrocytes in fibrin glue were very promising for clinical use of the three-dimensional constructs: They showed persistent size, stability and reexpression of cartilage-like collagens over a cultivation period of three months. Three-dimensional constructs of human chondrocytes and fibrin glue however showed a lacking stability in culture: They dissolved already after three weeks in culture without having had the opportunity to reexpress cartilage-like matrix. Therefore, our aim was to examine the cause of the decay in adding different proteinase inhibitors to the media during culture.

Methods: After patient consent the waste product of ten human nasal septa after septoplasty was used to isolate and amplify the chondrocytes. Cytotoxity tests of Aprotinin® as inhibitor of serinproteinases and Marimastat® as inhibitor of metalloproteinases were performed with those ten probes.

After the optimal concentration of the proteinase inhibitors was found, human chondrocytes of another ten nasal septa were isolated and amplified to suspend them in fibrin glue. To construct three-dimensional forms the suspensions were filled in chamberslides. Three-dimensional culture was performed with standard media without added inhibitors (A), standard media with added conservatives to inhibitors but no inhibitors as control (B), Marimastat® (C), Aprotinin® (D) and Marimastat® and Aprotinin® (E). Over a period of six weeks, once a week, not only the volume of the constructs were controlled and manual biomechanical testing done, but also cell viability, histochemical and immunhistochemical stainings were performed.

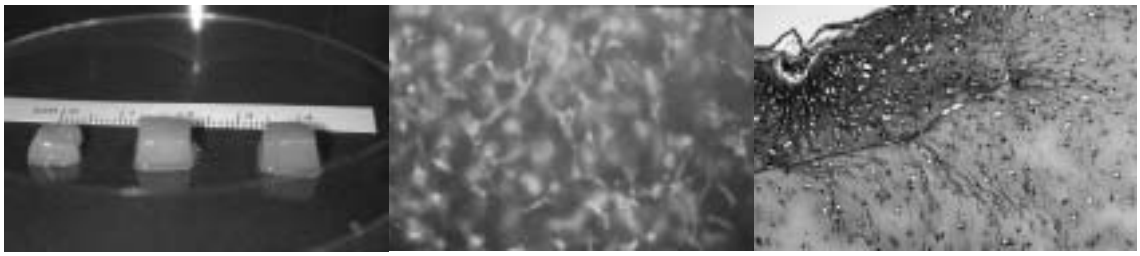

Fig. 1. Three-dimensional constructs of chondrocytes and fibrin glue after six weeks in culture: macroscopical aspect (group C, D, E), cell viability test and histochemistry.

Table 1
Methods and principles of cell selection

Methods for positive cell selection	Methods for negative cell selection
Immunological enrichment	Immunological depletion
Enrichment by cell culture	Depletion by cell culture
Physical enrichment	Physical depletion
	Pharmacological depletion

Results: Optimal concentration was defined as highest concentration of Aprotinin® and Marimastat® with no cytotoxity and was achieved with 1.6 μg Marimastat® / ml media and 4000 KIE Aprotinin® / ml media.

The three-dimensional constructs in standard media (A) and control media (B) showed reproducable dissolvement after three weeks of culture. The constructs with added Marimastat® (C) starting shrinking after two weeks down to a 50% shrinkage and a gelatinous consistence after six weeks. The constructs with added Aprotinin® (D) showed only slight shrinkage of down to 90–95% and a firm consistence within the six weeks of culture. The constructs with added Marimastat® and Aprotinin® (E) expressed only slightly improved stability compared to D with shrinkage of down to 95% and a persistent firm consistence. Cell viability staining showed that the chondrocytes within the fibrin glue were alive during the duration of culture. Histochemical staining showed homogenously distributed cells with chondrocyte-like morphology including chondroms but immunhistochemical staining revealed only little expression of cartilage-specific collagens (chondroitin-6-sulfate) (Fig. 1).

Conclusion: Aprotinin® showed to be a suitable proteinase inhibitor to keep three-dimensional constructs of chondrocytes and fibrin glue stable and in shape. However, to make fibrin glue a suitable biomaterial for the clinical use of tissue engineered three-dimensional cartilage constructs, stimulation of the chondrocytes to redifferenciate and produce cartilage-like matrix within the fibrin glue has to be improved.

Methods of cell selection in haematology and oncology

William H. Krüger
Department of Internal Medicine C – Haematology, Oncology, Transplantation, Ernst-Moritz-Arndt-University, Ferdinand-Sauerbruch-Str., 17487 Greifswald, Germany
Tel.: +49 3834 86 22007; Fax: +49 3834 86 22012; E-mail: william.krueger@uni-greifswald.de

Introduction: The field of cell selection in haematology and oncology has expanded dramatically during the last 15 years. The rationale for cell selection is to enrich or deplete a distinct population of cells either *in vitro* or *in vivo*. Cell selection can be done *in vivo* and *in vitro*. A method for cell selection can be designed as a negative selection as well as a positive selection or as a combined protocol. It must be mentioned that even a conventional chemotherapy or clinical use of antibodies such as anti-thymocyte-globulin may be regarded as a kind of cell selection. However, this article focuses on newer approaches of cell selection in autologous and allogeneic progenitor cell transplantation and for laboratory purposes. An overview is given in Table 1 [1].

Immunological cell selection: Immunological cell selection is in use for clinical graft engineering and for laboratory purposes. In clinical setting the main application is the selection of cells carrying the CD34-antigen [2]. These cells represent the progenitor-compartment of haemopoiesis. Main goal

of this approach in allogeneic stem cell transplantation is the partial or nearly complete depletion of T-lymphocytes to diminish graft-versus-host disease in the HLA-mismatched or haploidentical setting [3]. Another approach is the isolation of progenitor cells for *in vitro* manipulation such as retroviral gene-transfer or gene-marking [4]. Most numerous purpose for $CD34^+$-cell selection in autologous setting was an indirect removal of contaminating tumour cells, however, this indication has been abandoned due to absent or uncertain clinical significance of these contaminants [5,6].

The field of cell therapy after bone marrow transplantation has progressed rapidly. First approaches were donor lymphocyte transfusion for the treatment of relapsed leukaemia [7]. Follow up has shown that long term remissions are realistic after this cell therapy. Infusion of EBV-specific cytotoxic donor lymphocytes (CTL) represents a promising approach for the treatment of EBV-associated lymphoproliferative disease after allogeneic BMT with a chance of curing [2]. Devices for the immunological selection of lymphocyte subpopulations and dendritic cells have become available and are easy to handle. One major application of immunological cell selection in the laboratory is the enrichment of distinct haemopoietic populations or disseminated solid cancer cells for *in vitro* expansion and characterisation [8]. *In vitro* depletion of target cells by immunotoxins was in use during the 90ies for purging of contaminating lymphoma cells from autografts [1,9].

Cell culture: Cell selection by culture methods for enrichment of viable tumour cells was developed by the group of J.G. Sharp. They used different media to enrich tumour cells from lymphoma and solid cancer patients from bone marrow aspirations and autografts [10]. Despite this method is quite successful in lymphomas, there are special problems to be considered particularly when solid cancer cells shall be isolated [11,12]. *In vitro* cell expansion to grow small populations of haemopoietic cells to large-scale grafts was published by some investigators. Haemopoietic stem cells can be cultured in liquid media over several weeks. Requirements are a special media, the supplementation with cytokines such as IL1, IL3, IL6, erythropoietin, and SCF, an incubation temperature of 33 °C, and a so-called feeder layer consisting of stromal cells. Optimal culture conditions lead to a 33 to 115 fold expansion of CD34-positive stem cells and to the expansion of progenitor cell populations with different steps of differentiation. The labour intensity and the success of cytokine-mobilisation of $CD34^+$-cells limited the clinical use of *ex vivo* expanded haemopoietic cells [1].

Pharmacological selection: Depletion of leukaemia or cancer cells from autografts by incubation with cytotoxic agents has been investigated comprehensively by several groups in preclinical as well as in clinical trials. Most investigators used mafosfamide or 4-hydroxycyclophosphamide (4-HC) respectively, or etoposide (VP-16) alone or in combination. Cyclophosphamide is an inactive predrug which needs toxification in the liver *in vivo*. Thus, for *in vitro* purging of tumour cells it is necessary to use the activated metabolites 4-HC or mafosfamide. The incubation of autografts with cytotoxic agents has no selective effect on cancer cells. However, it could be shown that cells of lymphatic and myeloid leukaemias, lymphoma cells, breast cancer, neuroblastoma, and Ewing-sarcoma cells are significantly more susceptible to 4-HC and mafosfamide than haemopoietic stem cells. These differences result from a higher intracellular expression of the detoxificating enzyme aldehyddehydrogenase in the haemopoietic stem cells [13]. Mafosfamide has been used successfully to purge autografts from patients with acute myeloid leukaemias with increased survival rates compared to autotransplantation with non-purged marrow grafts. A major disadvantage of mafosfamide purging is the delayed engraftment with the risk of bleeding and severe infections due to prolonged neutropenia and thrombopenia [14]. A very interesting method of pharmacological *in vivo* negative cell selection is the retroviral transduction of certain cell populations with the thymidine-kinase gene, e.g., for the purpose of adoptive immune therapy after allogeneic bone marrow transplantation. Cells, e.g., lymphocytes, are transduced *in vitro* and infused

to the patient. *In vivo* these genetically modified cells can be eliminated in the case of need by simple treatment with ganciclovir.

Physical selection: Recently, phototoxicity has been used to eliminate tumour cells from autografts or to modulate or treat graft versus host disease after allogeneic BMT. MDR-overexpressing tumour cells were exposed to photosensitisers such as dihaematoporphyrinether or benzoporphorinderivates and eliminated by UV-irradiation from dilutions up to four log steps fold. Phototherapy after sensitising lymphocytes with 8-methoxypsoralen is a very promising approach for prevention and treatment of graft versus host disease [1,2,15].

Future considerations: These developments are facilitated by the commercial availability of selection systems and devices, their diversity, and by the simplicity of performing these methods. Careful methods of immunological cell selection allow recovery of different cell populations without causing damage. Less sophisticated methods such as purging with cytotoxic agents with severe toxic side effects on the desired cell populations have become replaced by newer approaches. The clinical value of new treatment modalities such as antisense-oligonucleotide exposition, ribozyme-cleavage or phototherapy is currently not predictable.

References

[1] W. Krüger, N. Kröger, K. Gutensohn, F. Tögel and A.R. Zander, Cell selection in marrow and stem cell transplantation, *Transfusionsmed* **26** (1999), 130–138.

[2] Hematopoietic Stem Cell Therapy. 1 ed. Philadelphia: Churchill Livingstone, 2000.

[3] Y. Reisner and M.F. Martelli, Transplantation tolerance induced by "mega dose" CD34+ cell transplants, *Exp Hematol* **28**(2) (2000), 119–127.

[4] A.B. Deisseroth, Z. Zu, D. Claxton, E.G. Hanania, S. Fu and D. Ellerson et al., Genetic marking shows that Ph+ cells present in autologous transplants of chronic myelogenous leukemia (CML) contribute to relapse after autologous bone marrow in CML, *Blood* **83**(10) (1994), 3068–3076.

[5] E.A. Stadtmauer, D.E. Tsai, C.J. Sickles, R. Mick, S.M. Luger and D.L. Porter et al., Stem cell transplantation for metastatic breast cancer: analysis of tumor contamination, *Med Oncol* **16**(4) (1999), 279–288.

[6] W.H. Krüger, N. Kröger, F. Tögel, H. Renges, A. Badbaran and R. Hornung et al., Disseminated breast cancer cells prior to and after high-dose therapy, *J Hematother Stem Cell Res* **10**(5) (2001), 681–689.

[7] H.J. Kolb, A. Schattenberg, J.M. Goldman, B. Hertenstein, N. Jacobsen and W. Arcese et al., Graft-versus-leukemia effect of donor lymphocyte transfusions in marrow grafted patients. European Group for Blood and Marrow Transplantation Working Party Chronic Leukemia, *Blood* **86**(5) (1995), 2041–2050.

[8] W. Krüger, C. Datta, A. Badbaran, F. Tögel, K. Gutensohn and I. Carrero et al., Immunomagnetic tumor cell selection-implications for the detection of disseminated cancer cells, *Transfusion* **40**(12) (2000), 1489–1493.

[9] A. Freedman, J.W. Friedberg and J. Gribben, High-dose therapy for follicular lymphoma, *Oncology* (*Huntingt*) **14**(3) (2000), 321–326, 329.

[10] S.S. Joshi, A. Kessinger, S.L. Mann, M. Stevenson, D.D. Weisenburger and W.P. Vaughan et al., Detection of malignant cells in histologically normal bone marrow using culture techniques, *Bone Marrow Transplant* **1**(3) (1987), 303–310.

[11] J.G. Sharp, S.S. Joshi, J.O. Armitage, P. Bierman, P.F. Coccia and D.S. Harrington et al., Significance of detection of occult non-Hodgkin's lymphoma in histologically uninvolved bone marrow by a culture technique, *Blood* **79**(4) (1992), 1074–1080.

[12] W. Krüger, A. Lange, A. Badbaran, K. Gutensohn, N. Kröger and A. Zander, Detection of disseminated epithelial cancer cells by liquid culture–factors interfering with the standardization of assays, *Cytotherapy* **5**(3) (2003), 252–258.

[13] D. Meier-Tackmann, D.P. Agarwal, W. Krueger, C. Dereskewitz, H.T. Hassan and A.R. Zander, Changes in aldehyde dehydrogenase isozymes expression in long-term cultures of human hematopoietic progenitor cells, *Adv Exp Med Biol* **414** (1997), 47–57.

[14] N.C. Gorin, M. Labopin, L. Fouillard, G. Meloni, F. Frassoni and A. Iriondo et al., Retrospective evaluation of autologous bone marrow transplantation vs allogeneic bone marrow transplantation from an HLA identical related donor in acute myelocytic leukemia. A study of the European Cooperative Group for Blood and Marrow Transplantation (EBMT), *Bone Marrow Transplant* **18**(1) (1996), 111–117.

[15] F. Sieber, Phototherapy, photochemotherapy, and bone marrow transplantation, *J Hematother* **2**(1) (1993), 43–62.

Tissue Engineering of the Skin

Effects of gender and age on vibrational resolution of the skin

S. Mounier
Institute for Applied Computer Science, Forschungszentrum Karlsruhe, Germany
Tel.: +49 7247 82 5757; Fax: +49 7247 82 5786; E-mail mounier@iai.fzk.de

Introduction: Force feedback systems are typically used in teleoperation and virtual reality systems and integrated into joysticks or data-gloves [1,2]. Whereas commercially available myoelectric hand prostheses do not have a force feedback system. Some of them have a closed-loop force feedback that acts like a reflex [4] but no one has an external force feedback to the user. Without a force feedback system the user has to control the grasping by vision [3]. Thus the benefit of a hand prosthesis can be improved [5]. A force feedback system translates a sensed pressure force from a prosthesis contacting an object or surface into a sensory feedback to the user. Vibrotactile actuators are compact, cheap and can be easily integrated in the socket.

The knowledge of the vibrational resolution of the skin is essential to implement a future appropriate vibrotactile force feedback in a prosthetic hand. While most studies cover the vibratory perception threshold using non-portable actuators, little data is available on the perception of frequency changes using portable actuators. The vibration sensitivity of the skin depends on the frequency, the contact surface, and the actuator configuration [6]. The aim of this study is to determine if the frequency discrimination varies with age and gender for a specific actuator with the potential to be integrated in the prosthesis.

Methods: The subjects were 30 right-handed healthy persons ranging in age from 23 to 35 and from 44 to 60, classified into four groups: younger men, elderly men, younger women, and elderly women. According to its operating voltage, a pager motor was able to generate sinusoidal vibrations in a frequency range between 60 and 320 Hz. These vibrations were delivered to the volar skin surface of the forearm. The contact surface is about 1.7 cm^2. The frequency discrimination is determined by the correct recognition of ascending and descending frequency steps. The mean of the minimum frequency discriminations of three series constituted the vibrotactile sensitivity.

Results: The correct recognition rate for the younger men is about 61%, for the elderly men about 64%, for the younger women about 66% and for the elderly women about 44%.

The Weber ratio of the vibrational resolution of the skin for each group is a descending curve (see Fig. 1). For ascending frequency steps, above 100 Hz the younger women are more sensitive than the elderly women and for men that is above 210 Hz. For descending steps there is no significant difference between the male groups whereas the elderly women are more sensitive than the younger women. A reason of the difference between the elderly women and the three other groups can be occurred by the low correct recognition rate of elderly women.

Discussion: The study confirms the occurrence of maximum sensitivity above 250 Hz reported in the literature [6]. However, the frequency discrimination appears not to vary significantly with age and gender. In the future this vibration sensitivity will be measured and compared with patients.

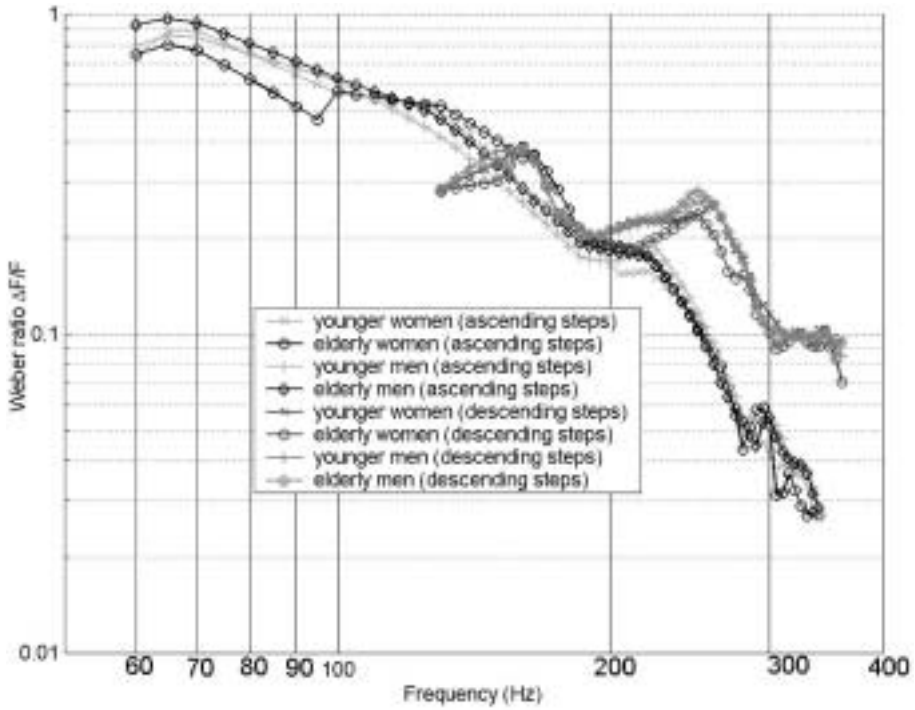

Fig. 1. Frequency discrimination of the skin.

References

[1] M. Bouzit, *Conception et mise en oeuvre d'un gant de données à retour d'effort pour la télémanipulation d'objets virtuels et réels*, PhD thesis, Université Pierre et Marie Curie, Paris, France.
[2] G.C. Burdea, *Force and Touch Feedback for Virtual Reality*, John Wiley and Sons, Inc., ISBN:0-471-02141-5, 1996.
[3] P.E. Patterson and J.A. Katz, Design and evaluation of sensory feedback system that provides grasping pressure in a myoelectric hand, *Journal of Rehabilitation Research and Development* **29**(1) (1992), 1–8.
[4] G. Puchhammer, *The tactile slip sensor: Integration of a miniaturized sensory device on an myoelectric hand.* In Orthopädie-Technik Quarterly, English, edition I/2000.
[5] R.N. Scott, *Feedback in myoelectric prostheses*, Clinical Orthopaedics and Related research, Philadelphia, 1990, pp. 58–63.
[6] R.T. Verrillo, Psychophysics of vibrotactile stimulation, *The journal of the Acoustical Society of America* **77**(1) (1985), 225–232.

Modification of polymeric surfaces for optimal growth of cells

K. Rieß[a], P. Wünsche[a], S. Kutschke[b], R. Poll[b] and P. Bloss[a]
[a]*Kunststoff-Zentrum in Leipzig, Erich-Zeigner-Allee 44, D-04229 Leipzig, Germany*
Tel.: +49 3414941 810; Fax: +49 3414941 555; E-mail: riess@kuz-leipzig.de
[b]*Technical University Dresden, IBMT, G.-Schumann-Str. 11, 01062 Dresden, Germany*

Introduction

To cultivate cells in bioreactors, optimal growing conditions are necessary. The properties of the cell culture medium, for example its temperature and partial pressures of oxygen and carbon dioxide, and

Table 1
Results of XPS-analysis

Sample		C	O
Material	Surface treatment	[Atomic-%]	[Atomic-%]
Nunclon^{TM}	with	95.9	4.1
Nunclon^{TM}	without	87.5	12.5
PS (BASF)	with corona treatment	94.3	5.7
PS (BASF)	without corona treatment	85.2	14.8

the surface properties of the breeding ground are important environmental conditions for optimal growth of adherend cells. The bioreactor has to achieve these conditions, and therefore, it should consist of modular components for an optimal growth of different kind of cells. We need exchangeable breeding ground, e.g. The use of polymers plays an increasing roll for the economical ex vivo cultivation of cells. The properties of polymer bulk materials are expedient concerning mouldability or stiffness, for example. Additionally, the surface properties of polymers can be adapted to optimal cell growth. This includes wettability and texture [1,2].

Materials and methods

We have used polystyrene (PS, BASF AG), a cyclic olefin copolymer (Topas^{TM}, Ticona GmbH) and two different types of polyurethane (PUR, Sonderhoff GmbH, Rühl AG & Co) as bulk materials of the breeding ground of our bioreactor. These materials allow sufficient mechanical stiffness, excellent optical transparency and easy manufacture of the bioreactor. The used adherend cells are murine fibroblasts and human endothel cells. We applied these cells to test the influence of modified polymer surfaces on there growth. To change the surface properties from hydrophobicity to hydrophilicity we treated the surface by corona discharge, an atmospheric plasma. The modified surface properties were analyzed by XPS, by contact angle measurement and by microscopic verification of the cell growth. The growth experiments are carried out in self-constructed modular perfusion culture chambers with exchangeable breeding grounds. We used cell culture polystyrol (Nunclon^{TM}, Nunc GmbH & Co. KG) as reference.

Results

1. XPS-Analysis: The treatment by corona discharge increases the oxygen concentration in the PS surface by about 3 times. The oxygen concentration of the corona treated PS is comparable with this one of the optimised Nunclon^{TM} surface (Table 1). We assume, the cell growth improves by increasing oxygen concentration in the surface of the breeding ground.

2. Storage after corona treatment: The cell growth depends also on storage conditions after surface treatment. In Figs 1 and 2, the contact angle of water of the surface-treated polymers stored in standard atmosphere (22°C, 50% relative humidity) and in de-ionised water as a function of the storage time in these media is shown.

The plateau value of the fitted curves in case of storage in standard atmosphere will be achieved with a time constant of about 4 days (Fig. 1). On the contrary, the contact angle changes more complex during the storage in water. These curves can be described mathematically by an exponential approximation to a linear decay followed by a plateau after about 14 days (Fig. 2).

We performed the determination of the surface tension at the initial state and at the final state after 23 days storage. The results show an increase of the polar part of the surface tension at PS and COC in the final state relative to the start values. The results of the PUR-systems show a high polar part of the

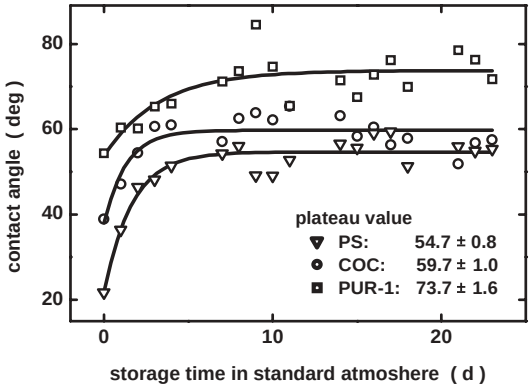

Fig. 1. Contact angle of PS, COC, PUR-1 stored in standard atmosphere.

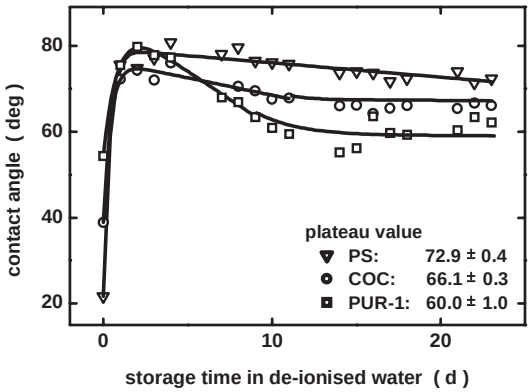

Fig. 2. contact angle of PS, COC, PUR-1 stored in de-ionised water.

surface tension in the initial material and a decrease of the polar part by corona treatment and storage. Compared to NunclonTM, the corona treatment generates higher polar parts of the surface tension at all used polymers.

3. Cell growth after corona treatment: We have found that the cell growth was positively affected by corona treatment. Additionally, the storage medium has a strong influence on the cell growth too. A stronger cell growth was observed on breeding grounds stored in de-ionised water compared to storage in the standard atmosphere. The growth of murine fibroblasts was accelerated on PS and COC. On PUR it was only a weak growth. For the growth of murine fibroblasts, COC has proven as the best material of the examined polymers used as breeding ground, whereas the PUR-systems were particularly favorable for the growth of endothel cells.

Summary

The investigations presented here show that for sufficient cell growth, additionally to the selection of the optimal bulk material, the material itself and its surface modification are crucial. We have shown that corona treatment of polymer surfaces is successful to achieve sufficient growth of different kinds of cells. An optimal breeding ground was found for the cultivation of murine fibroblasts and endothel cells. A high polarity of the polymer surface was favourable in the case of PS and COC, whereas for the PUR systems it has harmful effect.

Acknowledgement: We thank the BMBF for the financial support (project number 03/4010F).

References

[1] H.B. Lee, J.W. Park and H.B. Lee, Cell adhesion and growth on polymer surfaces with hydroxyl groups repared by water vapour plasma treatment, *Biomaterials* **12** (July 1991), 443–448.
[2] A. Welle, E. Gottwald and K.F. Weibezahn, Patterned polymer surfaces for cell culture applications, *Biomed Tech* (*Berl*) **47**(Suppl 1) (2002), Pt 1:401–403.

Methods of Cell Selection in Haematology and Oncology

Cell selection for gene therapy

M.S. Staege
Children's Cancer Research Center, Martin-Luther-University Halle-Wittenberg, Germany
Tel.: +49 345 5522947; Fax: +49 345 5522945; E-mail: martin.staege@medizin.uni-halle.de

Introduction: Introduction of transgenes into a variety of cell types has been used for experimental treatment of several diseases. Technical improvements have resulted in gene transfer efficacies that allow large scale transfer of transgenic cells in clinical studies. However, serious adverse side effects of transgenic cells have been described, indicating that the safety of methods for gene transfer and cell selection is still dissatisfying. The most important technique for selection of the relevant target cell is immunomagnetic bead selection. The same technique can be used for the selection of successfully transfected cells.

Genetically modified haematopoietic stem cells (*HSC*)*:* HSC are nearly ideal targets for gene therapy [14]. For a limited number of monogenic diseases, the successful correction of the underlying gene defect by *ex vivo* gene transfer into HSC was demonstrated and techniques for selection of HSC by immunomagnetic beads are routine in clinical practice. However, some major problems have been observed [1]. Stable expression of transgenes usually requires stable integration into the genome and the risk of insertional mutagenesis is evident. Oncogene activation by insertional mutagenesis has been observed in mice and humans, underscoring the necessity for vector optimization. *In vitro* manipulation and expansion of HSC before and after gene transfer is another critical point. Loss of pluripotency as well as malignant transformation has been observed after *in vitro* manipulation of HSC. In order to minimize these cell culture effects, high-efficacy gene transfer methods into non-dividing HSC are required.

Genetically modified antigen presenting cells and tumor cells: Presentation of tumor derived antigens by professional antigen presenting cells (APC), e.g. dendritic cells (DCs), has been used for the induction of tumor specific immune responses [4]. DCs can be generated from different sources after selection of precursor cells by plastic adherence or immunomagnetic beads [7]. With regard to GMP requirements, immunomagnetic bead techniques have the advantage of easier standardization and the general acceptance of these techniques in clinical practice. Tumor cell lysates and defined peptides can be used for the exogenous loading of HLA molecules on APC. Alternatively, tumor antigens can be expressed as transgenes in APC [5]. It was shown that the maturation status of DCs is a critical point for the decision between stimulation and tolerance induction [6]. One possibly important advantage of

transgenic APC is that the expression of the transgene can be restricted to mature DCs by the use of promotors that are only active in mature DCs [9].

Transgenic tumor cells expressing a range of different cytokines or co-stimulatory molecules have been used for induction of tumor specific T cells. Especially allogeneic tumor cells might be an alternative to professional APC in cases where no specific tumor antigens have been identified and where autologous tumor material could not be obtained in sufficient amounts for the pulsing of professional APC. However, unregulated transgene expression of normally highly regulated genes with immunomodulatory functions may cause unwanted side effects. It was demonstrated that prolonged administration of interleukin-2 cause depletion of tumor reactive T cells with subsequent loss of tumor protection in a mouse model [11]. In another example the unregulated expression of CD40 ligand results in defective T cell development in a mouse model for gene therapy of X-linked hyper IgM syndrome [2]. The optimization of vectors with large packaging capacities might allow the transfer of a transgene in combination with its natural regulatory elements [3]. At least for corrective gene therapy this should be desirable.

Genetically modified T cells: In addition to the low expression of co-stimulatory molecules on tumor cells, defects in antigen processing and presentation by tumor cells have been observed [12]. Genetically engineered T cells with chimeric receptors recognizing determinants on the surface of tumor cells without MHC-restriction are a highly elegant approach for circumventing these problems [8].

The main application for transgenic T cells, however, is the transfer of suicide genes into allogeneic T cells for control of graft versus host diseases (GvHD) [13]. In addition to high transfection efficacies, efficient selection and/or expansion of transfected cells are required. For this selection process antibiotics selection as well as selection on the basis of immunomagnetic beads has been employed. In addition to the advantage of easier standardization, the use of immunomagnetic beads avoid several problems occurring during antibiotics selection (long *ex vivo* cell culture, unspecific toxicity, immunogenicity of the marker transgene, and loss of antigen reactivity of selected T cells) [10].

Conclusions: Genetic engineering of cells opens several new perspectives for the treatment of hematological diseases and cancer. However, selection of the target cell as well as selection of the engineered cell is of utmost importance. In addition, experimental evidence clearly indicates that cells with highest and stable transgene expression are not necessarily the "optimal" cells, especially for immunogene therapeutic approaches.

References

[1] C. Baum, J. Düllmann, Z. Li, B. Fehse, J. Meyer, D.A. Williams and C. von Kalle, Side effects of retroviral gene transfer into hematopoietic stem cells, *Blood* **15** (2003), 2099–2114.

[2] M.P. Brown, D.J. Topham, M.Y. Sangster, J. Zhao, K.J. Flynn, S.L. Surman, D.L. Woodland, P.C. Doherty, A.G. Farr, P.K. Pattengale and M.K. Brenner, Thymic lymphoproliferative disease after successful correction of CD40 ligand deficiency by gene transfer in mice, *Nat Med* **4** (1998), 1253–1260.

[3] E.M. Borst and M. Messerle, Construction of a cytomegalovirus-based amplicon: a vector with a unique transfer capacity, *Hum Gene Ther* **14** (2003), 959–970.

[4] E.G. Engleman, Dendritic cell-based cancer immunotherapy, *Semin Oncol* **30** (2003), 23–29.

[5] J. Humrich and L. Jenne, Viral vectors for dendritic cell-based immunotherapy, *Curr Top Microbiol Immunol* **276** (2003), 241–259.

[6] K. Mahnke, E. Schmitt, L. Bonifaz, A.H. Enk and H. Jonuleit, Immature, but not inactive: the tolerogenic function of immature dendritic cells, *Immunol Cell Biol* **80** (2002), 477–483.

[7] F. Meyer-Wentrup and S. Burdach, Efficacy of dendritic cell generation for clinical use: recovery and purity of monocytes and mature dendritic cells after immunomagnetic sorting or adherence selection of CD14+ starting populations, *J Hematother Stem Cell Res* **12** (2003), 289–299.

[8] C. Rössig, C.M. Bollard, J.G. Nuchtern, C.M. Rooney and M.K. Brenner, Epstein-Barr virus-specific human T lymphocytes expressing antitumor chimeric T-cell receptors: potential for improved immunotherapy, *Blood* **99** (2002), 2009–2016.
[9] R. Ross, S. Sudowe, L. Beisner, X.L. Ross, I. Ludwig-Portugall, J. Steitz, T. Tuting, J. Knop and A.B. Reske-Kunz, Transcriptional targeting of dendritic cells for gene therapy using the promoter of the cytoskeletal protein fascin, *Gene Ther* **10** (2003), 1035–1040.
[10] D. Sauce, M. Bodinier, M. Garin, B. Petracca, N. Tonnelier, A. Duperrier, J.V. Melo, J.F. Apperley, C. Ferrand, P. Herve, F. Lang, P. Tiberghien and E. Robinet, Retrovirus-mediated gene transfer in primary T lymphocytes impairs their anti-Epstein-Barr virus potential through both culture-dependent and selection process-dependent mechanisms, *Blood* **99** (2002), 1165–1173.
[11] P. Shrikant and M.F. Mescher, Opposing effects of IL-2 in tumor immunotherapy: promoting CD8 T cell growth and inducing apoptosis, *J Immunol* **169** (2002), 1753–1759.
[12] M.S. Staege, S.P. Lee, T. Frisan, J. Mautner, S. Scholz, A. Pajic, A.B. Rickinson, M.G. Masucci, A. Polack and G.W. Bornkamm, MYC overexpression imposes a nonimmunogenic phenotype on Epstein-Barr virus-infected B cells, *Proc Natl Acad Sci USA* **99** (2002), 4550–4555.
[13] P. Tiberghien, Use of suicide gene-expressing donor T-cells to control alloreactivity after haematopoietic stem cell transplantation, *J Intern Med* **249** (2001), 369–377.
[14] J.L. Vollweiler, S.P. Zielske, J.S. Reese and S.L. Gerson, Hematopoietic stem cell gene therapy: progress toward therapeutic targets, *Bone Marrow Transplant* **32** (2003), 1–7.

Cell-Engineering and Stem Cells

BMP-2 promotes chondrogenic and adipogenic differentiation of ES cells

N.I. zur Nieden, G. Kempka and H.J. Ahr
Research Toxicology, Bayer AG, D-42096 Wuppertal, Germany
Tel.: +49 1 403 220 8684; Fax: +49 1 403 220 0834; E-mail: nicole.zur.nieden@gmx.net

Introduction: Embryonic stem cells are pluripotent continuously growing cells isolated from the inner cell mass of the mouse blastocyst and can be maintained in permanent culture [1]. Their characteristic features include an unlimited self-renewing capacity and the expression of the pluripotency markers alkaline phosphatase and the germline-specific transcription factor Oct-4. The proliferation of ES cells is controlled by cytokines of the Interleukin-6 superfamily. Under the influence of Leukemia Inhibitory Factor (LIF), a pleiotropic hormone of the IL-6 class, ES cells can be maintained *in vitro* in an undifferentiated state without loosing their pluripotent characteristics [2]. Upon the withdrawal of LIF, a fascinating step in their development occurs, in which the cells combine to form so-called embryoid bodies (EBs). Inside the EBs the cells differentiate spontaneously into cell types of all three germ layers. The yield of differentiation into an intended lineage can be greatly enhanced by the addition of growth factors or induction substances. For instance, it has been shown that retinoic acid induces neural differentiation [3], vitamin D3 forces ES cells to undergo osteogenesis [4] and BMP-2 pushes ES cells to the chondrogenic fate [5]. This study shows that ES cells were induced to differentiate *in vitro* into chondrocytes and adipocytes under the influence of Bone Morphogenetic Protein-2 (BMP-2). We also show that transforming growth factor-beta1, ascorbic acid and insulin further enhance differentiation.

Methods: Cells of the mouse ES cell line D3 were kept in permanent culture under the influence of LIF and differentiated via hanging drops as described [4,6]. Various combinations of medium additives were examined for their capability to enhance chondrogenic differentiation (Tbl.1). Applied concentrations were 10 ng/ml BMP-2, 2 ng/ml TGF-beta1, 50 μg/ml ascorbic acid and 1 μg/ml insulin. For quantitative

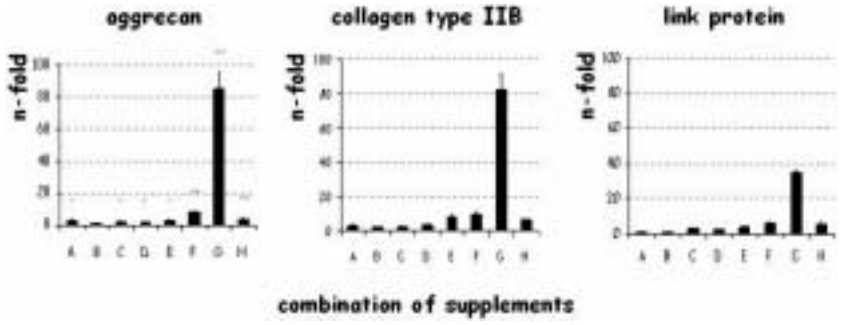

Fig. 1.

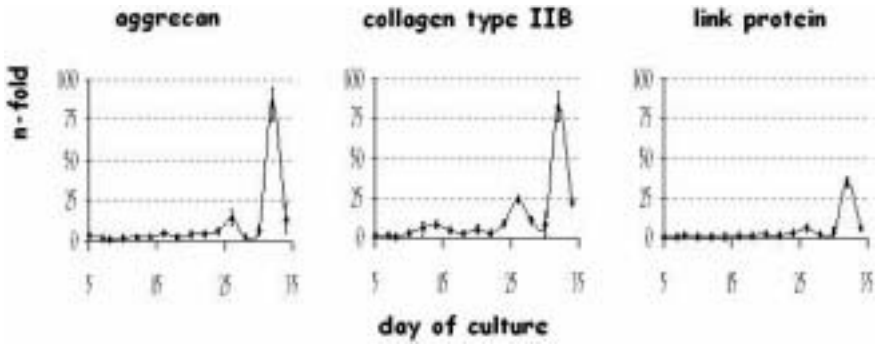

Fig. 2.

Fig. 3.

PCR total RNA was isolated from 20 EBs per probe as described [6]. Primer sequences can be provided. Target gene C_T-values were standardized against GAPDH expression and induction of expression in treated EBs was normalized to control EBs.

Results: Expression of genes associated with cartilage tissue such as collagen type II (COL II), aggrecan and link protein were examined by means of real-time quantitative PCR in EBs. Expression of COLII isoform B, the isoform specific for mature cartilage, and aggrecan was increased more than 80 fold above control values when cultures were supplemented with BMP-2 and TGF on days 3-5 and BMP-2, ascorbic acid and insulin from day 5 onwards as compared to 2.5 fold when treated with BMP-2 alone (Fig. 1). Those cartilage markers were highly expressed as early as day 25–28 of embryonic stem cell culture (Fig. 2). Starting with the fourth week of culture aggregates formed in the supplemented

cultures, consisting of small round cells, which stained positiv with alcian blue. This dye specifically stains proteoglycans that are expressed in cartilage tissue. Significant immunostaining for the COL II protein was observed at day 30 in treated cultures corresponding to the active secretion and formation of an extracellular matrix found with chondrocytes. The COL II antibody identified the fibrillary organization of the collagen molecules in the extracellular matrix. Chondrogenic differentiation was confirmed by positive immunostaining for adult proteoglycans. The signalling pattern shows a similar with the extracellular matrix associated distribution as was found with the COL II antibody. Staining appeared to be diffuse as the extracellular matrix is stained not single cells. Oil-Red-O staining showed the presence of adipocytes in the same cultures. The adipocyte specific transcription factor PPAR gamma was already expressed at day 12 and preceeded the expression of markers for mature adipocytes such as SCD and GLUT4 (Fig. 3).

Conclusion: All examined genes associated with chondrogenesis and adipogenesis, respectively, were expressed in a time-dependent pattern *in vitro* corresponding to the *in vivo* development of the embryo. These facts allow for the usage of this *in vitro* system for the study of mechanisms involved in BMP-2 induced chondrogenesis and adipogenesis.

References

[1] M.J. Evans and M.H. Kaufman, Establishment in culture of pluripotent cells from mouse embryos, *Nature* **292** (1981), 154–156.
[2] R.L. Williams, D.J. Hilton, S. Pease, T.A. Willson, C.L. Stewart, D.P. Gearing, E.F. Wagner, D. Metcalf, N.A. Nicola and N.M. Gough, Myeloid leukemia inhibitory factor maintains the developmental potential of embryonic stem cells, *Nature* **336** (1988), 684–686.
[3] G. Bain, D. Kitchens, M. Yao, J.E. Huettner and D.I. Gottlieb, Embryonic stem cells express neuronal properties *in vitro*, *Dev Biol* **168** (1995), 342–357.
[4] N.I. zur Nieden, G. Kempka and H.J. Ahr, *In vitro* differentiation of embryonic stem cells into mineralized osteoblasts, *Differentiation* **71** (2003), 18–27.
[5] J. Kramer, C. Hegert, K. Guan, A.M. Wobus, P.K. Müller and J. Rohwedel, Embryonic stem cell-derived chondrogenic differentiation *in vitro*: activation by BMP-2 and BMP-4, *Mechanisms of Development* **92** (2000), 193–205.
[6] N.I. zur Nieden, G. Kempka and H.J. Ahr, Molecular multiple endpoint embryonic stem cell test – a possible approach to test for the teratogenic potential of compounds, *Toxicol and Appl Pharm* (2003), accepted.

3. Analysis, Modelling and Prototyping

Mathematical modeling and computer imaging of non-linear phenomena in biomedical systems and signals

N.K. Bystrova[b], V.S. Bystrov[a] and M.M. Marinina[b]
[a]*Institute of Mathematical Problems of Biology RAS, Pushchino, Russia*
E-mail: bystrov@impb.psn.ru
[b]*Institute of Theoretical and Experimental Biophysics RAS, Pushchino, Russia*
E-mail: nkbys@mail.ru

Introduction: All vital processes of alive systems have nonlinear character. Thus the features of processes in each concrete case can have diagnostic and prognostic value. However it is necessary to be able to

allocate most necessary and informative parameters from the set of all attributes describing nonlinear dynamics of organisms or researched living system. One of the ways of the investigation of such dynamics is the study of various transients. For example, the study of individual features of the cardiovascular system (CVS) can be carried out by the heart rate (HR) variability registering (pulsogram) in the transients under various functional tests.

Methods: The test is applied to active orthoclinostatic tests (AOCT). Though this method is already pleased developed, not all parameters describing these transients are investigated enough. The change of CVS functional state is especially precise reflected in the transitive region of pulsogram. It is shown, that the type of transient of HR reaction at AOCT reflects peculiarities of a functional condition of an organism [1,2]. For example, the change of the volunteer functional status finds reflection in change of HR reaction at AOCT, especially in a phase of transition. Referring to Fig. 1 it will be presented three pulsograms of the same volunteer, which were registered at noted days with change of blood pressure (BP) registration too.

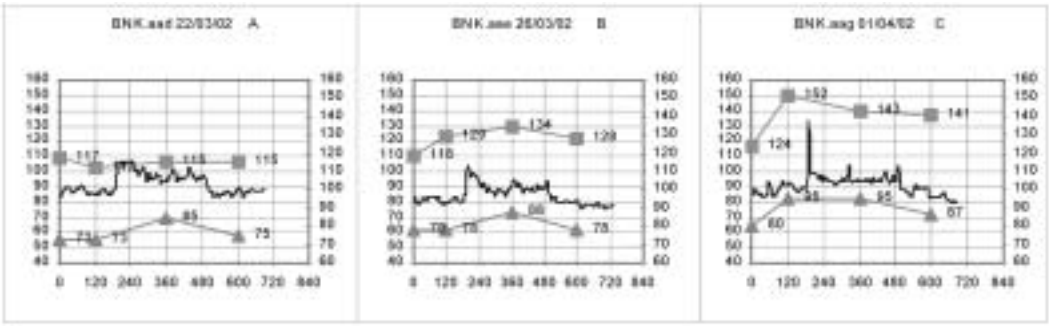

Fig. 1. Influence of the varied functional state on the pulsogram type at AOCT. (The upper line-systolic BP, the lower line-diastolic BP).

Models: Transition processes in non-linear systems maybe described by the second-order non-linear differential equation [3] of the following type with nonlinear term of power $N (N = 2, 3)$:

$$\frac{d^2Y}{dt^2} + p_0\frac{dY}{dt} \pm (p_1Y - Y^N + p_2) = 0, \tag{1}$$

where $Y = Y(t)$ is studied function of the transition process and p_0, p_i are the system's dimensionless parameters. The system have a transition from one state $Y_1 = Y(0)$ into second state $Y_2 = Y(t \to \infty)$ and under these conditions the solution $Y(t)$ of the Eq. (1) is the curve shape of transients, which includes the external actions in parameter p_2 (external fields, e.g. electric field). The parameter p_0 describe the damping processes and the velocity of kink (soliton) propagation. The different relations between parameters p_0, p_i the solution of Eq. (1) $Y(t)$ would have very various type of their curve shape. Perhaps as oscillation mode, as kink mode, as attenuation or decaying mode. In general case the integration of (1) is possible only numerically and for this purpose (1) was presented in the form of two first-order equations system, which were studied numerically using own program TRAX presenting the solution in the graphical imaging form.

Results: The proposed and analyzed nonlinear differential equation correspond the stationary solution (first integral) of the modified Korteweg-de Vriez – Burgers equation ($N = 3$) for nonlinear stationary waves in the dissipative media and Landau-Khalatnikov transient equation for second order ferroelectric-like phase transition between two states [3]. We obtain the following criteria for main 2 types of AOCT signal shapes (Fig. 2), available for further analysis.

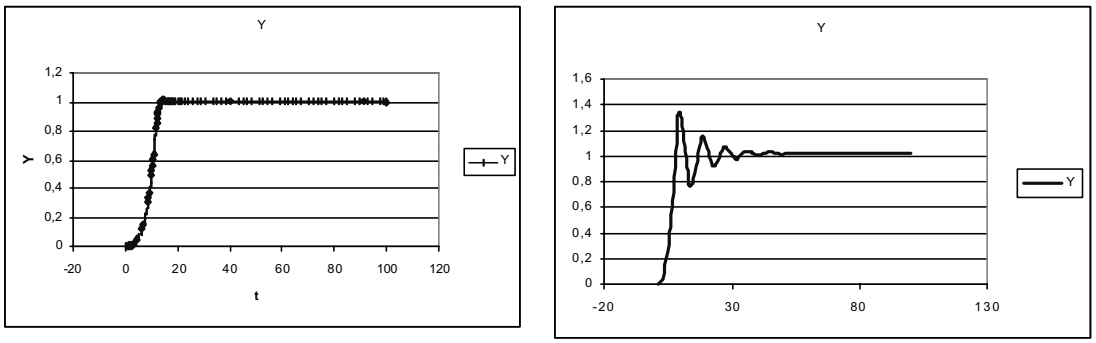

a) $p_0^2 > 4p_1$ - without peak *Kink-like* type b) $p_0^2 < 4p_1$ type with peak and oscillations decay

Fig. 2. Criteria for two types of HR signal shapes (if external action – field – is absent, parameter $p_2 = 0$): a) kink-, b) soliton-like.

References

[1] N.K. Bystrova, M.V. Marinina, E.V. Sadyrina, M.V. Sivashev, Pulsometry of transition process under active orthoclynostatic test, *J. Arrhythmology* **27** (2002), 18–20.
[2] N. Bystrova, M. Marinina and M. Sivashev, Heart Rate Telemetry Registration under Various Functional Tests, in: *Sci. Proc. RTU*, Ser. 6, Is. 9, RTU: Riga, 2002, pp. 90–93.
[3] V. Bystrov, T. Tazieva, A. Sapronova and N. Bystrova, Non-linear dynamical models of transitional processes in the biological and ferroelectric-like systems, ibid, pp. 155–158.

Rapid prototyping of porous hydroxyapatite for the application as bone substitute material

U. Deisinger[a], F. Stenzel[b], J. Lehmann[c] and G. Ziegler[a,b,c]
[a]*Friedrich-Baur-Research Institute for Biomaterials, University of Bayreuth, 95440 Bayreuth, Germany*
E-mail: ulrike.deisinger@fbi-biomaterialien.de
[b]*BioCer EntwicklungsGmbH, Bayreuth, Germany*
[c]*Institute for Materials Research, University of Bayreuth, 95440 Bayreuth, Germany*

Introduction: There is an increasing demand of bone graft material in clinical applications. Besides the use of autogene bone (own bone from the iliac crest e.g.), allografts or xenografts (bone from humans or animals) the tissue engineering of bone is a great challenge. Therefore, calcium-phosphate scaffolds have often been used [1–3] because hydroxyapatite ceramic is biocompatible and the inorganic part of bone consists of a mineralogically similar phase.

In this work porous scaffolds of hydroxyapatite ceramic were produced via two different rapid prototyping techniques. Hereby, the porosity was tailored, so that the resulting bone substitute material is adapted to the requirements of the implantation site. As rapid prototyping techniques a direct and an indirect processing route were investigated.

Materials and methods: For the direct rapid prototyping technique commercially available raw powder was processed to flowable granules suitable for the 3D-printing process, where an appropriate binder is printed layer by layer onto a ceramic powder bed. Therefore, a slurry containing raw powder and different organic additives wasas spray-dried. The resulting granules were characterized via scanning

electron microscopy (SEM) and tested in the 3D-printing process. The green samples were sintered at 1250 ªC. The green and sintered parts were characterized using helium pyknometer and SEM.

For the indirect rapid prototyping process, aqueous hydroxyapatite slurries with high solids contents and low viscosities were prepared. A commercially available hydroxyapatite powder was used as raw material. Polymeric models, made via a rapid prototyping technique, were infiltrated with these slurries. The polymer was pyrolysed during an adapted heat treatment, and subsequently, the ceramic was sintered. In the case of the slurries, special attention was focused on the organic additives, which influence the rheological behaviour and the wettability. The material properties were characterised during the different processing steps using rheometer, laser particle size analyser, helium pyknometer, SEM and X-ray diffractometer.

Results and discussion: For the direct rapid prototyping technique hydroxyapatite granules were processed for the special requirements and binder-systems were tested for 3D-printing. The resulting granules from the spray-drying process were compact and almost ball-shaped with a median particle size of approx. 120 μm. The powder consisting of granules revealed good flow properties so that a recoating of the powder bed was well achieved. The binder system was adapted to the organic additives of the granules. With this system green samples were printed (at Caesar, Bonn, Germany and FGB, University of Munich, Germany), which revealed a good strength and edge stability. These parts were sintered without any crack formation. SEM-images of the sintered samples showed a homogenous structure, although the shape of the granules was partly still visible. The single layers of the 3D-printing process were not detectable. A microporosity of approx. 2 μm in diameter can clearly be seen. This microporosity enhances the degradation of the hydroxyapatite. The macroporosity, i.e. the porosity created by the 3D-printing process, can be modified by changing the data for the printing process. The resolution of this process is limited by the size of the granules. Therefore, to get an improved resolution of the printed structures, the size of the granules should be lowered to a medium particle size of 80 μm as a next step.

In the indirect process polymeric models, which were produced via rapid prototyping techniques, were infiltrated with an aqueous hydroxyapatite slurry. The commercially available raw material had a specific surface area of 64 m^2/g. Using this powder, only slurries with a solids content of 35 wt% and a high viscosity could be prepared. Calcining the powder at 900 °C reduced the specific surface area to 12.5 m^2/g. With the calcined powder slurries with a solids content of 55 to 65 wt% were achieved. The slurries exhibited a shear thickening flow behaviour whereas the viscosity increased with rising solids content. The flow behaviour was also affected by the character and the amount of the dispersant. Other additives like the binder changed the viscosity as well, but to a minor degree. Crucial for the infiltration of the polymeric models is the wettability of the slurries on the polymer. A tenside was added to lower the surface tension of the slurry, and thus, to get a better wettability. After infiltration of the polymeric models the polymer was pyrolysed and subsequently the ceramic was sintered. Thus, a negative image of the polymeric model was achieved as ceramic. To receive crack free porous hydroxyapatite scaffolds with sufficient mechanical properties the polymeric models have to be optimised, e.g. the volume fraction of the polymer should be lowered. The pore structure of the ceramic scaffold can be adapted to the requirement of the implantation site by tailoring the structure of the polymeric models during the production via rapid prototyping.

Conclusions: For the production of hydroxyapatite scaffolds with tailored porosity the material processing for two rapid prototyping techniques was described. For the 3D-printing process flowable granules were produced and could be adapted to an appropriate binder system. For the indirect rapid prototyping process aqueous hydroxyapatite slurries with high solids contents and low viscosities were

produced. The wettability was improved by adding specific tensides. Both techniques show promising results to develop hydroxyapatite scaffolds which will be used in cell cultivation in a next step. A tailoring of the pore structure can be made by adapting the data of the rapid prototyping process.

Acknowledgements: This work is part of the research joint venture FORTEPRO, which is supported by the Bayerische Forschungsstiftung (Germany).

References

[1] Y. Lee, Y. Seol, Y. Lim, S. Kim, S. Han, I. Rhyu, S. Baek, S. Heo, J. Choi, P. Klokkevold and C. Chung, Tissue-engineered growth of bone marrow cell transplantaion using porous calcium metaphosphate matrices, *Biomed Mater Res* **54** (2001), 216–223.

[2] R. Martinetti, A. Belpassi, A. Nataloni and C. Piconi, Porous Hydroxyapatite Cell Carrier for Tissue Engineering, *Key Engineering Materials* **192–195** (2001), 507–510.

[3] A. Tampieri, G. Celotti, S. Sprio, A. Delcogliano and S. Franzese, Porosity-graded hydroxyapatite ceramics to replace natural bone, *Biomaterials* **22** (2001), 1365–1370.

Anatomical Rapid Prototyping models with soft and hard tissue representation for surgical planning

S. Irsen[a], H. Seitz[a], C. Tille[a], G. Bermes[a], E. Wolfinger[b], R. Sader[b] and H.-F. Zeilhofer[b]
[a]*Caesar research center, Ludwig Erhard Allee 2, 53175 Bonn, Germany*
Tel.: +49 228 9656 264; Fax: +49 228 9656 117; E-mail: irsen@caesar.de
[b]*Department of Reconstructive Surgery, University Hospital Basel, 4031 Basel, Switzerland*

Surgical planning tries to minimize the duration of surgery to reduce the risk of complications. Rapid Prototyping models of body sections in need of surgery help surgeons to prepare operations in close detail, especially in cranio-maxillofacial surgery. These Rapid Prototyping models find application in different ways. They are used for communication between surgical team members, radiologists, surgeons and patients as well as for preparing complex surgeries.

Physical models generated by stereolithography (SL) are especially suited for an application in surgical planning. SL models are translucent to view internal structures; they can be sterilized and used in the operating room. SL models also allow the improved visualization of anatomical features, such as tumors by selectively coloring within the model. Today, common rapid prototyping (RP) techniques only allow building models in a limited number of different materials and mostly in one color. With Stereolithography the color-coded representation of different internal anatomical structures within one model is possible by the use of a new kind of SL-material. Figure 1A shows a stereolithography model of a human skull with a colored tumor. But for the planning of soft-tissue alterations these models are not sufficient because of the material properties, especially the restricted color and haptical representation.

This paper presents a new approach to build medical models for surgical planning with realistic haptic and optical representation of different types of tissue. This new type of models is realized by the combination of different Rapid Prototyping techniques i.e. stereolithography for the hard tissue models and vacuum casting for a very realistic representation of soft tissues. The use of vacuum casting techniques allows building parts of an anatomical model in different materials with variable material properties and colors. In the presented case the patient's skin was realized in skin-colored silicon. The

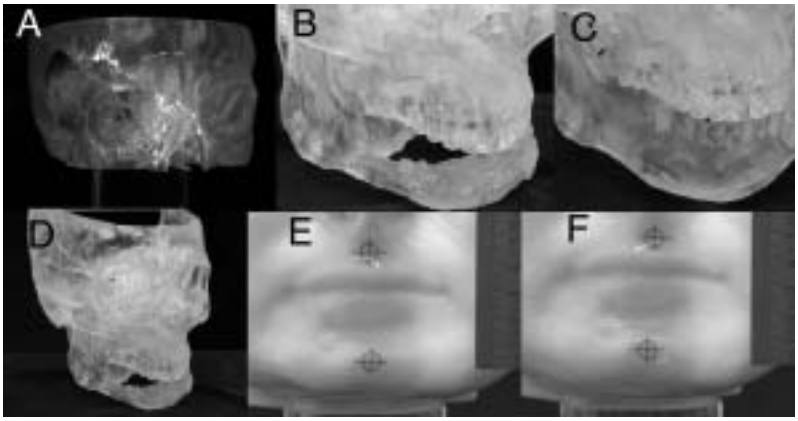

Fig. 1. Different Rapid Prototyping models for surgical planning. A = Representation of a colored SL-model. B–F = case study of a surgical planning with a combined hard and soft tissue model.

hardness of the used material can be adjusted with different additives to simulate different kinds of tissue and to create very realistic haptic representation of the model. Figures 1(B)–(F) show a case study of a patient with bone-defect of the mandible after trauma. Figure 1(B) illustrates the skull model of the patient in the actual state while in Fig. 1(C) a surgical planning for bone augmentation with an individual transplant of the iliac crest has been performed. The Figs 1(E) and (F) show the same skull models plus the representation of the patients skin. In Fig. 1(F) the changes of the chin caused by the surgery are noticeable. This is possible by the use of a soft tissue model that adapts to the changed mandible. These combined models can help surgeons in the craniofacial surgery to control the aesthetic aspects of the surgery.

Assessment of lower limb cross-sectional geometry using CT image analysis

T. Jämsä, O. Parviainen, I. Salmela* and P. Pulkkinen
Department of Medical Technology, University of Oulu, Oulu, Finland
Tel.: +358 8 537 5982; Fax: +358 8 330 687; E-mail: timo.jamsa@oulu.fi

Introduction: Osteoporosis is a disorder that causes increasing medical and social costs, especially in developed countries. The standard clinical assessment of osteoporosis is based on bone density measurements using dual-energy X-ray absorptiometry (DXA). However, DXA is a projectional method that gives the density of a two-dimensional projection. Therefore, density measurements by DXA are biased with bone size and cortical thickness [1], and with soft tissue as well [2].

Several studies have shown that the changes in bone geometry, especially in cortical bone, give a detailed figure on bone loss and fracture risk [3–6]. The strength of bone is influenced by bone material and by the distribution and organization of the material. Biomechanically, bone geometry is the primary factor in defining bone strength. Here we evaluated the reliability of a clinical CT scanner in evaluating bone and soft tissue geometry of lower limb.

*Current address: Division of Biophysics, Department of Physics, University of Oulu, Oulu, Finland.

Table 1
Reproducibility error (CV_{rms}) of different bone, muscle and fat parameters of lower limb. Duplicate measurements, $N = 15$

	Mid femur	Proximal tibia	Distal tibia
Bone circumference	0.20	0.48	2.09
Cortical CSA	0.32	0.49	2.10
Cortical thickness	0.53	0.55	2.88
Maximal CSMI of cortical bone	0.26	1.45	2.34
Minimal CSMI of cortical bone	0.20	0.93	2.54
Cortical attenuation	0.27	0.54	3.02
Trabecular attenuation			1.24
Muscle CSA	0.53	0.83	
Fat CSA	0.72	0.66	

Methods: Healthy premenopausal females (age 35–40 years) were scanned with a Siemens Somatom Emotion spiral CT scanner. Subject positioning was standardized, and one qualified radiographer performed the measurements. Fifteen subjects were scanned twice to evaluate the reproducibility of the analysis, repositioning the subject between the measurements. Duplicate scans of another three subjects were performed by another radiographer. Three cross-sectional scans were made, one at mid-femur (50%), one at proximal tibia (67%) and one at distal tibia (5%). The scan line was adjusted using the scout view of the scanner software.

The images were saved in DICOM-format and analysed using the GEANIE 2.1 bone analysis software (BonAlyse Ltd, Jyväskylä, Finland). Bone circumference, cortical cross-sectional area (CSA), cortical thickness, cross-sectional moment of inertia (CSMI), cortical and trabecular attenuation, and muscle and fat CSA were measured from the left leg.

The root-mean-square coefficient of variation CV_{rms} (%) was calculated from the duplicate measurements as a measure of reproducibility error. The inter- and intraobserver error of computerised image analysis was evaluated by repeated analysis of fourteen image sets, taken from the duplicate scans of seven subjects.

Results: The results of the reproducibility study are shown in Table 1. The CVrms values for the geometry parameters of cortical bone were 0.20–0.53% for mid-femur, 0.48–1.45% for proximal tibia and 2.09–2.88% for distal tibia. The reproducibility error of cortical attenuation was 0.27% at mid-femur and 0.54% at proximal tibia. At distal tibia, the reproducibility error of attenuation was 3.02% for cortical bone and 1.24% for trabecular bone. The CVrms values for muscle area at femur and tibia were 0.53% and 0.83%, respectively. The reproducibility error of fat area was 0.72% at femur and 0.66% at tibia. The results were significantly worse when the three subjects scanned by the other radiographer unfamiliar with the procedure were included in the calculation.

There was no inter- or intraobserver error in the bone analysis or in the soft tissue analysis at tibia. At mid-femur, there was some inter- and intraobserver error in fat area, the values being 0.23% and 0.46%, respectively. There was also a slight intraobserver error of 0.16% in the muscle area at mid-femur.

Discussion: The study shows that the geometry analysis of bone, muscle and fat at the lower limb is relevant using a standard CT scanner and the GEANIE bone analysis software, except for the geometrical evaluation of distal tibia. Standardized subject positioning and scanning procedure are essential for reproducible results. The lower reproducibility in the geometrical analysis of distal tibia indicates that the irregular, more conical shape of the bone ends limits the reliability of CT in the evaluation of geometry there. However, the measurement of trabecular attenuation, which is related to apparent density, is relevant at distal tibia. This study shows that not only bone but also soft tissue can reliably be evaluated from clinical CT scans.

Conclusion: The geometry analysis of bone, muscle and fat of lower limb is relevant using a standard CT scanner with standardized subject positioning and the GEANIE bone analysis software, except for the geometrical evaluation of distal tibia.

Acknowledgements: This study was financially supported by the National Technology Agency of Finland.

References

[1] C.R. Carter, M.L. Bouxsein and R. Marcus, New approaches for interpreting projected bone densitometry data, *Journal of Bone and Mineral Research* **7** (1992), 137–145.
[2] H.H. Bolotin, H. Sievänen and J.L. Grashuis, Patient-specific DXA bone mineral density inaccuracies: quantitative effects of nonuniform extraosseous fat distributions, *Journal of Bone and Mineral Research* **18** (2003), 1020–1027.
[3] J. Cordey, M. Schneider, C. Belendez, W.J. Ziegler, B.A. Rahn and S.M. Perren, Effect of bone size, not density, on the stiffness of the proximal part of normal and osteoporotic human femora, *Journal of Bone and Mineral Research* **7**(Suppl. 2) (1992), S437–S444.
[4] C.C. Glüer, S.R. Cummings, A. Pressman, J. Li, K. Glüer, K.G. Faulkner, S. Grampp and H.K. Genant, Prediction of hip fractures from pelvic radiographs: the study of osteoporotic fractures, *Journal of Bone and Mineral Research* **9** (1994), 671–677.
[5] J. Partanen, T. Jämsä and P. Jalovaara, Influence of the upper femur and pelvic geometry on the risk and type of hip fractures, *Journal of Bone and Mineral Research* **16** (2001), 1540–1546.
[6] H.G. Ahlborg, O. Johnell, C.H. Turner, G. Rannevik and M.K. Karlsson, Bone loss and bone size after menopause, *The New England Journal of Medicine* **349** (2003), 327–334.

Poster Presentation

Identificaton of human kinematics by FSBM algorithm

Ana Kuzmanic and Josip Music
Faculty of Electrical Engineering, Mechanical Engineering and Naval Architecture/Department of Biomechanics and Automatic Control Systems, Split, Croatia

Abstract: In this paper a novel procedure for human kinematics identification is presented. The whole procedure gives succesive vector presentation of human locomotion in saggital plane for any desired point on human body. Software used is based on FSBM (Full Search Block Matching) algorithm and is written in C-program language performed under Linux operating system.

Introduction: The basic idea in this work is to propose new methodology for obtaining kinematic variables by generation of vectors presenting motion of the point of interest. During initial measurements and software processing of data it was shown that this kind of image processing enables identification of motion that gives more information than usual marker or markerless identification procedure. Movements of as many as needed corresponding points of interest on foot, leg and HAT (head-arm-trunk) are generated and vectors are attached to piont. The vector represents differences in translational coordinates between succesive frames resulting in graphicaly presented movements with numerical data available as well. Software used is based on FSBM algorithm [1], in Linux and the graphical presentation is done in Matlab.

Methods and results: Measurement of kinematic data are based on two-dimentional sequence tracking using one TV-camcoder. The subject was recorded with Sony Digital 8 camcoder, DCR-TRV 110E in right saggittal plane at self-selected speed of slow walking, during one cycle of gait. Camcoder was

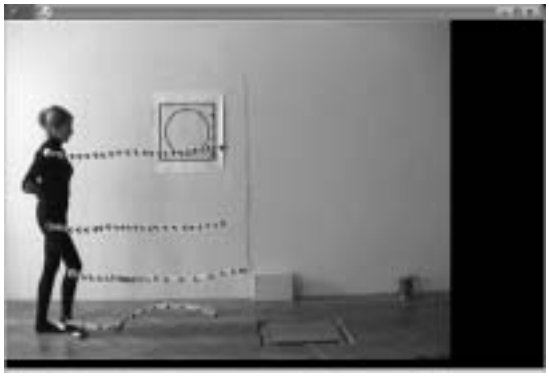

Fig. 1. Trajectories of desired points.

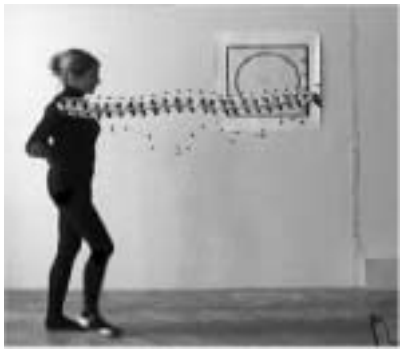

Fig. 2. Mismatched coordinates.

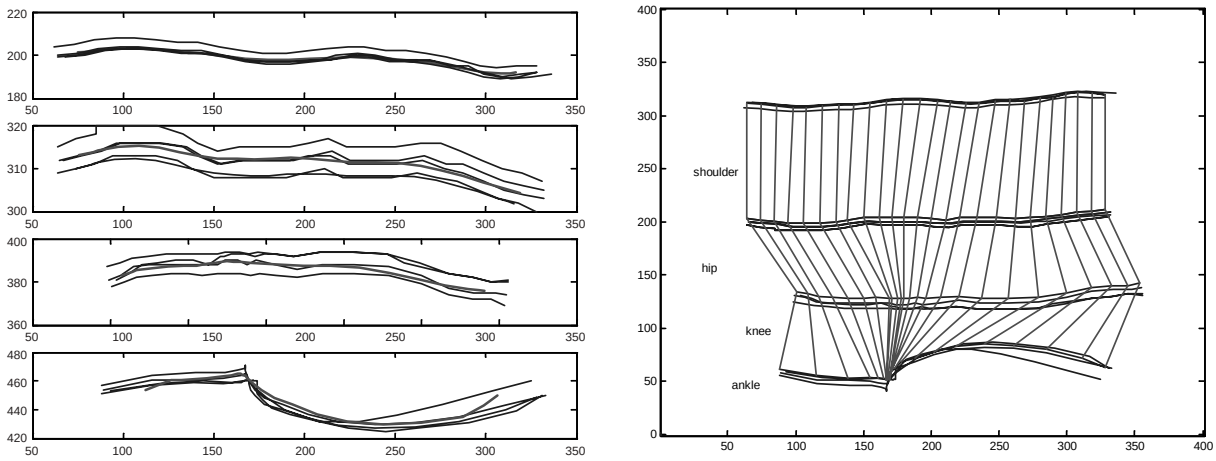

Fig. 3. Numerical data of tracking algorithm.

adjusted at 25 frames/sec [2]. Point coordinates were automaticaly measured and tracked during the sequence with software wich uses FSBM algorithm. FSBMA is considered to be the most accurate of all block matching algorithms but being computationaly expensive at the same time. FSBM approach analyses color images by their RGB components and is based on method wich considers an image region around selected point. One image is taken as referent and subsequent as search images.

User initialises procedure in first image of sequence defining desired points coordinate. It represents the upper left corner of referent block wich is going to be tracked. The size of referent block is chosen to be 8×8 pixels. After that program automatically defines the search region of 38×38 pixels. Every single block for each RGB component within this area is compared with values of referent block ranging from 1 to 64. If the difference between blocks is equal or less than value of a priori determined threshold, the value of coincidence counter is increased by 1. Considering possible illumination changes in image, it was experimentaly shown that threshold 10 is acceptable since it gives the best possible results. Final value of counter establishes percentage of correspondence among two successive frames. The block with highest value is matched and displacement is seen as vector positioned from center of initial block to center of matched block. Now, the matched block is taken as referent one and whole algorithm is repeated same way until the last frame of sequence.

The result of procedure are coordinates of desired point displayed as trajectories as shown in Fig. 1.

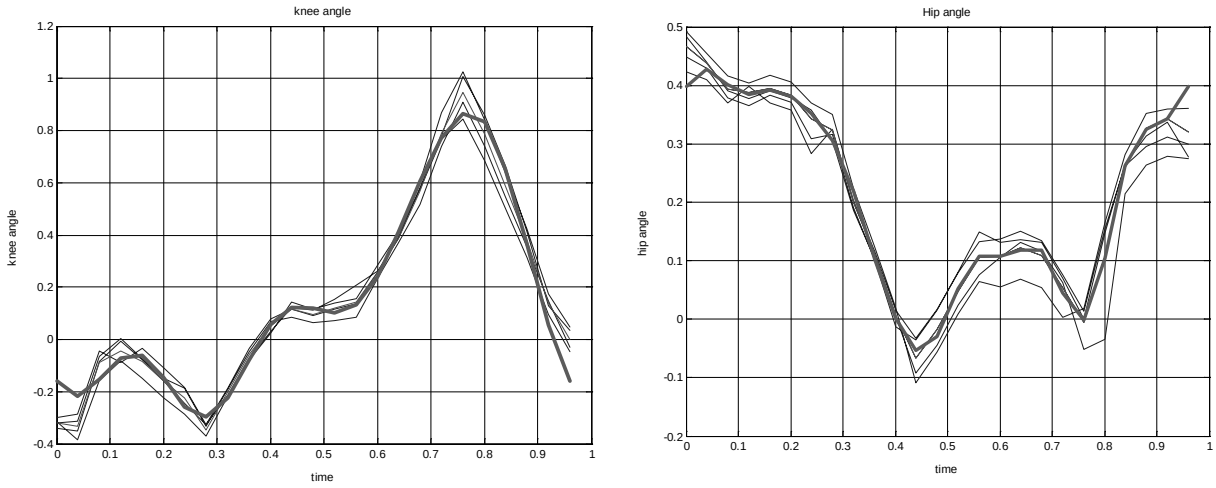

Fig. 4. Resulting joint angles of hip and knee.

However, during the sequence false trajectories can be generated. In order to eliminate these appearances, multiple points in proximal vicinity of desired one can be tracked. The false trajectories can be easily excluded because they don't follow the uniform flow of majority. Figure 2 shows obvious mismatched coordinates.

As a case example of kinematic identification we have chosen to track characteristic points of the human body positioned on shoulder, hip, knee and ankle. In order to visualize joint angles, numerical data of tracking algorithm were transferred to Matlab as shown on Fig. 3. In this case low-pass moving average filter is performed by replacing each data point with the average of the neighbouring data points defined with span. Resulting joint angles of hip and knee are shown in Fig. 4.

The numerical derivation can be applied to determine velocities and acceleration.

Conclusion: In order to prevent false matches it is desireable to pay attention to disadvantages of FSBM algorithm considering color and regions in image. Due to larger unicolored areas and legs occluding each other during a walking sequence, a lost of track can appear. This can be avoided by including colored clothes of recorded subject as well as with accentuation of tracking regions with different colored marks (not necessary classical markers). The proposed method for kinematic identification gives results that are comparable with the results obtained using standard marker tracking methods. Also the effectivness of algorithm can be verified by repeating the procedure on larger set of different samples and than statistical methods can be performed.

Acknowledgement: This work is sponsored by Ministry of Science and Technology of Republic of Croatia, project No. 023022 "Biomechanics of Human Locomotion, Control and Rehabilitation".

References

[1] C.-K. Cheung, Fast motion estimation techniques for video compression, PhD thesis, CityU, Image processing laboratory, 1998. http://www.image.cityu.edu.hk/˜ckcheung/thesis/thesis.html.

[2] A. Kuzmanic and T. Grujic, Identification of kinematic and kinetics of human gait, Proc. EMBEC'02, Vienna, Austria, 2002, pp. 824–825.

[3] V. Zanchi, M. Cecic and V. Papic, Visualisation of human motion kinematics in state space, *Journal of International Federation for Medical & Biologcal Engineering* **37**(2) (1999), 846–847.

Bioinformatics

Multidimensional scaling for stratifying Chagas' disease

L. Marmol-Herrera and K. Warwick
University of Reading, Department of Cybernetics, Reading, UK
Tel.: +44 118 3788210; Fax: +44 118 3788220; E-mail: ljmarmol@medscape.com

Introduction: In this study, we used an unsupervised statistical method, multidimensional scaling, to group different stages of the chronic Chagas' disease solely on the basis of some parameters (feature data) obtained from the electrocardiogram digital analysis. Our goal was to determine whether the feature data alone were sufficient to stratify 56 subjects in a clinically meaningful manner.

The diagnosis of myocardial damage in patients suffering from the early and asymptomatic stages of the Chagas' disease is currently carried out through invasive methods [4]. Therefore, it is highly desirable to stratify the different stages by non-invasive measurements related to the transmission of the cardiac impulse through the conduction system of the heart (electrocardiogram) and to the autonomic nervous system (heart rate variability).

Multidimensional scaling (MDS) is an iterative process used for constructing a low-dimensional representation of high-dimensional data, which facilitates visualization and analysis of patterns in the data [1]. In the Chagas' disease problem explained previously, the major interest is focused on determining from the pre-selected features obtained from electrocardiographic registers, those that are relevant for the non-invasive diagnosis of early myocardial damage.

Methods: Raw data was recorded by an acquisition system designed by the Biomedical Engineering Group of the University of Los Andes [3], and includes hardware for conditioning and digital acquisition of the signal as well as software for averaging of the electrocardiogram (ECG). Measuring the time interval between successive normal cycles or complexes, interbeat interval variations (RR intervals) were obtained.

The data analysed here are made up of 17 healthy individuals, and 39 patients with Chagas' disease in three different stages. The subjects have been classified according to the evolution of the disease and some invasive tests [2] as:

Control Group. Healthy patients without cardiac abnormalities. *Group IA.* Chagasic patients with subcellular damage in the heart. ECG normal. Left cineventriculography normal. Endomyocardial biopsy abnormal. They are asymptomatic. *Group IB.* Chagasic patients with segmental wall motion in the heart. ECG normal. Left cineventriculography abnormal. Endomyocardial biopsy abnormal. They are asymptomatic. *Group II.* Chagasic patients with advanced damage in the heart. Left cineventriculography and endomyocardial biopsy are abnormal. They do not present congestive cardiomyopathy. They are symptomatic.

The control group and the group II have been called "extreme groups", since each group represents two extreme conditions over the total set of groups; meanwhile group IA and group IB have been called "intermediate groups", as representing the evolutive and intermediate stages of the disease, both being stages of the indeterminate phase of chronic Chagas' disease

Each subject is represented by a vector with 7 features, which were previously selected from the electrocardiographic signals in [2]. These features were calculated by using different digital signal processing techniques (FFT, wavelets, fractals), and evaluated to be considered as prospective features.

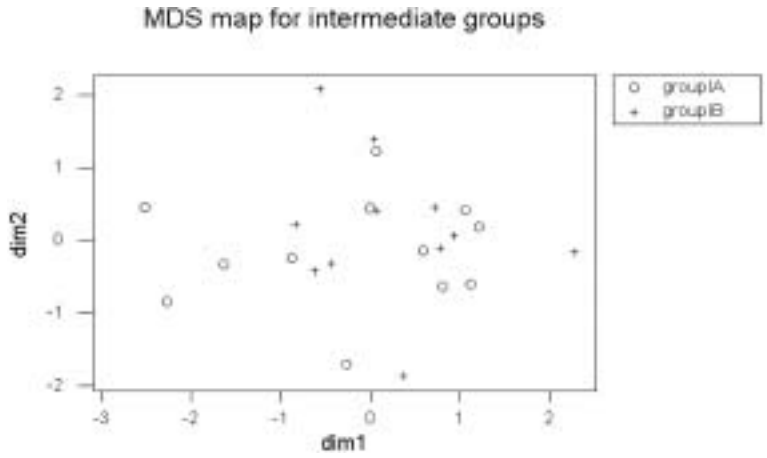

Fig. 1.

Many statistical techniques requires that the underlying data are distributed as multivariate normal. Multidimensional scaling imposes no such restrictions. The purpose of Multidimensional Scaling is to provide a visual representation of the pattern of similarities or distances among a set of objects. For this particular case study, the objects are represented by the patients or vectors. MDS plots the objects on a map such that objects that are very similar to each other are placed near each other on the map, and objects that are very different from each other, are placed far away from each other on the map. With the set of features for each object or vector, it is very difficult to visualize similarities unless the data can be represented in a small number of dimensions. Thus, a dimension reduction (usually two dimensions) is necessary.

To build an optimal representation the MDS algorithm minimizes an index called “stress”. This is the overall measure of how the distances in the configuration ordinally fit the data – a measure of a badness of fit. Therefore, when stress is closer to zero, there is a better representation.

Results: The result of MDS application to the initial data is a two dimensional picture of a set of points representing the objects considered. MDS-based analysis resulted in good separation of the 4 classes of patients provided. Extreme groups were clearly represented by separate clusters. However, the two intermediate stages showed a more diffuse separation from the other extreme stages. Figure 1 shows that there is a sort of separation between groups IA and IB, but the clarity of the final configuration according to a minimum stress and a number of dimensions easy to interpret is not sufficient for discrimination.

Conclusions: The methods evaluated in this paper are easy to implement without a priori assumptions related to data. The results demonstrated that a non-invasive classification of Chagas’ disease stages based solely on digital signal calculated feature data is feasible and potentially informative. The visualization of data obtained seems attractive for the initial discrimination of patients in the chronic asymptomatic phase of the disease, in order to determine whether some of them require additional invasive tests to establish the disease stage. These results show that it is possible to use some indices derived from digital signal processing techniques as electrodiagnosis indicators to evaluate the evolution of the disease.

References

[1] T.F. Cox and M.A.A. Cox, *Multidimensional Scaling*, London: Chapman & Hall, 1994.

[2] L. Marmol-Herrera, Artificial intelligence methods for the diagnosis of myocardial damage in Chagas'disease using electrocardiographic signals, PhD Thesis, University of Reading, 2000.
[3] R. Medina, D. Jugo and H. Carrasco, An Acquisition and Processing System for the High Resolution Surface Electrocardiogram, Proc. 14th Int. Conf. IEEE Eng. in Med. and Biol. Soc., 1992, pp. 779–780.
[4] World Health Organization: Division of Control of Tropical Diseases – Chagas Disease. http://www.who.int/ctd/html/chag.html, 2003.

In vivo micro-CT based finite element modelling to study adaptive bone response in guinea pig tibiae

L. Muraru[a], S.V.N. Jaecques[a], H. Van Oosterwyck[a], E. De Smet[b], M. Wevers[c], I. Naert[b] and J. Vander Sloten[a]
[a]*K.U. Leuven, Division of Biomechanics and Engineering Design* (*BMGO*), *Belgium*
[b]*K.U. Leuven, Department of Prosthetic Dentistry, Belgium*
[c]*K.U. Leuven, Department of Metallurgy & Materials Engineering* (*MTM*), *Belgium*
Tel.: +32 16 327747; Fax: +32 16 327994; E-mail: Oanamaria.Muraru@mech.kuleuven.ac.be

Introduction: This study focuses on the bone adaptive response around early loaded oral implants. A combined approach was followed, consisting of an animal experiment and a finite element simulation. As to the latter, it is important that individualised image-based finite element models are created in order to accurately calculate the stress and strain distribution in bone around loaded implants.

Materials and methods: Currently, guinea pigs were used as an animal model. Custom made titanium implants were placed percutaneously in both tibiae of skeletally mature guinea pigs. Mechanical loading was applied as a sinusoidal varying bending load, starting one week postoperatively during four weeks. The amplitude and the frequency of the mechanical load are the varied parameters in the animal experiment.

Due to the high resolution needed to visualise the bone geometry and the bone adaptive response to the loading regime, microfocus computed tomography (μCT) was used to follow up *in vivo* peri-implant bone adaptation. With μCT a fully three-dimensional characterisation of bone tissue around the implant at different time points within the same animal can be obtained [1]. Four *in vivo* μCT scans (pre-operatively, one week after implantation ("vivo 1"), after two weeks of stimulation ("vivo 2") and just before euthanising the animal) and one post mortem μCT scan were taken.

Individualised FE models were derived from the *in vivo* μCT images and from the post mortem μCT images. Correct bone and implant geometry, as well as the correct position of the implant with respect to the bone were incorporated. Heterogeneous bone elastic properties were implemented using a (linear) relationship between μCT image grey values and E-modulus. Static loading conditions, corresponding to the *in vivo* test conditions (eccentric force of 4N leading to a bending moment of 0.08 Nm) were applied. The implant-bone interface was modelled with a finite tensile strength. In this case, when interface tensile stresses exceed the interface tensile strength relative motion will occur.

Results and discussion: No deterministic radiation side effects were clinically observed up to the end of the study. The streak artefacts induced by the titanium implant and the general noise due to the low radiation dose regime made the bone segmentation more difficult than in the case of conventional post-mortem μCT. They may also influence the assignment of bone elastic properties based on voxels' grey-values. In order to more rigorously implement bone elastic properties, an accurate relation between μCT grey values and bone elastic properties will have to be established experimentally.

Fig. 1. Equivalent elastic strain distribution (in microstrain); post mortem also shown after metal artefact correction (right picture).

Fig. 2. Equivalent Von Mises stress distribution (in MPa); post mortem also shown after metal artefact correction (right picture).

For the time points modelled here, the interface tensile strength was exceeded, resulting in debonding and relative motion. In debonded regions interface stresses cannot be transferred from the implant to the bone, leading to lower stresses in these regions and an asymmetric peri-implant stress and strain distribution. Figures 1 and 2 show the equivalent elastic strain distribution and equivalent Von Mises stress distribution, respectively, in corresponding sagittal cross-sections through the tibia. High cortical stresses and strains ($>$ 5000 microstrain, time point "vivo1") were noticed near the implant neck at the distal side and near the implant apex at the proximal side. A decreasing evolution in peri-implant strain distribution between "vivo 1" and "vivo 2" can be noticed. This evolution is not coherent up to the last time point ("post mortem", after 4 weeks of mechanical stimulation). However, the influence of metal artefacts is not negligible, as can be seen in Figs 1 and 2 when the artefact-corrected post-mortem model is compared with the original post-mortem model. After correction for the metal artefacts, the results from low-noise post mortem μCT correspond well with observations made on histological sections of the same location.

Conclusions: A method was developed to derive μCT based FE models of bone-implant structures *in vivo*.

In vivo μCT image quality is very important for the accuracy of the FE models. More analyses will be needed to confirm the strain decreases already observed for one animal over the considered time points. Future work will involve metal artefacts reduction, noise reduction and validation of the calculated strains.

Reference

[1] S.V.N. Jaecques et al., Feasibility of monitoring bone remodelling around loaded percutaneous tibial implants in guinea pigs by in vivo microfocus computed tomography (μCT), in: Proc. Computer Assisted Radiology and Surgery 2001, H.U. Lemke et al., ed., Elsevier ICS1230, 2001, pp. 402–407.

ESB: Satellite Symposium: Implant Fixation

Autonomous compensation for tissue and patient motion during robot-assisted surgery

A. Ranftl[a], K. Denis[a], J. Vander Sloten[a], J. De Schutter[b], H. Bruyninckx[b] and J. Bellemans[c]
[a]*Division of Biomechanics and Engineering Design* (*Mechanical Engineering*), *KU Leuven, Belgium*
[b]*Division of Production Engineering, Machine Design and Automation* (*Mechanical Engineering*), *KU Leuven, Belgium*
[c]*Division of Orthopaedics UZ Pellenberg, KU Leuven, Belgium*
Tel.: +32 16 32 75 34; Fax: +32 16 32 79 94; E-mail: Andrea.Ranftl@mech.kuleuven.ac.be

Introduction: In the Division of Biomechanics and Engineering Design earlier projects in the field of robot-assisted surgery have developed procedures for static registration in orthopaedics. With respect to total knee arthroplasty (TKA) registration by means of surface matching [3] as well as by means of an intramedullary rod [2] were introduced. Furthermore a markerless registration technique by surface matching was developed for total hip arthroplasty (THA) [5]. Drawback of these methods is that during the operation process the tibia (see Fig. 1) respectively the hip have to be clamped invasively to prevent movements of any kind. Clamping is essential to obtain accurate cavities in the bone, which is needed to achieve good initial implant fixation. This is due to the inability of the robot to react autonomously on position changes in the workspace. This fixation can lead to lesions in soft and hard tissue. Furthermore in case of sudden and unexpected movements of bones or the robot during the operation the registration has to be renewed. This can be impossible at an advanced stage of intervention.

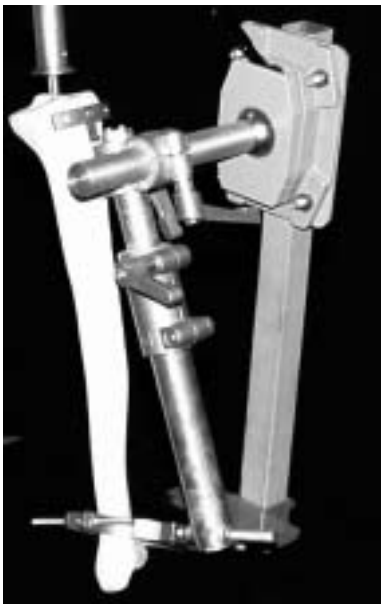

Fig. 1. Invasive clamping of the tibia.

In this abstract a procedure, called dynamic registration, will be proposed which copes with the above mentioned problems. For this purpose results of the Division of Production engineering, Machine Design

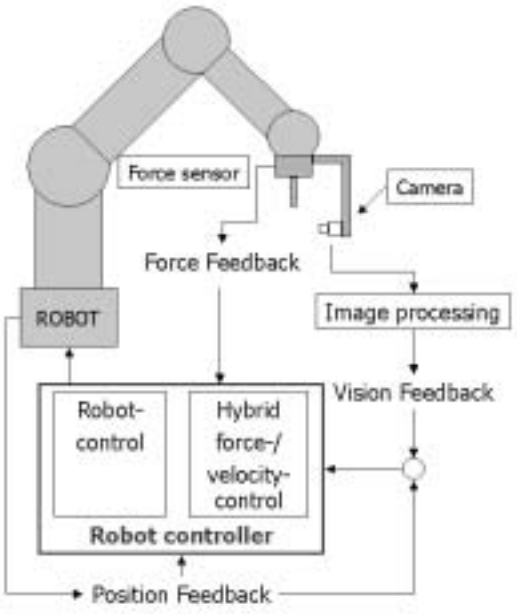

Fig. 2. Blockdiagram of the dynamic registration.

and Automation in the field of visual servo control will be applied. With the help of hybrid vision and force control the robot end-effector is forced to follow a planar contour. The vision provides feedforward information of the end-effector trajectory and the force control prevents the end-effector from loosing the contact with the contour [1]. Our objective is to develop a control strategy which combines and extends the achieved results. With the help of so-called dynamic registration it is possible by means of visual feedback to compensate movements of the patient autonomously by the robot. The drawbacks of invasive clamping by static registration methods are therefore removed.

Methods: Dynamic registration stems from the in control theory well known visual servo control. Thereby machine vision closes a control loop for position control [4]. The camera records the movements in the working space of the robot. With this information the position changes can be calculated and be sent as setpoints for the end-effector to the robot joint controller. The whole process including all data streams and the robot motion have to be realized in a real-time environment to ensure an appropriate reaction of the robot. The experimental set-up of the department consists of a six degree of freedom industrial Stäubli RX 130 robot and a conventional Philips INCA 311 camera. It includes an internal processor and is supported by a vision library in C/C++. It has furthermore to be considered that the whole technical assembly has to fit in an operation theater and must not bother the staff.

The main objective is to develop a control scheme as outlined in Fig. 2 for the robot position control which includes three feedback loops: The precise position of the end-effector provided by the joint controller, the force feedback which records the interventions of the end-effector in the working space as already realized in earlier approaches [2,3,5] and the vision loop to observe motions in the environment of the robot. With these three control loops the robot is able to compensate unexpected movements automatically during the operation. The proposed control strategy will initially be applied to robot assisted surgery in the field of orthopaedics. In particular the procedures mentioned for TKA will be extended and the previously obtained results of accuracy studies will be taken as benchmarks and

references. One of the main goals is to show the feasibility of the proposed control strategy in robot-assisted surgery.

Results and conclusion: The authors have proposed a control scheme which will enable the robot to react autonomously on movements in the workspace. With the help of vision feedback the previously developed hybrid force/velocity control in robot-assisted TKA is extended to replace the invasive clamping by a more moderate one to spare soft and hard tissues. It should be stressed that in this line of work the intention never lies in replacing the surgeon by the robot. His responsibility will rather be shifted to higher level tasks such as the supervision of the whole process and the planning of the applied procedure. In the future this approach will also be applied to other fields of surgery (e.g. cardiac surgery) where invasive clamping of the tissues is not possible and therefore the application of robot-assisted procedures is restricted.

References

[1] J. Baeten, Integration of vision and force for robotic servoing. PhD thesis, Katholieke Universiteit Leuven, B-3001 Leuven, Belgium, December 2001.
[2] K. Denis, G. van Ham, J. Bellemans, L. Labey, J. Vander Sloten, R. Van Audekercke, G. Van der Perre and J. De Schutter, How correctly does an intramedullary rod represent the Longitudinal Tibial Axes? *Clincal Orthopaedics and related Research* **397** (2002), 424–433.
[3] K. Denis, G. Van Ham, J. Vander Sloten, R. Van Audekercke, G. Van der Perre, J. De Schutter, J. Bellemans and G. Fabry, Registration of the tibia in robot-assisted total knee arthroplasty using surface matching. Computer Assisted Rediology and Surgery, 17th International Congress and Exhibition, London, June 25–28, 2002, pp. 664–669.
[4] S.A. Hutchinson, G.D. Hager and P.I. Corke, A Tutorial on Visual Servo Control, *IEEE Transactions on Robotics and Automation* **12**(5) (October 1996), 651–670.
[5] G. Van Ham, Development of a markerless registration method and a semi-active control strategy for robot-assisted orthopaedic surgery. PhD thesis, Katholieke Universiteit Leuven, B-3001 Leuven, Belgium, September 2002.

Reliability of an accelerometer in the assessment of body movements

E. Vihriälä[a], J. Oksa[b], J. Karkulehto[c], R. Korpelainen[d], R. Myllylä[a] and T. Jämsä[e]
[a]*Department of Electrical and Information Engineering, University of Oulu, P.O. Box 4000, FIN-90014 Oulu, Finland*
E-mail: evihrial@ee.oulu.fi
[b]*Oulu Regional Institute of Occupational Health, Oulu, Finland*
[c]*Medical Engineering, The Oulu Polytechnic Institute of Technology, Oulu, Finland*
[d]*Department of Sports Medicine, Oulu Deaconess Institute, Oulu, Finland*
[e]*Department of Medical Technology, University of Oulu, Oulu, Finland*

Introduction: Human body movements, such as tremors and exercises, have generally been measured with optical motion analysis [3]. This technique, however, has its limitations, the most serious being that the measurement setup is fixed to one place and that the measurement period is limited. Accelerometers, on the other hand, enable the continuous measurement of movements over long periods without interruptions. In addition, the measurements are not spatially limited.

In earlier studies, accelerometers have been successfully applied to the observation of human motions [2], and previous validation studies [1] have shown that the agreement between the accelerometric

Table 1
Confidence and prediction intervals. Combination of all measurements

Interval	Value
95% confidence interval for b (form.4).	0.0126
95% confidence interval for a_{acc}.	0.108 (g)
95% prediction interval for a_{acc} (the worst case).	0.617 (g)
Residual standard deviation s_r.	0.308 (g)

method and other more conventional methods is high. This paper extended the variety of examined exercises and the range of measured acceleration amplitudes. The aim of the present study was to evaluate the reliability of a tri-axial accelerometer in the assessment of body movements by comparing it with a conventional motion analysis system.

Methods: To achieve equal calculus basis with the accelerometric method, the position-time information provided by a motion analysis system was converted into accelerations. The agreement between the two measuring methods was determined by means of regression and correlation (correlation coefficients) analysis. Accelerations were measured with two prototypes. The first one operated with a laptop computer (Compaq Armada E500, Hewlett-Packard Company, US), while the other one incorporated a datalogger (Tattletale Model 8v2 Data Logger, Onset Computer Corporation, US). Both prototypes operated with a sampling rate of 400Hz/Channel. The 3d-sensor of the acceleration measuring devices was constructed with three orthogonally connected commercial accelerometers (SCA-320, VTI Technologies, Finland). Motion analysis was performed with a commercial analysis system with two video cameras (MacReflex, Qualisys Ab, Sweden), operating with a rate of 100 frames/s and ground reaction forces were measured with a force plate sensor (Kistler 9287 A, charge amplifier Kistler 9865 C, Kistler Instrumente AG, Winterthur, Switzerland). Acceleration measurements of a set of standardized exercises (walking, running, jumping, etc.) were carried out in two stages. At the first stage, accelerations were measured using the prototype with the laptop computer ($n = 169$). Next, a new set of measurements were performed with the prototype incorporating a datalogger ($n = 403$). At last, to get a wider sampling, all results were combined . Both average acceleration values (10 test subjects, first stage measurements) and maximum peak values (10 test subjects, second stage measurements) were examined. The 3d-accelerometer was attached either directly on the skin using an adhesive tape or over clothing using a belt. The marker for the motion analysis system was placed on top of the accelerometer's sensor. The sensor attachment sites vary being either ankle, knee, thigh or waist. Only accelerations with an upward direction were analysed.

Results: The correlation coefficient while all results were combined was $r = 0.989$.

The regression line equation was $a_{acc} = a_{ma}1.02 + 0.0277g$, where

$a_{acc} =$ estimated acceleration for the accelerometer and

$a_{ma} =$ acceleration measured with the motion analysis system.

Residual standard deviation, prediction interval and confidence intervals are presented in Table 1 and Fig. 1.

Discussion: This study showed a high agreement between the video-based and accelerometric methods in the assessment of body movements. The observed slight deviation between the methods may be due to their different operating principles. Video-based analysis has only a limited ability to detect accelerations and requires generally at least three position detections to obtain one acceleration value. First, position1, position2 and the corresponding speed are calculated, followed by a calculation of position2, position3 and the corresponding speed, before a change in speed (acceleration) can be determined. If the acceleration peaks are high and their durations short, the determined accelerations may easily be

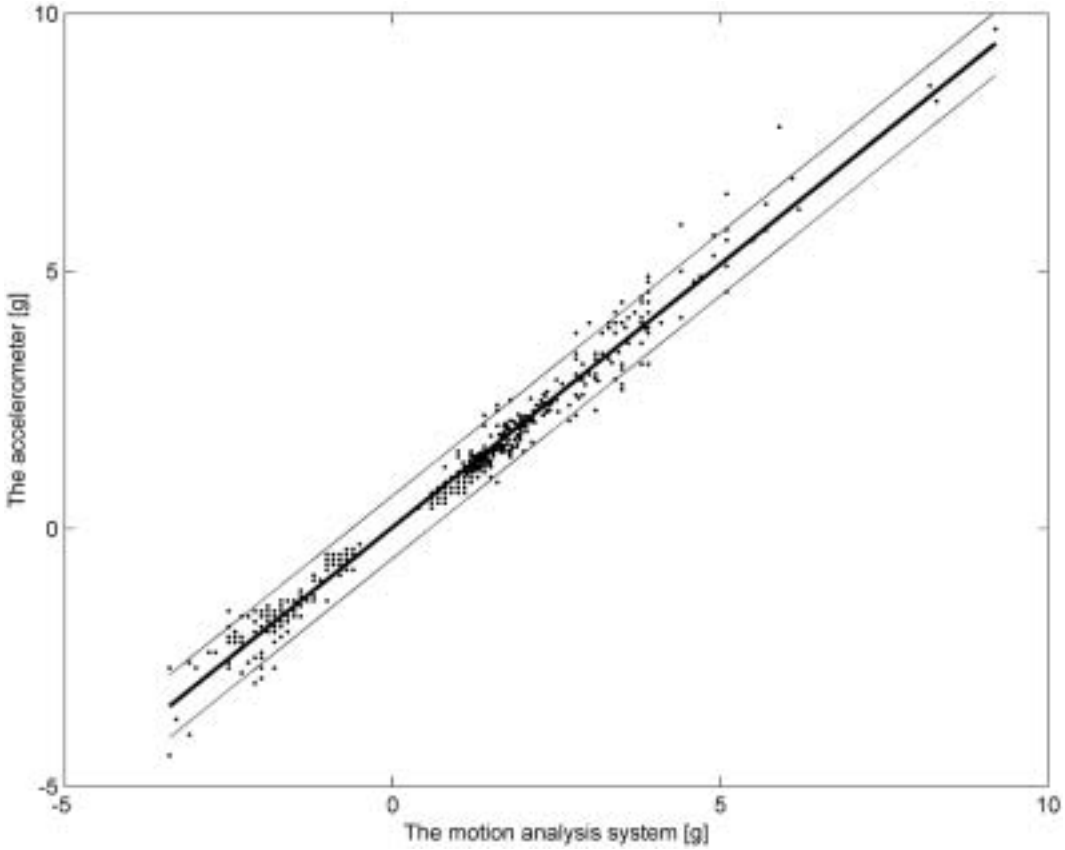

Fig. 1. Regression line and the 95% prediction limits. Combination of all measurements ($n = 572$).

attenuated (depending on the time resolution of the system). This conclusion is actually affirmed by the fact that slope b was higher than 1. Also, Fig. 1 shows that the motion analysis system produces lower values at high accelerations than the accelerometric method.

Conclusions: In comparison with the motion analysis system, accelerometers seem better suited for observing different patterns of physical exercises and are more accurate at high accelerations. However, if the exercises to be measured consist of very slow movements and accelerations, motion analysis gives more reliable results.

Acknowledgements: The authors wish to thank the National Technology Agency of Finland for financial support.

References

[1] R. Mayagoitia, A. Nene and P. Veltink, Accelerometer and rate gyroscope measurement of kinematics: an inexpensive alternative to optical motion analysis systems, *Journal of Biomechanics* **35** (2002), 537–542.

[2] M. Sekine, T. Tamura, M. Ogava, T. Togawa and Y. Fukui, Classification of acceleration Waveform in a continuous walking record, Proceedings of the 20th Annual International Conference of the IEEE Engineering in Medicine and Biology, Vol. 20, No 3, 1998.

[3] P. Van Gheluwe, P. Roosen and K. Desloovere, Rearfoot Kinematics During Initial Takeoff of Elite High Jumpers: Estimation of Spatial Position and Orientation of Subtalar Axis, *Journal of Applied Biomechanics* **19** (2003), 13–27.

4. Biosignals and Sensors

Analysis of T-wave shape variability in HR ECG mapping

M. Fereniec[a], G. Karpiński[b], R. Maniewski[a], G. Opolski[b], H. Rix[c] and A. Zbieć[a]
[a]*Institute of Biocybernetics and Biomedical Engineering PAS Warsaw, Poland*
[b]*Chair and Department of Int. Medicine and Cardiology, School of Medicine, Warsaw, Poland*
[c]*Université de Nice, Sophia Antipolis, France*

Introduction: The non-invasive assessment of the cardiac repolarization heterogeneity is of clinical importance. It is generally accepted that the repolarization inhomogeneity facilitates the re-entry phenomena causing the development of life-threatening ventricular arrhythmias, e.g. ventricular tachycardia [4]. This concerns, in particular, a large group of post myocardial infarction patients and patients with left ventricular hypertrophy.

The purpose of this study was to investigate the spatial changes of the repolarization period, in particular, T-wave in a high-resolution ECG recording. We have applied two different methods quantifying T-wave shape. First, the parameter called TSI parameter (T-wave Shape Index), sensitive for T-wave shape changes based on length of T-wave curve and integral of ECG amplitude in T-wave period was proposed [1]. The second method is based on distribution function method defined to detect signals shape differences. The preliminary results obtained from the analysis of a limited number of normal subjects and post-infraction patients with cardiac insufficiency confirm hypothesis that the spatial heterogeneity of repolarization phase increases after myocardial infarction.

Methods: The preliminary analysis of HR-ECG in the repolarization period was carried out on the set of data of 14 normal subjects and 12 post-infarction patients. The examination was carried out in the electrically shielded room using the high-resolution ECG measurement system [2].

The system consists of 64 low noise amplifiers with 16-bit A/D converters (BIOSEMI, the Netherlands). Digital signals were transformed to the serial optical format and then were transferred to the computer via an optical fiber. The data acquisition was controlled by the LabView measurement software. To improve the signal-to-noise ratio the cross-correlation averaging and filtering methods were applied to 64 signals obtained from the lead position on the torso according to the University of Amsterdam lead system [3,5].

The-wave Shape Index (TSI), is a quantitative measure of individual T-wave shape and a ratio of the integral of ECG amplitudes in the T-wave period and the total length of the T-wave curve. In the analysis the normalized TSI parameter is used.

The distribution function method is based on normalized distribution function adopted from statistics to signals analysis and allows to measure shape similarity between signals. Δ parameter is a quantitative measure of difference between certain pattern of T-wave, calculated from control group, and each individual T-wave. Spatial distributions around the torso of these two parameters were analyzed.

The proposed TSI parameter and Δ parameter were calculated for all 64 ECG signals of each subject and presented as iso-amplitude maps. For TSI parameter departure maps were created i.e. map of each individual subject was subtracted from the mean map calculated for control group.

Results: The obtained results show that in certain areas on the torso surface, differences of T-wave shape between normal subjects and post-infarction patients are clearly seen. Below are the departure maps of TSI parameter (Figs 1(a), (b) and (c)) and maps of Δ parameter (Figs 2(a), (b) and (c)).

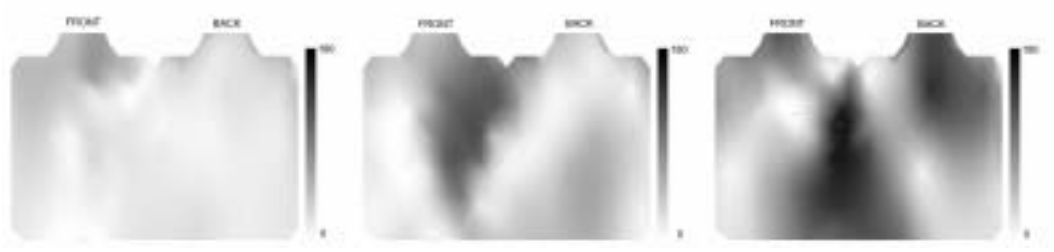

a) control subject b) patient after anterior infarction c) patient after anterolateral and inferior infarctions

Fig. 1. Departure maps of TSI parameter.

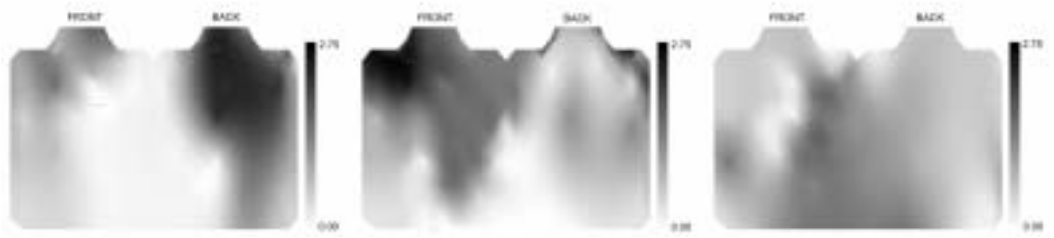

a) control subject b) patient after anterior infarction c) patient after anterolateral and inferior infarctions

Fig. 2. Maps of Δ parameter.

For TSI parameter differences in spatial variability of ventricular repolarization phase between healthy subject and patients are distinctly seen, for Δ parameter clear differences are seen only in precordial area due to large disparity of T-wave shapes in the group of healthy subjects in peripheral regions.

Discussion: Different parameters of repolarization phase assessment were introduced and it is well established that local changes of repolarization in the myocardium increase the risk for ventricular arrhythmia vulnerability. QT dispersion is the most often proposed parameter of repolarization inhomogeneity assessment, but the exact measurement of QT interval is practically difficult. The TSI parameter and Δ parameter were calculated for averaged beats in all 64 location on the thorax. Both proposed parameters are not depended on the accuracy of T-wave on- and offset detections. Only amplitude changes in the same time interval established time interval for all leads were taken into account.

It was observed that spatial heterogeneity of both parameters value are larger in examined patients with cardiac insufficiency then in normal subjects.

Obtained results indicate that spatial variability of both parameters might be a good marker of variability of T-wave morphology and could reflect spatial repolarization gradient.

References

[1] M. Fereniec, M. Kacprzak, G. Karpiński, R. Maniewski, G. Opolski and D. Ircha: Evaluation of T-Wave Morphology in High – Resolution ECG Mapping, *International Journal of Bioelectromagnetism* **4**(2) (2002), 101–102.

[2] M. Fereniec, M. Kacprzak, R. Maniewski, A. Zbiec and D. Ircha, The 64 channel system for high resolution ECG mapping, in Proceedings of Computers in Cardiology, 2001, 28:513–515.

[3] R. Hoekama, G. Uijen and A. van Oosterom, On Selecting a Body Surface Mapping Procedure, *J Electrocard* **32** (1999), 93–102.

[4] C.S. Kuo, K. Munakata, C.P. Reddy and B. Surawicz, Characteristics and possible mechanism of ventricular arrhythmia dependent on the dispersion of action potential durations, *Circulation* **67** (1983), 1356–1367.
[5] R.L. Lux, C.R. Smith, R.F. Wyatt, A.K. Evans, G.M. Vincent and J.A. Abildskov, Clinically practical lead systems for improved electrocardiography: Comparison with precordial grids and conventional lead systems, *Circulation* **59** (1979), 356–363.

Bioanalytical and Medical Trends in Sensor Applications

Project overview LOCOMED

M. Fleischer, E. Simon and K. Abraham-Fuchs
Siemens AG, Munich and Erlangen, Germany
Tel.: +49 89 636 40049; Fax: +49 89 636 46881; E-mail: Maximilian.Fleischer@siemens.com

Introduction to LOCOMED project: The project LOCOMED (Low-Cost Gassensor System in Mikrosystems Technology for Medicine and Biotechnology) is a joint university/industry research project devoted to the development of innovative sensors for medical use and biological process control. It was partly funded by the German Ministry for Education and Research in the framework of the successful program "micro system technique 2000+" and was executed under the supervision of VDI/VDE-IT (Teltow), with the project co-ordination done by the Siemens AG. Its duration ranged from January 00 to June 03.

The medical applications follow the approach, known since medieval times, that the smell of the body odor of humans or the exhaled air gives an indication for the presence of a diseases. The technical implementation was done by the development of new gas sensors for the detection of disease marker gases in exhaled air of humans. This additional diagnostic means is intended to give a contribution to the field of disease management. Besides ethical issues, there is a strong financial drive for this due to cost reductions that are available with the use of disease management (see Fig. 1).

The biotechnological applications relate to the detection of lead substances in biotechnological processes in the liquid phase, based on newly developed sensors. Such substances give an indication about the state of the biotechnological process as a foundation for a reliable process control. The cost saving potential for this applications are regarded as substantial, since few means for the on-line monitoring of biotechnological processes are available up to now.

Medical application: The choice of the medical application was done based on known clinical trials investigating disease marker gases in breath. On the other hand attention has to be paid to the patient numbers in the most widespread chronic diseases, hypertension (12 Mio), Asthma (4 Mio), Diabetes (4 Mio), congestive heart failure (1 Mio), values for Germany. Based on the assumption that the double number of the hospital cases gives a rough indication of the possible users of a breath analysis tool for disease management, the potential numbers of users have been estimated between 300000 and 600000 in Germany for these diseases.

The target of monitoring the acetone as a Diabetes marker in exhaled air had to be waived despite the advantage of the high acetone permeability from the blood to the alveolar gas. Reasons have been the high inter- and intra-patient variability (1,2–1880 ppb Acetone in breath), a low range of exploitable acetone concentration change from diabetic to non-diabetic of about a factor 2–3, and the availability of few relevant clinical trials.

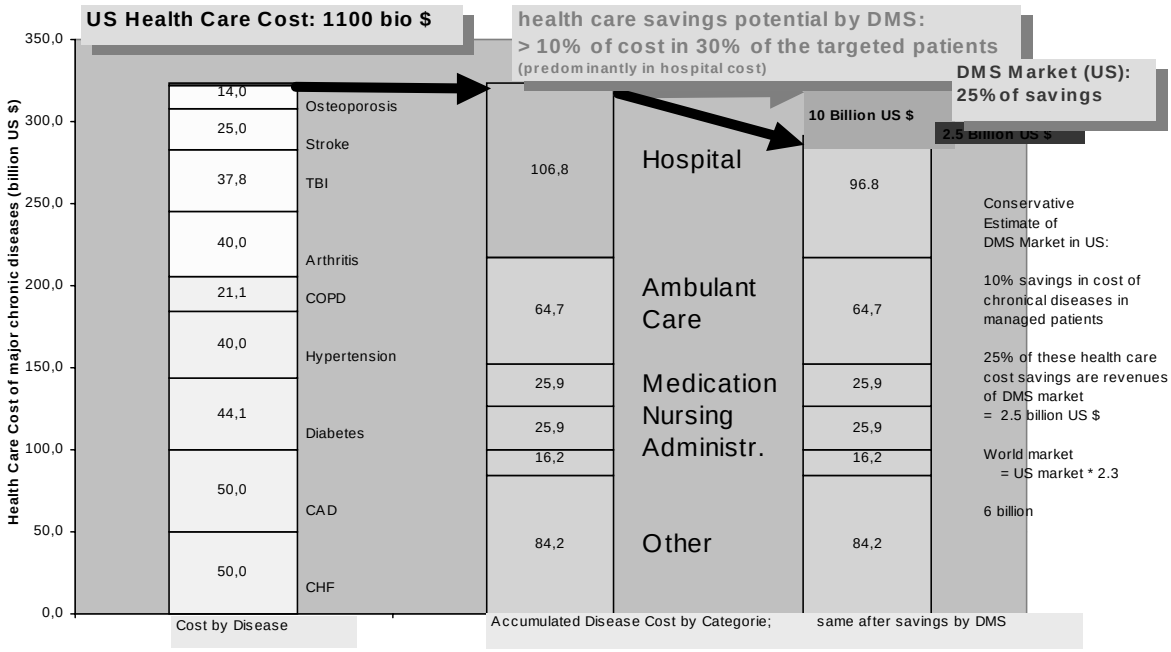

Fig. 1. Overview of US health care costs with an indication of the cost saving potential of stringent disease management (DSM) effort.

Table 1
Clinical trails investigating disease markers in breath since 1996

Analyte	Number of studies done	Topic
H2	86	Digestion: H2 as Indicator for incomplete usage of Hydrocarbons
NO	36	Asthma, esp. with children
Ethanol	22	Ethanol in blood
CO	8	Marker for oxidative Stress
NH3	6	Protein Digestion
Others		Isoprene (5), Pentane (3), Acetone (3), Methanol (2)

The motivation for selection of Asthma Bronchiale as medical target application were clearly given. Besides the fact that it is a widespread disease with 5–15% of the population in industrialised countries suffering from it, a well defined marker gas exists, This is nitrogenmonoxide (NO) which constitutes a general biomarker for pulmonary inflammation processes. To allow the detection of acute Asthma Bronchiale, NO gas concentration in breath: have to be detected which undergo a significant change from 5–10(24) ppb (normal) to a level of 30–100 ppb before an Asthma attack emerges. The use can be twofold: a raised level of NO gives an indication of Asthma Bronchiale for improved diagnosis. On the other hand, the use of inflammatory repressive medication decreases the NO level to normal values. The control of the NO concentration in breath therefore can be used for therapy control, with the NO level indicating the exigency of the use of another dose of medication.

Technology used: A novel gas sensing technology was investigated to selectively detect the low NO-levels. A new type of gas sensor [1] has been developed, which is based on a field effect transistor that has a suspended gate covered with a gassensitive layer. When the gas to be detected adsorbs at the gassensitive layer, a small voltage is generated at the surface of the sensitive layer (physically spoken, a change of the work function) and this voltage is amplified to give a variation in the transistor current. The

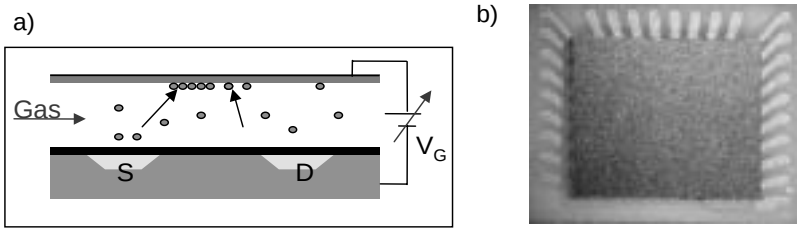

Fig. 2. Scheme of the gas sensors developed. a) The schematic view of the suspended gate FET. b) The actual realization with a Si-Chip (middle) region bonded onto a ceramic carrier substrate, with the larger dimension being roughly 1 cm.

Fig. 3. Sensor for detection of target substances in biotechnical liquids, based on the electrical readout of enzymatic procured detection processes.

basic set-up is given in Fig. 2. The technology of the suspended gate FET has been further developed to fulfil the sensing demands These devices are equipped with sensing layers based on porphyrine dyes [2, 3] that enable the gassenstive FETs to detect nitrogendioxide concentrations down to 10 ppb in the human breath. This is based on a transformation of NO to NO_2 by an oxidation step and the detection of the NO_2 by the gas sensor. Based on these sensors, a detection system for the NO in human breath have been developed. The detectability of the Asthma relevant concentrations is shown on the level of a laboratory demonstrator.

Other applications: Other activities in the field of breath analysis use sensors based on a conductivity-readout of polymers with extremely high susceptibility to other relevant trace gases in the human breath. Starting with the detection of ultra-low levels of Thymol, arrays for breath analysis have been constructed using this technology. It turned out that the application of polymer sensing technology can be extended to the detection of certain biological trace substances in liquids. Sensing layers with a big variety of detection properties have been developed by SENSOBI sensors company. Based on these, a sensor array with intelligent signal evaluation methods (based on the mathematics of patter recognition) have been developed, which is capable to distinguish different patters of detected species to allow the recognition of specific states of the medium under investigation.

The work on sensors for the liquid phase had another strong focus on sensors for monitoring biotechnical processes. and was mainly performed by the company TRACE. Examples for biotechnical processes to be monitored are beer fermentation, where the unintentionally generation of Diacetyl (2,3 Butadion) as a flavoring material gives rise to an unwanted butter-like taste. Other examples are the generation of acetic acid which occurs occasionally in the fermentation of E. coli, which limits then growth of the cells, or the monitoring of the level of Ammonia/Ammonium which is used as nitrogen source in

fermentation processes e.g. in the production of amino acids. For such applications, new sensors based on enzymatic reaction with electrical readout (amperometrical and voltametric) have been successfully developed, see Fig. 3. Based on the selective enzymatic decomposition of the analyte (substrate) to be detected, electrically active species are generated at the sensors surface that can be detected by electrical measurements done by the sensor in the biotechnical liquid. Target substances to be detected are Urea, Ethanol and Ammonia The functionality of the sensors has been demonstrated by the example of the detection of urea, ammonia and potassium.

References

[1] R. Pohle, E. Simon, M. Fleischer, H. Meixner, H.-P. Frerichs, M. Lehmann and H. Verhoeven, Proc. 12th International Conference on Solid-State Sensors, Actuators andMicrosystems, TRANSDUCERS 2003.
[2] M. Fleischer, E. Simon, E. Rumpel, H. Ulmer, M. Harbeck, M. Wandel, C. Fietzek, U. Weimar and H. Meixner, *Sensors & Actuators* **B83** (2002), 245–249.
[3] E. Simon, M. Fleischer and H. Meixner, Proceedings Eurosensors XVI, Prague, 15.-18.9.2002, p. 647.

Denoising of surface EMG signals: A comparision of wavelet and classical digital filtering procedures

Tamara Grujić and Ana Kuzmanić
Faculty of Electrical Engineering, Mechanical Engineering and Naval Architecture, University of Split, Rudjera Boskovica bb, 21000 Split, Croatia
E-mail: tamara.grujic@fesb.hr

Introduction: The scope of this work is the rejection of motion artefacts and white noise from EMG signals, both synthetic and experimentally recorded. Several filtering techniques were tested and compared: classical passband filtering procedures and wavelet based methods which use discrete wavelet transformation and application of thresholds. Several different wavelets and threshold methods were employed and results were compared.

The electromyographic (EMG) signal gives us the access to the physiological processes involved in producing joint movements [1]. The information extracted from the EMG signal can be exploited in several different applications [2]. One of such information is defined as muscle activation intervals, which is of paramount importance in numerous clinical applications [3]. The information acquired by the electromyographic signal is affected by white noise introduced by electronic equipment and by artefacts due to the movements of the electrodes over the skin. Motion artefacts are characterised by low-frequency components (0–15 Hz), with relatively high power. These noises strongly affect the detection of onset and cessation times of muscle activity. Therefore, in order to perform an accurate observation of muscle activity, the noise must be efficient removed from the signal.

All the data processing and graphical presentation of results is done by Matlab software package, MathWorks Inc.

Data acquisition: Electromyographic measurements were performed on one healthy adult, during gait trial. EMG signals were measured and collected by EMG system designed and developed at our laboratory, LaBACS, in collaboration with Laboratory of Biomedical Engineering, University of Ljubljana. Electromyographic activity of muscles tibialis anterior and soleus was recorded using a pair of concentric

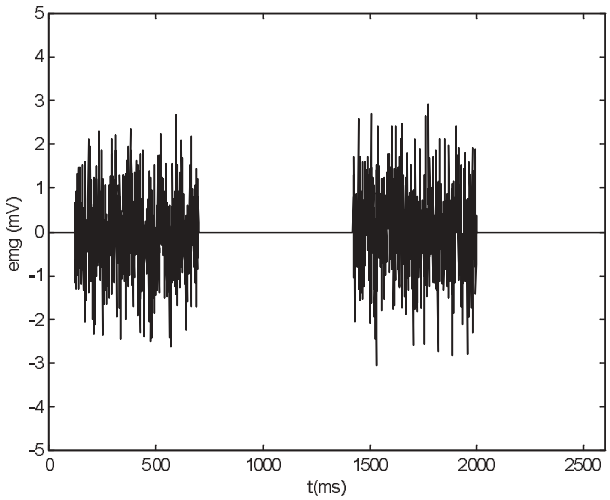

Fig. 1. Synthetic EMG signal.

surface Ag-AgCl electrodes, type P00S-blue sensor, from Medicotest Inc. manufacturer. The spacing between recording contacts was 30 mm. Measured signals were amplified by an bioamplifier with the following characteristics: the overall gain is 2000, the bandwidth is 3–500 Hz. The CMRR of the preamplifier has a high value of 130 dB, which ensures an optimal rejection of common mode input signal. The amplified signal is passed to 12-bit AD converter and sampled with sampling frequency of 1000 Hz.

White noise removal by DWT and thresholding: The general wavelet denoising procedure is as follows [4]:

- Apply DWT to the noisy signal to produce the noisy wavelet coefficients.
- Select appropriate threshold limit at each level and threshold method (hard or soft thresholding) to best remove the noises.
- Perform inverse wavelet transformation of the thresholded coefficients to obtain a denoised signal.

Three different methods for the calculation of threshold limits, implemented in Matlab's Wavelet Toolbox, were used in this work: Minimax method (minimaxi), Stein's Unbiased Risk Estimate method (rigrsure) and Visually calibrated method (sqtwolog).

Artefact removal from EMG signals by wavelets: EMG signals usually contain low frequency noise ranging from 0 to ~ 15 Hz. In this work the following procedure for the artefact removal is implemented:

- Prior to the decomposition of EMG signal by DWT, the level of decomposition, J is calculated as follows:
  $\frac{F_s}{2^{J+1}} \approx f_{\mathrm{noise}}$; if $F_s = 1000$ Hz and $f_{\mathrm{noise}} = 15$ Hz, J is obtained to be 5.
- DWT of J-th level is performed. Approximation coefficients on 5-th level, cA_5 represent EMG signal in frequency range from 0, up to $F_s/2^6 \approx 15$ Hz. Therefore, these coefficients represent artefact and will be removed (replaced by zero values) in order to clean artefact from the signal. Detail coefficient are left unchanged.
- Performation of signal reconstruction.

Implementation of WBNR on synthetic EMG signal: In order to test WBNR techniques and compare them to classical filtering methods, we have simulated the EMG signal, as follows. The synthetic

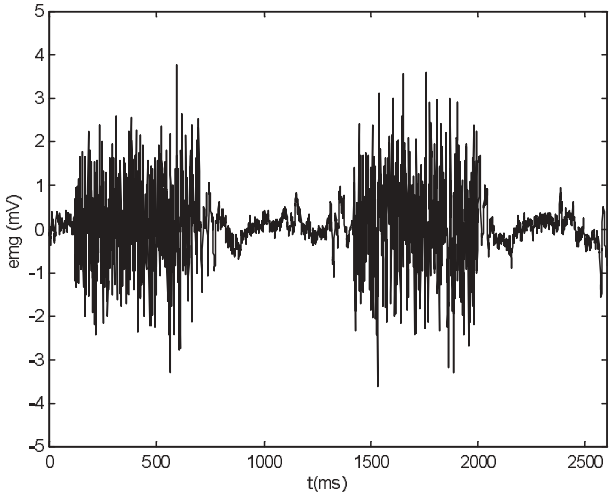

Fig. 2. Test signal: synthetic EMG signal+white noise+low fr. artefact.

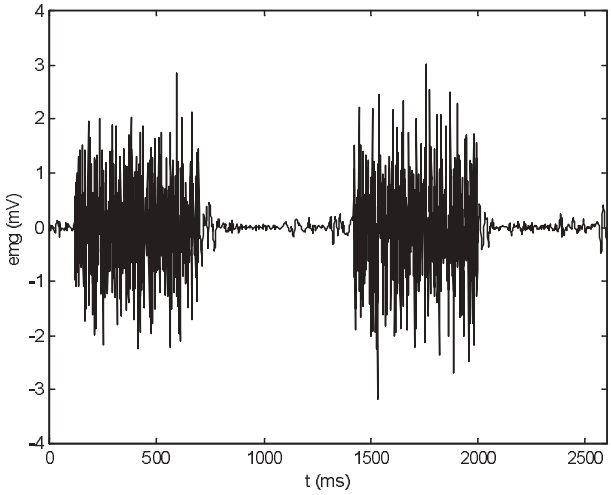

Fig. 3. Test signal filtered by db5 wavelet and soft rigrsure threshold.

electromyogram, shown in Fig. 1. was generated by amplitude modulation of Gaussian white noise, $N \sim (0, 1)$. Signal is consisted of two active intervals, separated by resting intervals with no EMG activity. Sampling frequency is 1000 Hz and the duration of signal is 2.6 s. Then, the signal is contaminated with normally distributed white noise, and with an artefact pattern, extracted from real EMG signal, measured on soleus muscle during gait. So obtained signal, shown in Fig. 2, consists of two different zones: a burst zone where noises and myoelectric activity coexist and an inter-burst zone where only noise contribution is present. The signal has the SNR $= 7.9$ dB and will be used as test signal. DWT with 5 decomposition levels was performed and following wavelets were used: Daubechies5 (db5), Daubechies8 (db8), Symmlet8 (sym8) and Coifflet5 (coif5). Low frequency artefact is filtered by elimination of approximation coefficients of the 5th level. White noise is filtered by thresholding detail coefficients of levels 1 to 5. Standard band-pass filters used for comparison with WBNR techniques were an eight order Butterworth filter and an eight order Chebyshev. Filter's coefficients were calculated

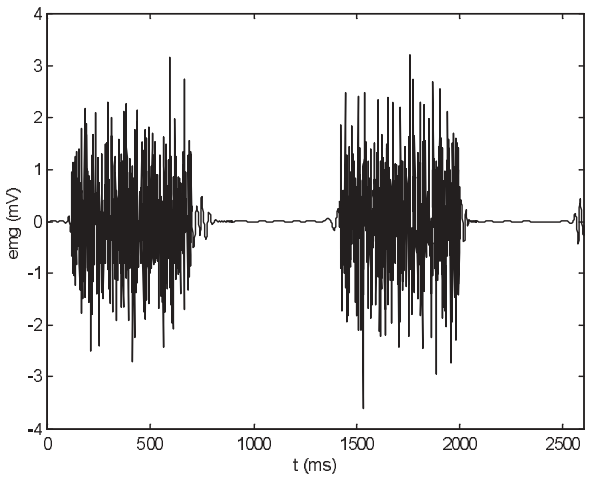

Fig. 4. Test signal filtered by db5 wavelet and hard sqtwolog threshold.

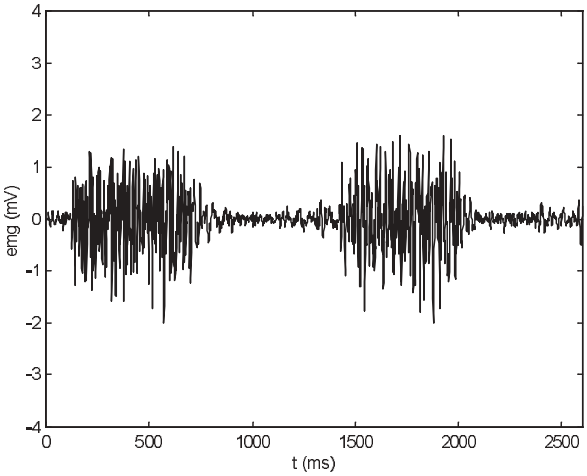

Fig. 5. Test signal filtered by Butterworth filter.

Table 1
Statistics collected for test signal

WAV/FILT	TH. METHOD	S/H TH.	SNR (dB)	SKP
Db5	sqtwolog	hard	6.7315	0.0907
Db5	minimaxi	soft	5.9797	0.1078
Db5	minimaxi	hard	8.1494	0.0654
Db5	rigrsure	soft	8.6413	0.0584
Db5	rigrsure	hard	8.6107	0.0588
Db8	rigrsure	soft	8.6352	0.0585
Db8	rigrsure	hard	8.5748	0.0593
Sym8	sqtwolog	hard	6.7193	0.0909
Sym8	heursure	soft	8.7734	0.0567
Coif5	sqtwolog	hard	6.7011	0.0910
Coif5	minimaxi	soft	6.1294	0.1042
Coif5	heursure	soft	8.6737	0.0580
Butt	–	–	1.5677	0.6130
Cheb	–	–	0.9478	0.5315

for band pass ranging from 15 to 200 Hz. Table 1 shows the results of applying a variety of wavelet transform and filtering techniques to the test signal.

As expected, the results are more dependent on the threshold method than on the choice of wavelet. Soft rigrsure threshold, applied with db5 wavelet (Fig. 3) gives the best statistical results (SNR = 8.6413 dB, MSE = 0.0584). But, this method is known to be conservative, especially comparing to visually calibrated method (sqtwolog threshold) which gives excellent visual results: white noise from the resting intervals is almost completely removed (Fig. 4). Thus, there is an apparent trade-off between high SNR values and good visual quality, which is a subjective merit measure. Test signal filtered by Butterworth filter is shown in Fig. 5. Noticeably attenuation of signal amplitude at active intervals is present. Also, intervals of muscle resting are still contaminated with white noise. Therefore, statistical results, SNR and MSE, are very poor, for Butterworth as well as for Chebychev filter (Table 1).

Noise removal from EMG signal recorded during gait: Figures 6(a) and (b) present an experimental raw myoelectric signal, recorded on muscle tibialis anterior as described in Section 2, and it's power

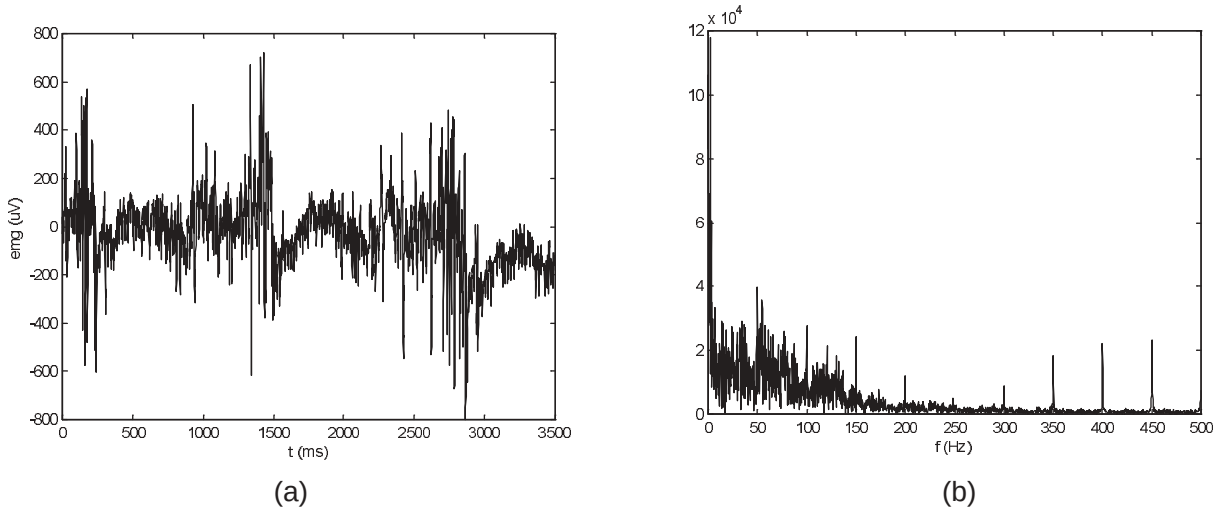

Fig. 6. (a) Raw signal recorded on *m. tibialis* anterior. (b) Power spectrum of the raw signal.

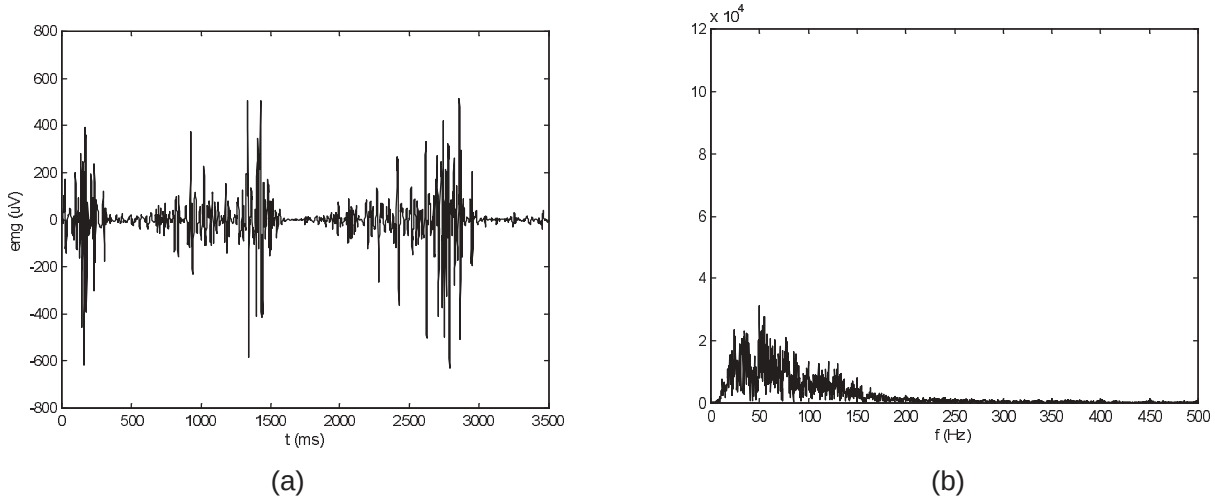

Fig. 7. (a) Signal filtered by wavelet method. (b) Power spectrum of signal filtered by wavelets.

spectrum. Signal is highly corrupted by artefact and white noise, and the accurate observation of muscle activity from the raw signal is not possible. Also, if we look at the power spectrum, the excessive presence of line interference on 50 Hz and higher harmonics can be noticed.

Figures 7(a) and (b) show EMG signal processed by wavelet and 8-th order bandpass (15–200 Hz) Butterworth filter, respectively. For wavelet filtering, fifth level decomposition with db5 wavelet, using soft sqtwolog threshold, was applied.

When comparing filtered signals and their spectrums, it could be seen that visually quality of wavelet filtered signal is much better than signal filtered by Butterworth filter. There is still excessive presence of white noise in signal on Fig. 8(a) and, therefore, it is hard to distinguish muscle activation intervals from intervals with no muscle activity. Also, wavelet filtering is better at removing line interference noise, as can be seen if we compare power spectrums on Figs 7(b) and 8(b).

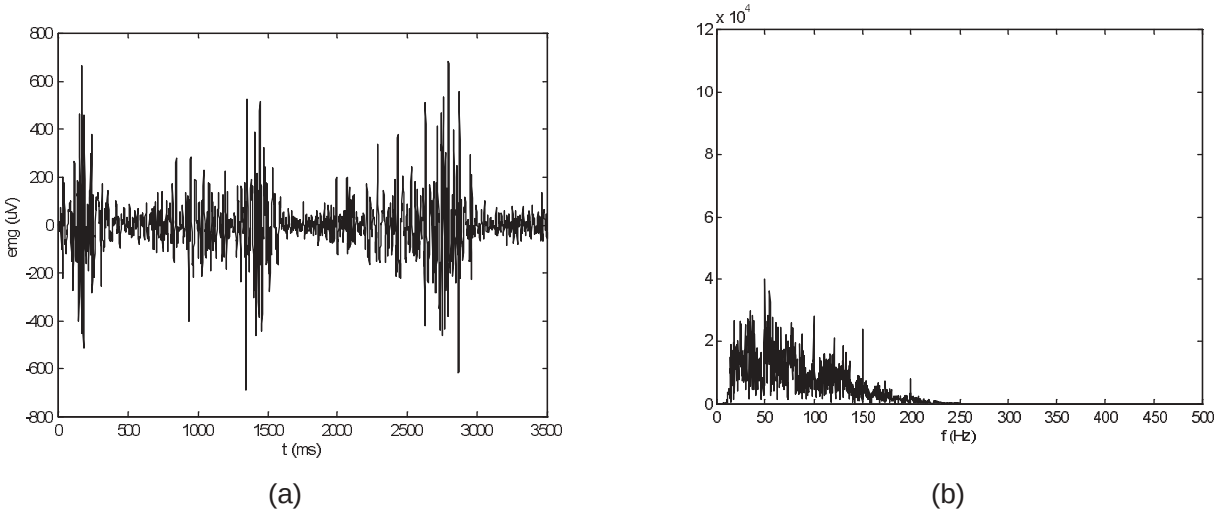

Fig. 8. (a) Signal filtered by Butterworth filter. (b) Power spectrum of signal filtered by Butterworth filter.

Conclusion: In this work the advantages of wavelet based noise removal techniques are emphasised. Quantitative merits as SNR and MSE of synthetically generated and denoised EMG signal were analysed and we can conclude that wavelet based denoising provides better results than widely used classical filtering methods.

Also, the efficiency of wavelet based noise removal has been tested on experimentally recorded EMG signal. Results show that reconstructed denoised signal clearly indicates muscle activity. Therefore, an accurate observation of activity that was not possible with conventional filtering methods, becomes possible with wavelets.

References

[1] C.J. DeLuca, The use of surface electromyography in biomechanics, *J. Appl. Biomech.* **13** (1997), 135–163.
[2] S. Micera, G. Vannozzi, A.M. Sabatini and P. Dario, Improving detection of muscle activation intervals, *IEEE Engineering in Medicine and Biology* **20**(6) (2001), 38–46.
[3] P. Bonato, T. D'Alessio and M. Knaflitz, A statistical method for the measurement of muscle activation intervals from surface myoelectric signal during gait, *IEEE Transactions on Biomedical Engineering* **45**(3) (1998), 287–299.
[4] M. Mitisi, Y. Mitisi, G. Oppenheim and J.M. Poggi, Wavelet toolbox user's guide, The Math Works Inc., 1996.g.

Intracanular electrical impedance imaging

J. Jossinet and A. Desseux
National Institute for Health and Medical Research, INSERM U556, Lyon, France
Tel.: +33 472 68 19 46; Fax: +33 472 68 19 31; E-mail: jossinet@lyon.inserm.fr

Introduction: The evaluation of the lesion produced by the treatment of the localised prostate cancer by therapeutic ultrasound and the detection of residual cancerous tissue are hindered by the lack of specificity and sensitivity of ultrasonography [2,6]. Experiments in bovine liver in vitro have shown

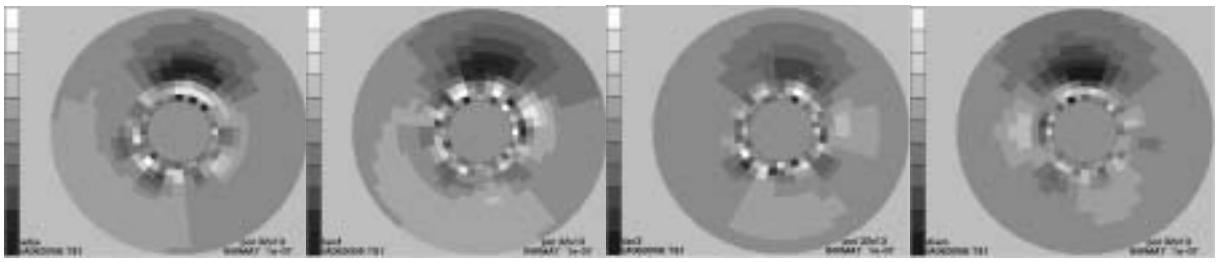

Fig. 1. The four tested drive patterns gave similar results. The displacement of the reconstructed target (darkest area) towards centre is attributed to the finite length of electrodes (50 mm). Diametric and fan3 drives shows lower noise level and smaller reconstruction lobes.

that the application of high intensity ultrasound gives rise to significant changes in a tissue's electrical impedance [7]. Electrical Impedance Tomography (EIT) gives images of the conductivity in the human body using surface electrodes [1], but is not suitable for prostate imaging, due to the size and location of this organ. The authors have developed Electrical Impedance Endotomography (EIE) where the electrodes are located on a probe placed at the centre of the region of interest [4,5].

Theory: The basic 2D mathematical model for EIE consists of parallel line sources on the surface of an insulating cylinder. In such a translationally uniform model, a disk of null conductivity surrounded by a conducting plane represents the probe and the medium to be imaged, respectively. The electrodes project as point sources regularly spaced at the circumference of the disk.

Application: The method was first tested *in vitro* using a 16-electrode prototype probe designed for this purpose [3] and a single frequency (8 kHz) hardware system. Figure 1 shows conductivity images reconstructed from an insulating target (6 mm in diameter) in tap water (of conductivity 38.5 mS/m) and located at 3 times the radius of the probe, according to 4 drive patterns (adjacent, fan4, fan3 and diametric) defined formerly [5]. At the real scale, with a probe 8 mm diameter, this represents a perturbation of about 1 mm located at a distance of 12 mm. This situation is compatible with the exploration of the prostate using a urethral probe.

Conclusion: EIE enables the visualisation of conductivity perturbations near the probe. The sensed volume is compatible with the exploration of the prostate using a urethral probe. Electrical Impedance Endotomography is also potentially usable for the intracanular exploration of vessels and ducts where it is possible to pass a catheter probe. The optimisation of the signal/noise ratio and the improvement of reconstruction algorithms are foreseen next steps in the development of this method.

References

[1] K. Boone, D. Barber and B.H. Brown, Imaging with electricity: report of the European Concerted Action on Impedance Tomography, *J. Med. Eng. Technol.* **21** (1997), 201–232.

[2] E.J. Feleppa and R.D. Ennis et al., Spectrum-analysis and neural networks imaging to detect and treat prostate cancer, *Ultrasonic Imaging* **23** (1997), 135–146.

[3] J. Jossinet and E. Marry, Design of a multi-electrode impedance urethral probe, 6th ESEM Conference, 3–5 May 2001, Belfast, UK, *Technology and Health Care* **9** (2001), 93–95.

[4] J. Jossinet, E. Marry and A. Matias, Electrical Impedance Endotomography, *Physics in Medecine and Biology* **47** (2002), 2189–2202.

[5] J. Jossinet, E. Marry, A. Montalibet and A. Matias, Electrical Impedance Endotomography: Imaging tissue from inside, *IEEE Trans. on Medical Imaging* **21** (2002), 560–565.

[6] T.A. Kirkland and J.E. Lathem, The role of transrectal ultrasound (TRUS) in the evaluation of cancer of the prostate, *J. South Carolina Med. Ass.* **90** (1994), 217–219.

[7] C. Trillaud and J. Jossinet, Ultrasound induced changes in the bioelectric properties of a tissue, 3rd Annual Conference on Therapeutic Ultrasound, Lyon, 2003, in press.

Wireless monitoring of distributed intelligent medical sensor systems

C. Moor[a,b], M. Schmidt[c] and A. Bolz[a,b]
[a]*Institue of Biomedical Engineering, University of Karlsruhe, Germany*
[b]*Corscience GmbH & Co. KG, Erlangen, Germany*
[c]*Chair for Microwave Engineering and High Frequency Technology, University of Erlangen, Germany*
Tel.: +49 9131 977986 0; Fax: +49 9131 97798 59; E-mail: Armin.Bolz@ibt.uni-karlsruhe.de

Introduction: One vision that has always existed in the extraction of medical parameters is wireless signal derivation. The current standard in medical parameter derivation, however, requires that the patient be completely connected to various cables. The obvious disadvantages, which include the patient's and caregiver's immobility and the creation of artifacts when the cables are moved, could be avoided by using wireless transmission technology. Eliminating the cumbersome cable connection would therefore result in an easier medical routine.

Using wireless sensors requires that analog measurement signals must already be digitalized in the transmitter. This is done with an A/D converter, followed by a microcontroller. Since the microcontroller usually isn't worked to capacity by the conversion and transmission of data, it's possible to transfer the intelligence from the monitor to the dedicated sensors.

Materials: The first step in developing wireless medical sensors is the selection of the transmission technology. Since no visual connection can be guaranteed in classical cable applications, as can be found in rescue services, sleep medicine and in intensive care units, the infrared standard of the Infrared Data Association (IrDA) can be eliminated. Therefore, for the transmission of medical sensor data, only a radio connection is possible. In order to keep the development costs as low as possible, the use of standardized transmission methods is recommended. Already existing radio modules can be used with no further problems, which can be programmed over defined transmission protocols, and which already have error correction and are robust against disturbances. Also, standardized radio transmission has the advantage of being compatible with other standardized applications. Therefore it is often sufficient to equip the data transmitter, in this case the medical instrument, with a wireless interface. When PCs, Laptops or PDAs are used as the monitor, the standard interface is usually already integrated. Also, it should be taken into consideration that usually the data of more than one instrument must be displayed on a monitor. One example can be found in emergency medicine, where the EKG, oxygen saturation and blood pressure are the typical derived signals which appear on the monitor. The radio technology which fulfills all the above requirements is Bluetooth [1].

The first developed wireless sensors included the wireless EKG BlueECG and the pulse oximeter BlueOxy, introduced in [2]. Here, it was shown how Bluetooth technology can be used for the transmission of medical data.

Methods: One of the biggest challenges in the development of wireless medical instruments is the integration of the measurement sensors in the transmitter. This is necessary because the signals are analog when they're being derived, must sometimes be amplified, and then the signal is converted by an A/D converter from an analog signal (A_0) to the digital signal (D_0). In digital form, the signal can be sent wirelessly to a monitor (see Fig. 1).

Fig. 1. Data extraction of analog signals for wireless transmission, A_0: analog signal, D_0: digital signal, $\vec{D}_0$: pre-processed digital signal.

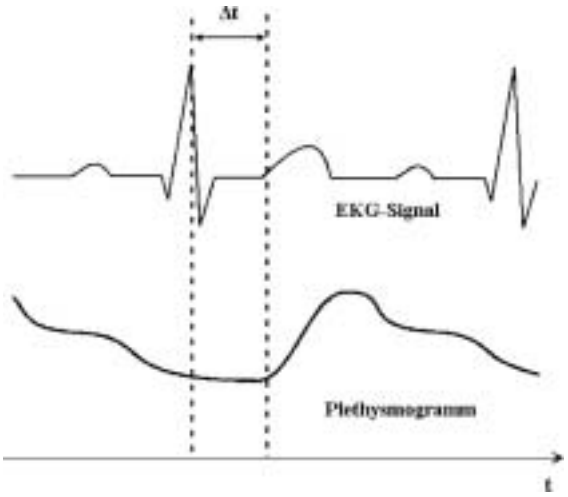

Fig. 2. Measurement of the average pulse transit time Δt.

In order to reduce the actual data to be transmitted, the next step is to integrate as much intelligence as possible into the sensor itself. A pre-processed measurement $\vec{D}_0$ is then transmitted. One example for the development of intelligent dedicated sensors is the measurement of the average pulse wave transit time over BlueECG and BlueOxy.

The pulse transit time is directly proportional to blood pressure and can therefore be used as an indicator for an elevation or drop in blood pressure. In order to determine the average pulse transit time, characteristic points in the time domain are calculated. The start-time is determined with the detection of the R-peak in the EKG, which approximately indicates the time when blood is expelled from the heart into the aorta. The end-time is determined by means of the artificial base of a peripheral pulse wave (see Fig. 2). A plethysmograph from a pulse oximeter finger sensor is suitable for the peripheral pulse wave [3].

The artificial base is best detected over two points, the base and the point of maximum incline in the plethysmograph. The tangents of both points are drawn, and the intersection of these lines is the artificial base. The advantage of this method is that information from two points is used, which makes it more robust against disturbances [3].

In order to be able to determine the PTT of the R-peak and the artificial base in the receiver, both signals are given a time stamp. This allows both sensors to be synchronized to each other in the Bluetooth monitor. The measurement can be extracted at the monitor by simply subtracting the two measured times.

Results: If calculations are carried out in the sensor, it's enough to send the final measurement $\check{D}_0$. This reduces the bit rate over the wireless interface, which also reduces the spent power. Since power consumption is the main exclusion criterion for wireless sensors, it's absolutely necessary to reduce this in any way possible.

Another advantage of having intelligence integrated in the sensor is the simple connection of instruments on various monitors. Since the absolute values on the monitor don't have to be calculated, the monitor only has to act as a display unit. This offers the developers of OEM devices (OEM – Original Engineered Manufacture) the possibility to demarcate their development and knowledge.

Discussion: When displacing intelligence into a battery operated autarkic system, it's always to be determined whether a low-consumption microcontroller is able to process the algorithms. The greatest advantage of this solution is lost when more power is needed in the end.

Conclusions: The determination of the PTT over the Bluetooth sensors BlueECG and BlueOxy is an example for the displacement of signal processing in wireless medical sensors. The announced microcontroller and Bluetooth modules are smaller and have higher processor performance with reduced energy consumption. The trend toward autarkic wireless medical sensor systems is, therefore, continuing.

References

(Conference Submissions)
[1] C. Moor, M. Schwaibold, J. Schöchlin and A. Bolz, Bluetooth als drahtloses Datenerfassungsnetzwerk für medizinische Anwendungen, *Biomedizinische Technik* **46**(1) (2001), 488–489.
[2] C. Moor, M. Schwaibold, H. Roth, J. Schöchlin and A. Bolz, Entwicklung drahtloser Sensoren auf Basis von Bluetooth, *Biomedizinische Technik* **47**(1) (2002), 325–327.
(Books)
[3] P. Elter, Methoden und Systeme zur nichtinvasiven, kontinuierlichen und belastungsfreien Blutdruckmessung, Dissertation Universität Karlsruhe, 2001.

Bioanalytical and Medical Trends in Sensor Applications

Organic layers for field effect application

A. Oprea, J. Claußen, C. Fietzek, M. Harbeck, H.-G. Mack and U. Weimar
Institute of Physical & Theoretical Chemistry, University of Tuebingen, Auf der Morgenstelle 8, 72076 Tuebingen, Germany
Tel.: +49 7071 2978765; Fax: +49 7071 295960; E-mail: alexandru.opera@ipc.uni-tuebingen.de

Introduction: The detection of specific gaseous or volatile compounds encountered in human breath can facilitate both medical diagnosis and patient ambulatory surveillance. Having the opportunity to control themselves their health state and to act in a suitable manner many patients will be able to further live a near normal life. This could be seen, from the medical side, as a more efficient and friendly medical practice. The possibilities offered by the chemical sensors [1], especially equipped with gas sensitive field effect transducers (FET) [2], have been already tested and focused investigations are in progress. We present now some experimental and theoretical results concerning organic layers sensitive to NO_2 and NH_3 required for asthma and protein digestion diagnosis – In asthma bronchialis actually NO is the disease trace present in exhalation. The lack of sensitive layers for NO implies however its catalytic oxidation to NO_2 [3].

Experimental: Several thin metal-phthalocyanine (MePc) and polymer layers were deposited by thermal vacuum evaporation and liquid phase pulverization (spray) onto gold/platinum/alumina or

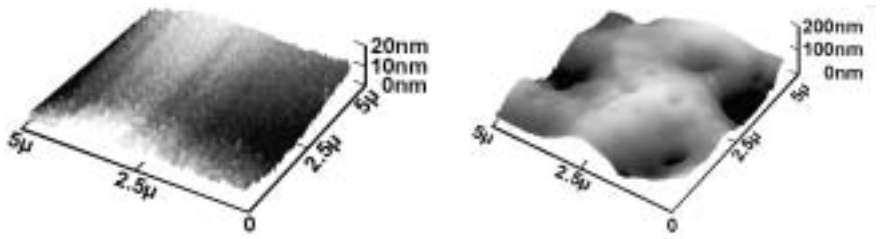

Fig. 1. AFM pictures of the bare Au/Ti/Alumina substrate (left) and a polyacrylic acid layer (right).

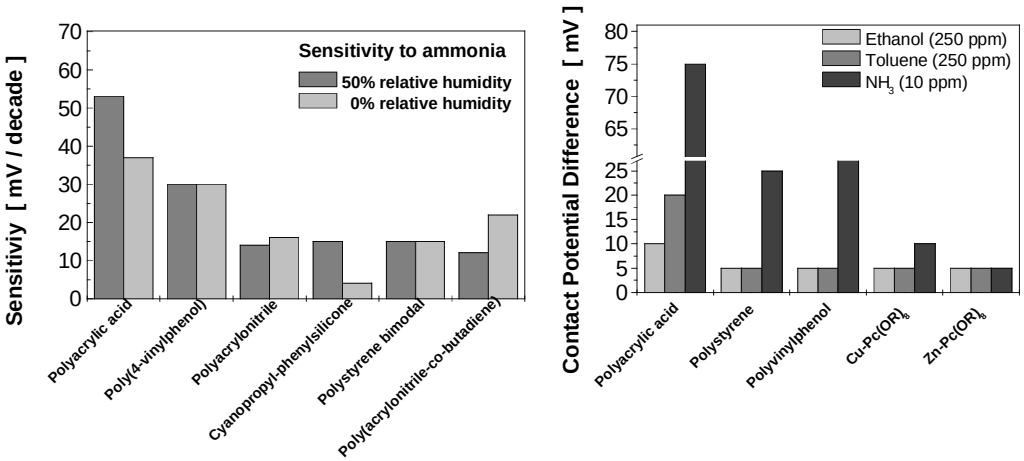

Fig. 2. The sensitivities (left) and the main cross sensitivities (right) presented by different sensing layers.

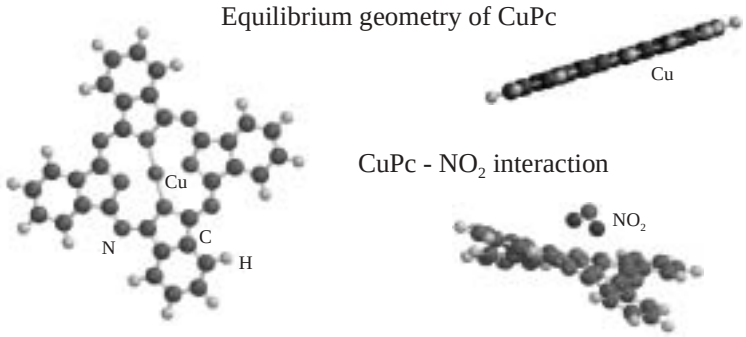

Fig. 3. The modification of the CuPc molecular structure under NO_2 influence. LDA computation.

gold/titanium/silicon substrates. Geometrical (thickness, coverage) and morphological (structure, roughness) parameters were investigated with a optical microscope and profiler, stylus profiler, electronic scanning microscope and atomic force microscope (AFM).

The potential difference (named contact potential difference, CPD) between the layer surface and a reference gold electrode was measured with a Besocke Delta-Phi Kelvin Probe. The standard response to the target analytes (NO_2, NH_3), other gases (CO, CO_2, methane) or vapours (water, ethanol, toluene) was considered the shift of this CPD parameter. In cooperation with E. Simon and M. Fleischer from

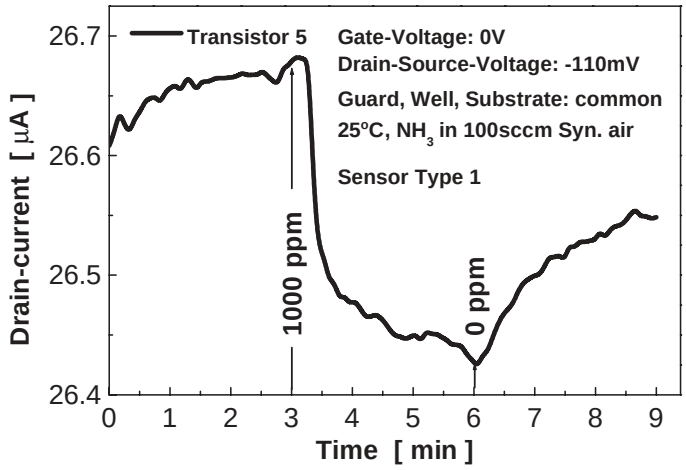

Fig. 4. The polyvinylphenol FET signal in the presence of the target analyte NH_3.

Siemens AG, also flip-chip suspended gate transistor structures with polymer gate were realized and gas tests performed. The metal-phthalocyanine layers were analysed additionally by *in situ* x-ray (XPS) and ultraviolet (UPS) photoemission spectroscopy in order to elucidate the influence of the analyte on the electronic structure of the sensitive layer and consequently the sensing mechanisms.

Theoretical: Ab initio calculation in the frame of the local density approximation (LDA) with Gauss orbitals were done (Jaguar 3.5 programme [4]) to simulate the gas-analyte interaction process.

Results and discussions: The thin sensitive layers prepared from the above mentioned materials show good structures with a reduced roughness (< 300 nm), suitable for field effect transducers. One typical example is depicted in Fig. 1.

The CPD response of the sensing films is depending nearly logarithmically on the concentration due to a Langmuir-type absorption isotherm. The sensitivity presented by CuPc to the target gas NO_2 was in the range of 30 mV/decade – 30 mV CPD shift are obtained for 10 times analyte concentration increase – with an estimated detection limit in the range of 50 ppb. Figure 2 depicts the sensitivities and the main cross sensitivities presented by different sensing layers. Polyacrylic acid is among the tested polymer layers the most sensitive to NH_3 in dry and humid air with a sensitivity of 53 mV/decade.

The response and recovery times of the investigated films were in the range of 30–120 s and respectively 100–500 s depending on temperature and humidity. Long term stability tests have been performed for some materials with encouraging results. Polyacrylic acid shows after more than 1 year, no or not very important functional changes or structural damages.

UPS experimental data revealed the contributions brought to the CPD shifts by different terms expressing the material structure and its interaction with the gaseous analyte. The theoretical simulation reproduced well the modification of the MePc electronic structure under analyte influence and gave an intuitive image of the interaction effects on the molecular structure (Fig. 3).

First sensitivity tests made with the flip-chip FET having polyvinylphenol sensitive layer were positive. An example sensor signal is shown in Fig. 4.

Further improvements in layer preparation, transistor production and mounting technology have still to be achieved for stable and reliable devices used in medical applications.

Conclusion: The performed studies pointed out that, battery driven devices with gas sensitive field effect transistors for the detection of specific analytes in human breath and/or ambient air are feasible.

Acknowledgements: The authors acknowledge the financial support by the BMBF (Project "LocoMED", 16SV1083/6).

References

[1] M. Fleischer, E. Simon, E. Rumpel, H. Ulmer, M. Harbeck, M. Wandel, C. Fietzek, U. Weimar and H. Meixtner, *Sensors and Actuators* **B83** (2002), 245–249.
[2] M. Fleischer et al., *Sensors and Actuators* **B80** (2001), 169–173.
[3] E. Simon, K. Abracham-Fuchs, M. Fleischer and H. Meixtner, Present volume.
[4] Jaguar 3.5 program, Schrödinger Inc., Portland, OR, 1998.

Analysis of cervical stabilization systems influence on changing in intervertebral disc pressure

C. Pezowicz[a,*], S. Szotek[a], J. Filipiak[a], R. Będziński[a], W. Jarmundowicz[b] and W. Szarek[b]
[a]*Institute of Machine Design and Operation, Wroclaw University of Technology, Wroclaw, Poland*
[b]*Department of Neurosurgery, Wroclaw Medical University, Wroclaw, Poland*

Introduction: Experimental investigations analyzing the intradiscal pressure of cervical spine are less common than other region of spine [1,2]. The aim of this paper is the comprehensive estimation of the influence of intervertebral stabilization in the cervical spine segment on the biomechanics of the cervical spine, particularly on the pressure changes within the intact and stabilised part of the spine. A biomechanical study was performed using cadaveric cervical spine.

Methods: The twelve cervical spines were used for this biomechanical testing. Specimens were divided into the following two groups: long spines (C2-C7) and short spines (C3-C6). The fresh spines were stripped of soft tissues, sparing the ligaments and articular structures. Radiographic and computer tomography examination of the specimens showed normal no degenerative changes and no deformity or anatomic defects. All biomechanical testing was performed on a biaxial material testing machine (MTS 858 Mini Bionix Test System), in a nondestructive manner. The upper and lower vertebral bodies of the specimens were mounted rigidly with two polyester resin cats and in cylindrical pots in a neutral upright orientation.

The loading types performed included axial compression, flexion and extension. In axial compression, the specimens were subjected to 200 N with a compressive preload 50 N. Flexion/Extension displacement $+15$ mm/-15 mm was applied. The biomechanical testing sequence of the spinal constructs was as follows: each specimen was first tested intact, subsequently, the specimen was destabilized, then reconstructed by using: bone graft, bone graft and anterior fixator plate.

During each biomechanical test, intervertebral disc pressure measured by a strain-gauged pressure transducer mounted in needle. The transducers were inserted into intact disc below and above planning and performed stabilization.

Conclusion: Investigations prove that difference of pressure in nucleus pulposus for healthy spine and after stabilization are significant. Stabilization of one segment cause to removement of one of important movement joint. In consequence of that change of movement appears in the part above and below stabilised part and, what is connected, in the changes of recorded pressure.

Acknowledgement: This work was supported by the State Committee for Scientific Research, grant No. 8 T07B 011 21.

*E-mail:celina.pezowicz@pwr.wroc.pl.

References

[1] D. Skrzypiec, C. Wigfield, P. Pollintine and M. Adams, The internal mechanical functioning of human cervical intervertebral discs, *Acta of Bioengi. and Biomech.* **4**(1) (2002), 54–55.
[2] J.C. Eck, S.C. Humphreys, T.H. Lim, S.T. Jeong, J.G. Kim, S.D. Hodges and H.S. An, Biomechanical study on the effect of cervical spine fusion on adjacent-level intradiscal pressure and segmental motion, *Spine* **22**(27) (2002), 2431–2434.

Bioanalytical and Medical Trends in Sensor Applications

Detection of breath gases via gas sensitive field effect transistors for asthma diagnosis

E. Simon, K. Abraham-Fuchs, M. Fleischer and H. Meixner
Siemens AG, Corporate Technology, D-81739 München/Erlangen, Germany
Tel.: +49 89 636 4433; Fax: +49 89 636 46881; E-mail elfriede.simon@siemens.com

Introduction: Investigations of the human breath with analytical methods have shown a correlation of volatile compounds with the occurrence of certain illnesses [1], therefore breath analysis can play an important role in the field of disease monitoring, therapy and diagnosis. Sensor systems promise a number of advantages as compared to traditional diagnostic techniques: not invasive, be expanded to mobile use (home care), highly suited for monitoring purposes. The medical community is especially interested in low cost and low power sensor devices for fast and convenient monitoring, especially with hand held devices. The application of work function type gas sensors based on field effect transistors (FET) has the potential to fulfil these requirements [2]. In the case of pulmonary inflammation processes of the lower respiratory tracts, e.g. asthma, the nitrogen monoxide concentration in breath increases. Normally, the amount of NO is between 5 ppb and 10 ppb. In case of an asthma disease (during asthmatic exacerbations) the NO concentration steps up to 80 or 100 ppb [3].

Methods: The screening of gas sensitive layers for the detection of NO was carried out using Kelvin probes (made by Besocke [4]). Different porphine dyes were prepared with different layer techniques like screen-printing technique or vapour deposition on a metallized alumina substrate. The gas sensor set up was carried out in hybrid flip chip technology. For that purpose the sensor layer is prepared on a gold metallized ceramic gate and electrically connected to the FET by conductive polymer bumps.

Results: During our investigations we found out that some porphine dyes are highly sensitive to nitrogen dioxide gas down to the lower ppb-range if they were used as gas sensitive layers for work function measurements. Especially phthalocyanines and protoporphyrines with or without Cu as metal atom, or with a side group derivatization showed a high NO_2 sensitivity [5]. Due to the thermal instability of the protoporphyrines only the phthalocyanines were taken for further tests. Cupper phthalocyanine showed the best performances concerning sensitivity, response time and selectivity. It has a low cross sensitivity to relevant breath gases like acetone, oxygen or ethanol and a low cross reaction to humidity which makes this sensor layer well suited for a breath analysis systems. Gas measurements with this sensor layer used in our suspended gate FET device showed a sensitivity of 42 mV/decade (in the range of 10 to 100 ppb NO_2) with a detection limit of 2 ppb and a log dependency of the sensor signal at different NO_2 concentrations. Due to a cross talk of the sensor device to ethanol and humidity additional sensors should be implemented in the asthma device in order to correct the sensor signal. The fact, that for the detection of asthma a NO sensor is required, an NO oxidation step to NO_2 by a catalyst is necessary. An

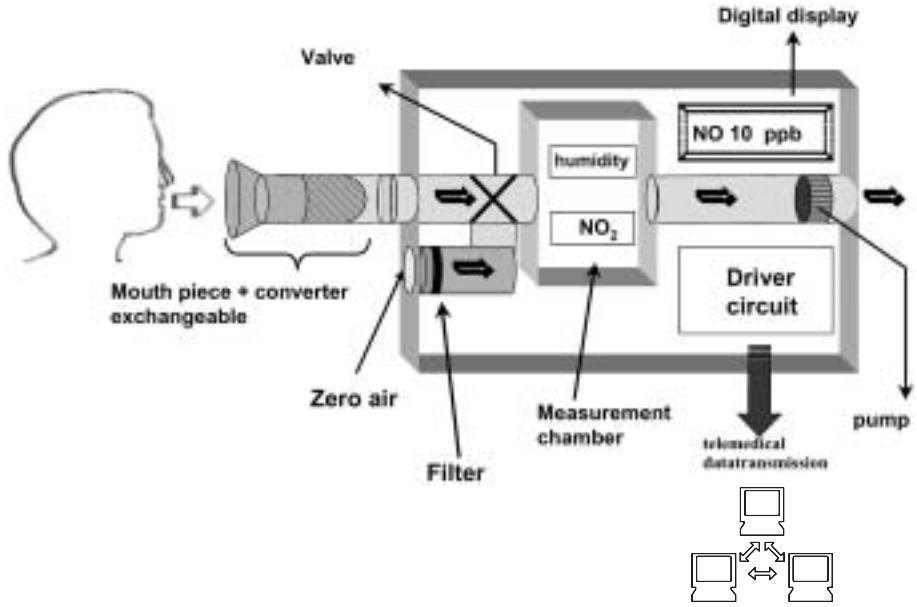

Fig. 1. Asthma prototype.

oxidation column consisting of $KMnO_4$ immobilized on silica gel placed in front of the NO_2 sensor is used for that purpose. The oxidation of NO to NO_2 is strongly dependent on the humidity concentration therefore a pure silica pre-column is integrated which reduces the humidity to values lower than 70% r.h. The high reproducibility (conversion rate is 95%, recovery is 82% at a gas flow of 2.5 l/min) and a delay time due to the oxidation of lower than 15 s allows therefore the detection of NO gas. In Fig. 1 the system configuration of an asthma prototype is presented.

The laboratory set up for the NO detection in breath was tested by simulating different breath maneuver with different NO concentrations at high humidity levels. A clear discrimination between the measurements with and without a NO to NO_2 oxidation column was found. The humidity was reduced to 68% and the conversion rate was about 98%. Only a small sensor reaction to humidity was detected. The correlation of the gas sensor signal and the NO respectively the NO_2 concentration was high ($R = 0.98$) together with a good reproducibility of the NO_2-GasFET sensor signal. These very promising measurements allows us to test this asthma sensor set up in field tests in a next step and show the way to develop a mobile asthma sensor for the low cost sector.

References

[1] M. Phillips, Breath Tests in Medicine, Scientific American, 1992, pp. 74–79.
[2] M. Fleischer, B. Ostrick, R. Pohle, E. Simon, H. Meixner, C. Bilger and F. Daeche, Low power gas sensors based on work function measurement in low-cost hybrid flip-chip technology, *Sensors and Actuators* **B80** (2001), 169–173.
[3] E. Baraldi, N.M. Azzolin, A. Cracco and F. Zaccello, Reference Values of Exhaled Nitric Oxide for Healthy Children 6–15 Years Old, *Pedriatic Pulmonology* **27** (1999), 54–58.
[4] K. Besocke and S. Berger, Piezoelectric driven Kelvin Probe for contact potential measurement, *Rev. Sci. Instrum.* **477** (1976), 840–842.
[5] E. Simon, M. Fleischer and H. Meixner, Porphin dyes – high potential sensor materials for work function type gas sensors in an asthma detection system; Conf. Proc. Eurosensors XVI in Czech Technical University Prague, Czech Republic, 15–18 September 2002.

II. Biosignals Bioengineering

Accuracy of the electronic palpation blood pressure measurement method versus the intra-arterial method

H. Sorvoja and R. Myllylä
University of Oulu, Department of Electrical and Information Engineering, Oulu, Finland
Tel.: +358 08 5532690; Fax: +358 08 5532774; E-mail: hannu.sorvoja@ee.oulu.fi

Introduction: The electronic palpation (EP) method [1] uses a standard occlusion cuff around the upper arm and a wristwatch type of multi-element pressure transducer array to sense pulsations on the radial artery. Measurements can be made both during inflating and deflating cuff. Diastolic blood pressure can be defined as the point where the pulse amplitude of the blood pressure signal starts to decrease, while systolic blood pressure was defined as the last pulse detected. However, cuff pressure affects not only amplitude, but also pulse transit time. As an increasing cuff pressure level approaches the pressure level in the brachial artery, the pulse transit time from the aorta to the radial artery is correspondingly delayed. In the ideal model, the time elapses continue to rise until the systolic pressure level is achieved. Thus, the maximum transit time change equals the time that the blood pressure pulse takes from the diastolic pressure to the systolic pressure point.

Methods: Two different groups, patients and healthy volunteers, were measured in a hospital environment. Array type of transducer was used to facilitate the placement of the wrist transducer, as the array element with the strongest pulsation is easy to pick out. As mentioned above, diastolic blood pressure determination is based on pulse transit time. To measure accurately the point of increasing of pulse delay, good timing base is essential. The best timing can be got from the other hands radial artery, and, if having same data processing, time difference can easily be defined.

Since radial artery EP-signals is already bandpass (1–15 Hz for healthy and 1.7–11 Hz for patients) filtered using analogical hardware filtering, same kind of filtering is done to intra arterial blood pressure signal. Owing to the 100 Hz sampling rate used in data acquisition, we had to interpolate the data matrices for better timing accuracy. According to our experience, an adequate resolution level was achieved at a ten-fold sampling rate. After interpolation, derivated signal is calculated and peak detection is defined for both pulses for time difference calculation. Matlab$^{\mathrm{TM}}$-software were used in all calculations.

Results: Systolic pressure was visually determined from the last palpated pulse and the diastolic blood pressure readings by the time delay method described above. Reference values were provided by the average intra arterial systolic and diastolic pressure. The mean error for the patient group (14 men and 6 women) is 0.7 ± 6.3 mmHg for systolic and 0.2 ± 5.3 mmHg for diastolic pressure. For the healthy group (12 men and 4 women), on the other hand, the average error is -2.6 ± 9.9 mmHg for diastolic and -4.6 ± 8.0 mmHg for systolic pressure.

Discussion: In principle, the electronic palpation method can be used with any transducer which measures pressure pulsations on the radial artery or a finger. When measuring cuff pressure and radial artery pressure pulses using two identical pressure array transducers with the same bandwidth, even pulse-by-pulse noninvasive blood pressure monitoring may be established.

Conclusion: Electronic palpation method had almost zero mean error in patient group and almost as good with young volunteers. This shows that the electronic palpation method has clinical value.

Reference

[1] H. Sorvoja, R. Myllylä, S. Nissilä, P. Kärjä-Koskenkari, J. Koskenkari, M. Lilja and A. Kesäniemi, A method to determine diastolic blood pressure based on pressure pulse propagation in the electronic palpation method. Engineering in Medicine and Biology Society, *Proc. of the 23rd Annual International Conference of the IEEE* **1** (2001), 3255–3258.

A method for transmitting data in a body area network (BAN) using capacitive coupling

L. Tebje[a], H. Dorn[b], H. Danker-Hopfe[b], W. Benecke[a] and R. Laur[a]
[a]*Microsystems Center Bremen (MCB), University of Bremen, Germany*
[b]*Department of Psychiatry and Psychotherapy, Charité University Medicine Berlin, Campus Benjamin Franklin, Germany*
Tel.: +49 421 218 7051; Fax: +49 421 218 4774; E-mail: ltebje@imsas.uni-bremen.de

Introduction: The miniaturization of medical sensors and signal processing electronics enables a high-quality medical supervision of humans in real life situations. Body-worn sensors and receivers are often referred to as Body Area Network (BAN) or Personal Area Network (PAN) where radio transmission technology is the usual approach to exchange data [1,4,5]. In this paper, a novel approach utilizing capacitive coupling between body-worn electrodes is described. The human body provides the return path for the electrical current (see Fig. 1). A similar technique has been presented by Zimmerman [6], who coupled the current capacitively into the body. To verify our approach, a clinical study has been conducted.

Methods: A measurement system was built, comprising a signal transmitter and a receiver galvanically isolated from the transmitter (see Fig. 2). The attenuation of the signal between transmitter and receiver was measured on ten test persons. Signal averaging is employed to improve the signal-to-noise ratio (SNR) and to reduce external interference. Both transmitter and receiver are electrically connected to the human body with ECG-electrodes. Capacitive coupling is accomplished employing the ground planes (area: 70 cm^2) of the devices as electrodes. The transmitter voltage was 4 V, for safety reasons a protection capacitor (100 nF) and resistor (1 kΩ) were used at the transmitter output. A capacitor of

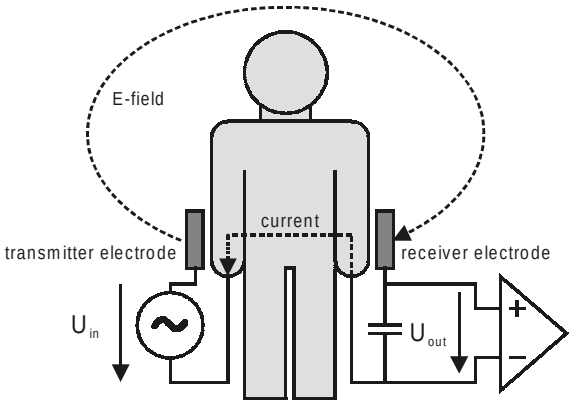

Fig. 1. Illustration of the transmission principle.

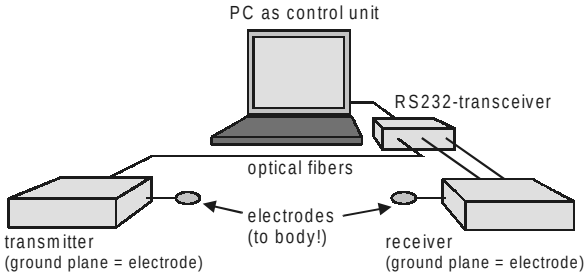

Fig. 2. Measurement system.

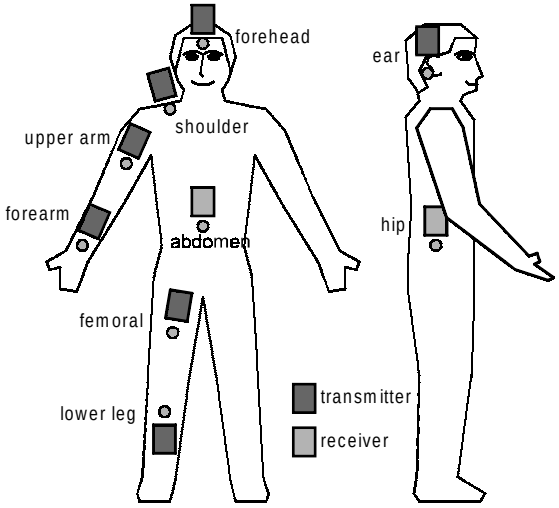

Fig. 3. Locations of transmitter and receiver.

Table 1
Transmitter locations

Position	Description
femoral	20 cm from middle of patella
lower leg	15 cm below patella
upper arm	10 cm proximal from elbow joint
forearm	5 cm proximal from wrist
shoulder	clavicula
forehead	3 cm above nasion
ear	mastoid

Table 2
Receiver locations

Position	Description
hip	lateral, 3 cm above crista iliaca
abdomen	directly above belly button

330 pF was used in parallel to the receiver input to obtain a defined input impedance. The different positions of receiver and transmitter are shown in Fig. 3, resulting in fourteen possible combinations.

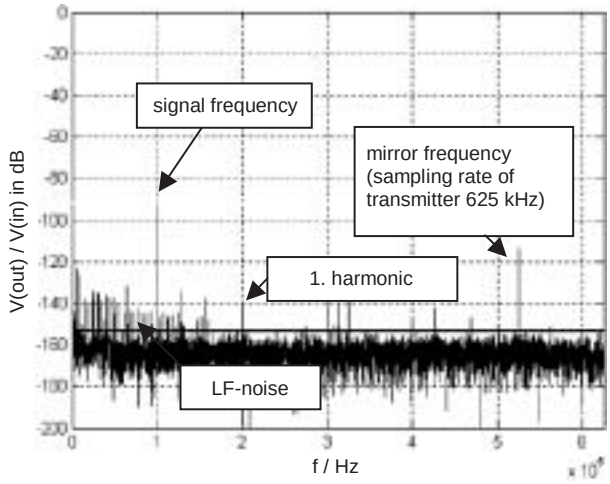

Fig. 4. Typical amplitude spectrum for $M = 128$.

One measurement cycle consisted of three single measurements at 20 kHz, 100 kHz and 180 kHz where the test person did not move followed by the same sequence where the person had to move the part of the body where the transmitter was located. This was carried out for every combination of transmitter and receiver locations. The receiver samples a time window of $N = 10000$ values and averages M consecutive time windows. The SNR then increases by a factor of the square root of M corresponding to 3 dB for every doubling of M [2]. The acquired signal is sent to the computer and evaluated using MATLAB. The Fast Fourier Transform (FFT) is applied to obtain the amplitude spectrum of the signal. Figure 4 shows a typical amplitude spectrum.

Results: The attenuation did not depend on frequency due to the capacitive voltage divider formed by the coupling capacitance through air and the parallel capacitor at the receiver input. For application in a Body Area Network, the channel capacity in bits per second (bps) is the most important parameter. The channel capacity C for a channel with additive white Gaussian noise can be calculated as [3] $C = B \cdot ld(1 + S/N)$ with B as used bandwidth, S as signal power and N as noise power. The signal power is obtained from the peak due to the sine function.

The noise power and therefore the SNR depend on the bandwidth. The average spectral noise voltage density was measured to be 180 nV per root-Hz. Assuming a constant spectral noise voltage density ($f > 150$ kHz in Fig. 4) and a bandwidth of 10 kHz, the channel capacity shown in Fig. 5 is obtained.

Conclusion: Capacitive coupling can be used in a BAN to transmit data from sensors attached to the body to a body-worn receiver. The obtainable data rates are on the order of several tens of kbps for a bandwidth of 10 kHz and an electrode area of 70 cm^2. A feature of this principle is its extremely low power consumption at transmitter output. Assuming a coupling capacitance of 1 pF, a total loss resistance of 2 kΩ (resistance of human body), a frequency of 100 kHz and a voltage of 8 V (peak to peak), the power consumed by the loss resistance becomes 6 nW. On the downside, the signal can be shielded by the human body. This could be circumvented by using electrodes wrapped around e.g. arm, leg or hip (belt).

References

[1] K.P. Fishkin, K. Partridge and S. Chatterjee, Wireless User Interface Components for Personal Area Networks, *IEEE Pervasive Computing* **1**(4) (2002), 49–55.

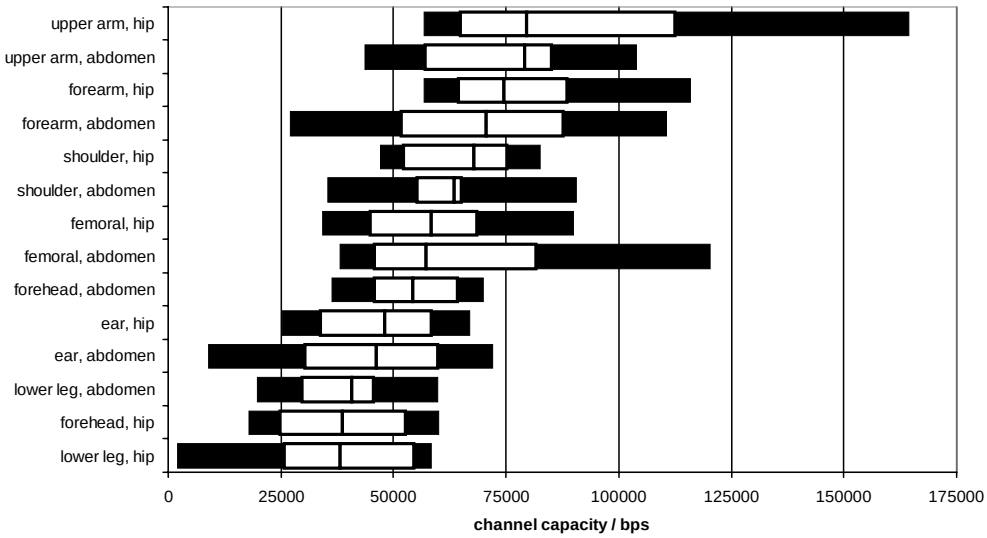

Fig. 5. Channel capacity for a bandwidth of 10 kHz for different transmitter / receiver locations. Black boxes mark 5% and 95% quantiles, white boxes: lower and upper quartile, middle line: median.

[2] P. Horowitz and W. Hill, *The Art of Electronics*, 2nd ed., Cambridge: Cambridge University Press, 1989, pp. 1026–1035.
[3] K.D. Kammeyer, *Nachrichtenübertragung*, 3rd ed., Stuttgart: Teubner Verlag, 1996.
[4] J.Y. Khan, J. Wall and M.A. Rashid, Bluetooth-Based Wireless Personal Area Network for Multimedia Communication, in Proc. of the First IEEE Int. Workshop on Electr. Design, Test and Appl. (DELTA 02), 2002.
[5] T.G. Zimmermann, Wireless networked digital devices: A new paradigm for computing and communication, *IBM Systems Journal* **38**(4) (1999).
[6] T.G. Zimmermann, Personal Area Networks (PAN): Near-Field Intra-Body Communication, Master Thesis, Massachusetts Institute of Technology, 1995.

Bioanalytical and Medical Trends in Sensor Applications

Micro-bioreactor-sensor systems for monitoring of biochemical parameters

W. Torbicz, D.G. Pijanowska and E. Remiszewska
Institute of Biocybernetics and Biomedical Engineering, Polish Academy of Sciences, Trojdena 4, 02-109 Warsaw, Poland
Tel.: +48 22 6595534; Fax: +48 22 6597030; E-mail: wtorbicz@ibib.waw.pl

Introduction: Application of silicon technologies and among them micromechanics for fabrication of microfluidics systems opened up a possibility for realisation of micro total analytical systems (μTAS), consisting of several blocks such as a sampler and a block for sample preparation and a sensing block for measurement of the concentration of a given biochemical analyte. The measuring procedure has been usually realised by means of (bio)sensors. However, in the case of complicated set of (bio)chemical reactions, the procedure is shared between: biosensors and/or bioreactors. One of the real problems in manufacturing of the μTAS systems is a local immobilisation of bioreceptors such as enzymes and antibodies onto micro structured surfaces of the bioreactors and the biosensors.

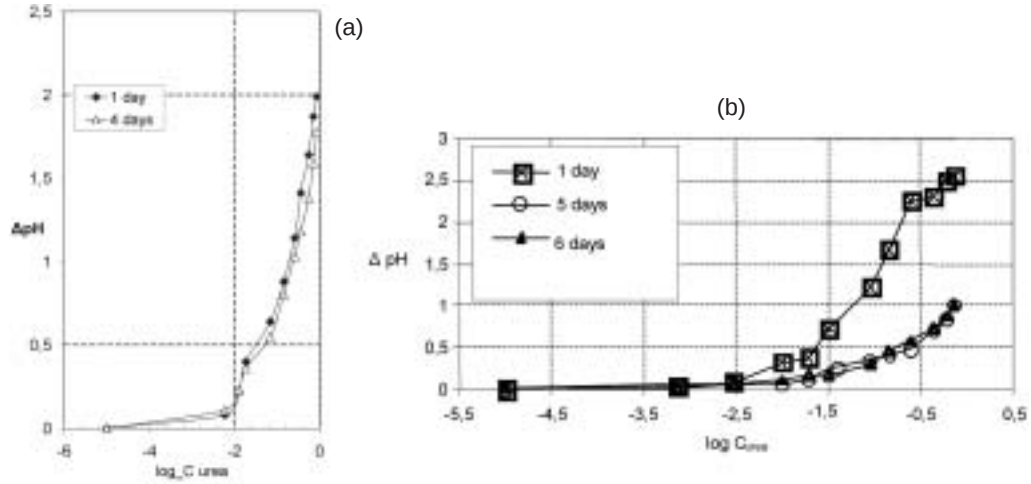

Fig. 1. Calibration curves for micro reactors. (a) With glass beads modified with GOPTES at pH 8.0. (b) Silicon lamella type modified with GOPTMS at pH 7.0.

In this paper we discuss the influence of different technological procedures assuring preservation of the activity of the immobilised urease, as a representative of bioreceptors. These chemically active components were used to create micro enzymatic reactors.

Materials and methods: Reagents applied for the immobilisation of urease: (1) 3-glicidoxypropyl-triethoxysilane (GOPTES) obtained from Fluka, (2) 3-glycidoxypropyltrimethoxysilane (GOPTMS) – Aldrich, (3) aminopropyltriethoxysilane (APTS) and glutaraldehyde from Sigma (4) urease from Jack Bean (EC 3.5.1.5) type IX, of activity 500 kU/g – Sigma, (5) urea as substrate for urease – Merck, (6) glass beads of diameter 0.75–1 mm as substrate for the enzyme immobilisation – Carl Roth GmbH.

A flow-through system operating in a closed loop mode was utilised for evaluation of the immobilisation procedures. Three types of micro reactors were realised: (1) flow-through column of 100 μl volume made in Pyrex with urease immobilised beads and two other fabricated in silicon – (2) with 62 parallel channels and common inlet and outlet (lamella) and (3) in a form of 1?m long meander single channel [2].

The urease was immobilised using four methods. Three of them: (1) entrapment within alginate gel beads, (2) adsorption onto nitrocellulose sheets and (3) chemical coupling to surface of silica gel beads through APTS and glutaraldehyde were used for the Pyrex column [1]. The fourth one, based on alkilation reaction between an amino groups on the enzyme and an epoxy rings of the silane [2], was applied for the glass of beads used in the Pyrex column and for the silicon type bioreactors.

The microreactors were tested in a flow-through system where the flow was driven using a peristaltic pump. Hydrolysis reaction of urea, catalysed by the immobilised urease, was analysed using recording of pH changes of the sample solution. Concentration of urea in the solution was changed by a standard addition method. Before the sample introduction into the measuring system, the micro reactors were rinsed with phosphate buffer solution. All measurements were taken at room temperature.

Results: For the micro reactor packed with urease immobilised onto NC sheets, the total change of pH was 3 units for the measured range of concentration of urea between 10^{-5} to $10^{-0.5}$ M. The linear range was $10^{-2.8}$ to $10^{-1.6}$ M. Similar results were obtained for urease immobilised within alginate gel. However the method failed to work due to a very poor mechanical stability of the gel.

Both the third and the fourth immobilisation methods are effective. However, the fourth one is relatively simple and the conditions for urease immobilisation in alkilation reaction are much milder for

the enzyme than for the immobilisation with APTS and glutaraldehyde. An example of the calibration curves obtained for the micro reactors with urease immobilised by GOPTES in solutions at pH 8.0 is shown in Fig. 1(a). The linear range for the micro reactor with urease immobilised with GOPTES is shifted in the direction of higher urea concentration in comparison to the micro reactors based on NC-sheets.

Since the immobilisation of the urease onto testing material (glass beads) with GOPTMS indicated more unequivocal results than for the GOPTES, immobilisation of the urease in silicon micro reactors was performed with the first silane. An example of the calibration curves obtained for the silicon micro reactors with urease immobilised with GOPTMS in solutions at pH 7.0 are shown in Fig. 1(b).

Discussion: The experiments indicated that there is a permanent decrease of the signal for microreactor packed with glass beads modified with GOPTES with urease immobilised at pH 7.0. Although, signal obtained for microreactor with urease immobilised at pH 7.0 is higher than for urease immobilised at pH 8.0, the later one exhibit better stability in time. In the case of micro reactors with glass beads modified with GOPTMS the influence of pH of buffer solution for urease immobilisation was not so clear. For both pH 7.0 and pH 8.0 there was a significant degrease of the output signal after the first day of operation. This can be explained by washing out of non-attached molecules from the micro reactors. Behaviour of the silicon micro reactors was similar to the model micro reactors made in Pyrex.

Conclusions: Four methods of urease immobilisation were compared. Immobilisation by the adsorption onto the NC sheets can be applied for micro reactor made by precision engineering and is rather not applicable as a method for biosensor and silicon type micro reactors preparation. All other described methods can be applied for preparation of both biosensors and micro reactors. In addition, the promising preliminary results, concerning chemical immobilisation, allow future works be oriented towards miniaturisation of micro reactors and its integration into a micro-analytical system.

References

[1] D.G. Pijanowska and W. Torbicz, The pH-detection of triglycerides, *Sensors and Actuators* **B78** (2001), 263–266.
[2] D.G. Pijanowska, E. Remiszewska, J.M. Łysko, J. Jaźwiński and W. Torbicz, Immobilization of bioreceptors for microreactors, *Sensors and Actuators* **B91/1-3** (2003), 152–157.

Master Programme in Biomedical Engineering

K.-P. Hoffmann[a] and H. Foth[b]
[a]*Hochschule Anhalt (FH), Bernburger Str. 55, 06366 Köthen, Germany*
Tel.: +49 3496 67 2322; Fax: +49 3496 67 2399; E-mail: hoffmann@et.hs-anhalt.de
[b]*Martin-Luther-Universität Halle-Wittenberg, Franzosenweg 1a, 06112 Halle/ Saale, Germany*
Tel.: +49 345 557 1630; Fax: +49 345 557 1871; E-mail: heidi.foth@medizin.uni-halle.de

The Biomedical Engineering programme is a joint venture between the Martin-Luther-University Halle-Wittenberg and the Hochschule Anhalt (University of Applied Sciences). This unique co-operation offers an excellent opportunity to combine theory and practice. The degree course is organised in modules which results in a great amount of flexibility. Furthermore the European Credit Transfer System (ECTS) enables students to transfer easily within an international university environment. The degree course is

divided into a project and course orientated programme. The introduction of a quality management for teaching and research and regular evaluation ensure a high quality of education.

The objective of the course is to give students an additional scientific qualification for an academic career, prepare them for working in an international environment or assist them undertake a professional reorientation. Students successfully completing the course are awarded a degree in Master of Engineering (MEng) in Biomedical Engineering, (3 regular semesters) or Master of Science (MSc) in Biomedical Engineering, (4 regular semesters planned to start in October 2004/05). Entry requirements are university graduates in engineering, the sciences or medicine. The course is taught in English and German. Enrolment is once a year in October and the enrolled students have a double registration at the Martin-Luther-University Halle-Wittenberg and the Hochschule Anhalt (University of Applied Sciences).

As mentioned above there are two different programmes. Programme A is more practically orientated and involves the students at an early stage in the course working on a project which is research based and leads to a publication (project oriented). Programme B is course oriented and involves more theoretical elements and more lectures.

The students can individually choose the subjects within the modules according to their own personal objectives. The personal timetable is organised and confirmed at the beginning of every semester with a mentor. Periods of study and exams at other universities (including the open university) are also considered. The timetable should enable the student to reach 100 credits. Programme A requires 40 semester week hours and Programme B requires 60 semester week hours.

The study programme is divided into the following modules:

1. Biomedical Engineering and Interdisciplinary Specialisation.
    1.1. Special Areas of Biomedical Engineering
    1.2. Applied Engineering and Information Technology
    1.3. Interdisciplinary Subjects.
    1.4. Project Work and Certificate (paper) (only for programme A)
2. Medical Research and Applied Biomedical Engineering
    2.1. Basic Medical Research (Preclinical Medicine)
    2.2. Clinical Research and Highly Specialised Medical Care (Clinical Medicine)
    2.3. Project Work and Thesis (paper, poster) (only for program A)
3. Project Work and the Preparation of the Master Thesis
4. Special Areas of Scientific Engineering (planned)

Because of the highly innovative character of biomedical technology the MBE graduates may find careers in a wide range of areas including research and development of the biomedical engineering, technical supervision and the civil service, in the application but also in sales and services of medical instruments in particular in medical institutions and hospitals.

The MBE graduates are the doctor's partners and are directly involved with the highly specialised medical care and developing solutions in basic clinical research. The instruments and systems developed by the MBE are essential tools for the doctor to help him recognise, treat, alleviate and observe illnesses and compensate disabilities. The precision of modern diagnostic methods and instruments enables an early and reliable diagnosis of numerous illnesses which increases the chances of healing.

Some examples of further possible career openings for MBE graduates are:

– International businesses (Management, Research and Development)

– Medical Institutions (Clinical Research, Highly Specialised Medical Care, Management)
– Research Institutes, University (Basic Research, Lecturing)
– Civil Service, Personal Management

Biomedical Engineering education for a research environment

D.W. Slaaf[a,b,*] and A.A.H.J. Sauren[a]
[a]*Department of Biomedical Engineering, Eindhoven University of Technology, Eindhoven, The Netherlands*
[b]*Department of Biophysics, Maastricht University, Maastricht, The Netherlands*

Introduction: Biomedical Engineering (BME) still is a rather new discipline. IFMBE defined BME as follows: "Medical and Biological Engineering integrates physical, mathematical, life sciences and engineering principles for the study of biology, medicine and health systems and for the application of technology to improve health and quality of life. It creates knowledge from the molecular to the organ system levels, develops materials, devices, systems, information approaches, technology management, and methods for assessment and evaluation of technology, for the prevention, diagnosis, and treatment of disease, for health care delivery and for patient care and rehabilitation". In BME education, knowledge about the functioning of the human body, understanding by using mathematical models and computer simulations, data collection and design of new techniques and research methods all play an important part. A Biomedical Engineer may interact with engineers of various disciplines, but also with biologists, biochemists, and medical specialists. After his training (B.Sc. and M.Sc.), a Biomedical Engineer may work in research, a hospital or in design or applications in industry. Depending on the specific requirements, further education may be required.

The Dutch situation: In the Netherlands, several levels of BME education exist: Higher Vocational and University Education. In Higher Vocational Education, the intended final qualifications are partly based on the professional profiles and/or professional competences drawn up by or in conjunction with the relevant professional field. In University Education, the intended final qualifications are based on requirements made by the academic discipline, the international academic practice and, if applicable to the course, the relevant practice in the prospective professional field. A University Bachelor possesses the qualifications that allow access to a minimum of one further degree course at University master's level as well as the option to enter the labor market. *A University Master possesses the qualifications to conduct independent academic research* or to solve multidisciplinary and interdisciplinary questions in a professional practice for which a University degree is required or useful.

Requirements for BME education: BME combines engineering with life sciences. The fact that more disciplines have to be studied and integrated, should not lead to superficial studying. A strategic choice of the core knowledge is of utmost importance. This was recognized by ABET, who formulate the requirements for a BME curriculum as follows:

The structure of the curriculum must provide both breadth and depth across the range of engineering topics implied by the title of the program.

The (undergraduate) program must demonstrate that graduates have:

*E-mail: DW.Slaaf@bf.unimaas.nl.

– An understanding of biology and physiology, and
– The capability to apply advanced mathematics (including differential equations and statistics), science, and engineering to solve the problems at the interface of engineering and biology;
– The ability to make measurements on and interpret data from living systems, addressing the problems associated with the interaction between living and non-living materials and systems.

BME programs require the presence of engineering sciences and biomedical sciences in one location or not too distant from one another, provided an ongoing collaboration exists. The specific contents of a BME education program depend on the availability of specific knowledge and research facilities, and on the type of career the engineers plan to pursue. The requirements for a career in research will differ from a career in a hospital. Given the many different professions where a Biomedical Engineer may function and the many different research topics where Biomedical Engineers are invaluable, many different roads will lead to a good finish. Consequently, BME education programs will develop strong local flavors.

The Eindhoven/Maastricht BME program started in 1997. Our BME program is a University education with an integrated, 5-year program where engineering and life sciences are implemented in the curriculum from the start, with one bachelor and two master programs with various tracks. It is research driven and oriented, and aims at educating engineers who will be employed in biomedical research and development. Various departments contribute in the education of our students: Medicine and Health Sciences (Maastricht), Applied Physics, Chemical Engineering & Chemistry, Electrical Engineering, Mechanical Engineering, and Mathematics & Computing Science (Eindhoven).

The domain: good engineering background combined with life sciences. The research interests of the constituting groups "color" the program. This is most visible in the integrated parts of the bachelor education and in the master tracks.

Three educational programs are offered: undergraduate program (B.Sc.) in Biomedical Engineering, graduate program (M.Sc.) in Biomedical Engineering, and a graduate program (M.Sc.) in Medical Engineering

The bachelor phase provides the student with a solid scientific base: physics/chemistry (30%), mathematics (25%), engineering (25%) and biology/medicine (20%). Courses are restricted to a certain domain and supply the building blocks for a base of theoretical knowledge. In the Design-Centered Learning (DCL evolved from Problem-Based Learning and is aimed at the integration and application of knowledge as well as the acquisition of general research and engineering skills) blocks, students work actively and cooperatively on multidisciplinary design tasks. It takes about 60% of study time in the bachelor phase and is the integrating part of the education. DCL ranges from case studies (1st and 2nd year) to projects (3rd year) and Skills labs (3rd year).

The master phase: The Biomedical Engineering program aims at educating engineers capable of organizing and executing both fundamental and applied research in the field of biomedical engineering at the initial phase of their career. Although this multidisciplinary study is based upon the integration of physical, engineering and life sciences, specialization in several disciplines is possible. The graduate student focuses on complex subject matter, involving innovation of existing concepts or development of new concepts. The BME Master program is "colored" by the locally available expertise as exemplified by the following master tracks: Molecular Bioengineering, Biomechanics and Tissue Engineering, and Biomedical Imaging and Modeling.